STUDIES ON THE SYNTHESIS, CYCLODEXTRIN INCLUSION AND BIOLOGICAL ACTIVITY OF AJOENE ANALOGUES AS POTENTIALLY NOVEL ANTI-CANCER AGENTS

BY

Tozama Qwebani

Thesis Presented for the **Degree of**

Master of Science in Chemistry

Faculty of Science

UNIVERSITY OF CAPE TOWN

August, 2009

Supervisors

Professor Roger Hunter and Professor Mino R. Caira

Certification

As the candidate's supervisor, I have approved this dissertation for submission.

Professor Roger Hunter

Signature: _____

Date: 30 | 11 | 2009

As the candidate's co-supervisors, I have approved this dissertation for submission.

Professor Mino Caira

Signature: _____

Date: 2e Nov 2009

Declaration

I declare that this thesis is my own work. Where collaboration with other people has taken place, or material generated by other researchers is included, the parties and/or materials are indicated in the acknowledgements and/or are explicitly stated with references as appropriate.

This work is being submitted for the Master of Science in Chemistry at the University of Cape Town. It has not been submitted to any other university for any other degree or examination.

Tozama QWEBANI

27/11/2009.

Date

Dedication

To my dear parents, who did everything possible to educate me.

Abstract

The first part of the thesis describes synthesis of 10-(4-methoxyphenyl)-4,5,9-trithia-deca-1,6-diene (**25**) as an ajoene mimic and as a mixture of *E/Z*-geometrical isomers using new synthetic methodology. 4,5,9-trithia-dodeca-1,6-diene 9-oxide (**43**), 4,5,9-trithia-dodeca-,6-ene 9-oxide (**44**) and 2,3,7-trithia-deca-4-ene 7-oxide (**45**) were also successfully synthesized as a mixture of *E/Z*- separable geometrical isomers using the same synthetic methodology. The synthesis involved a radical addition and a chemoselective oxidation as key steps. Characterisation was carried out by ^{1}H NMR, ^{13}C NMR, IR and HRMS spectroscopies.

The second part of the thesis describes the preparation and characterization of an inclusion complex formed between 10-(4-methoxyphenyl)-4,5,9-trithia-deca-1,6-diene 9-oxide (**25**) as a mixture of *E/Z*-isomers with heptakis (2,3-tri-O-methyl)-β CD) TRIMEB. Characterisation of the complex was achieved using ^{1}H NMR spectroscopy, Powder X-ray diffraction, hot stage microscopy and Differential Scanning calorimetry. Single crystal X-ray diffraction revealed that the complex is orthorhombic, crystallizing in the space group $P2_12_12_1$ with unit cell parameters a = 14.7900(2), b = 21.4857(2), c = 27.9036(4) Å and Z = 4 complex units per cell. The guest molecule adopts a hairpin conformation with the sulfoxide moiety located near the cavity 'roof' and the methoxyphenyl and allyl residues directed towards the secondary rim of the host molecule.

The final part describes the biological activity of the synthesized ajoene analogues together with that of the inclusion complex regarding their ability to inhibit cell growth of WHCO1 cancer cells using an MTT colourimetric assay. The WHCO1 cell-line is an oesophageal cancer cell-line of South African origin which was originally established from surgical biopsies of primary oesophageal squamous cell carcinomas. All the biological tests were conducted at the UCT Medical School. IC_{50} values were calculated and compared with that of ajoene. Their biological activity has been found to increase with the lipophilic character in the chain.

Acknowledgements

To my heavenly Father 'The steps of a righteous man are ordered by the Lord' having you as a father has made me to be righteous. You opened doors that I thought were never possible to be opened, you made me understand science when I was about to give up thinking it is only for Einstein, you gave me peace in the mist of the storm, you showered me with love and faithfulness and held me close to your arm. You proved yourself to be faithful. You made me meet people who assisted me and without their assistance this thesis would not have been possible. What then can I say to you father Jesus? All glory, honour and adoration belong to you. Ndiyabulela kakhulu Tata.

Prof Roger Hunter and **Prof Mino Caira**, you believed in me succeeding in science before I even believed in myself as an undergraduate. You nurtured and trained me as the father does to his daughter, you always welcomed me to your office as if you had no other work to do. You introduced me to science literature and allowed us to publish some of that literature before completing my masters. You became more than supervisors and equipped me with necessary skills and knowledge for the working world. Words can not fully express what I'm trying to say, I felt honoured being supervised by you for the qualities and values you give to your students, which I have embraced, and if the fruit is not yet visible it surely will be sooner or letter and for that I will forever be grateful, thank-you.

My sincere gratitude to **Dr Phillip Richards**, **Dr Catherine Kaschula**, **Dr Vincent Smith**, **Dr Nashia Stellenboom**, **Mr Scebi Mkhize and Miss Dyanne Cruickshank** all your assistance and encouragement to the success of this thesis is highly appreciated. When the puzzle was still in pieces you assisted me to complete it, I will forever be **grateful**, **THANK-YOU**. I would also like to extend my gratitude to both **Prof Hunter and Prof Caira's laboratories,** it has been great working with all the **team members.**

I would like to thank both my sponsors : **Council of Scientific Industrial Research (CSIR)** and **University of Cape Town, Department of Chemistry Equity Development Programme**, this research would have not been possible without your assistance, **THANK YOU**.

My parents, **Mrs P.B and Mr T.A Qwebani,** your love of letting go have thought me to make and stand in my decision at a very early stage of my tertiary life. You sacrificed a lot for us to get education, your spirit of excellence, determination and commitment in your work has made me to be likewise. As the saying goes, 'The branch does not fall far form its tree.' I'm here because of the qualities that I have seen and embraced from you. From the younger age you thought us about God and sent us to church that which I have embraced and God, who has proved himself to be faithful. Your leadership qualities, values and humanity have thought me to embrace opportunities, to pray and work harder on achieving my goals. Tata you introduced Maths 24 when I was in Grade 4 to our home, we use to play maths in our supper table unknowingly that you were sharpening an important skills in our brains that has been important in all spheres of my life, ...Mama you finished your BA degree while having a family and working in due time that thought me the importance of having a vision and working it out. Forever I will be grateful. You are the best Parents in the Whole World Wide.

My Siblings, **Zimasa** and **Bhut' Vuyani**: Your assistance and belief in me has made me to believe in myself and work hard. Your assistant in maths and science while in high school has been a stepping stone to be where I am today. Many thanks you are the best siblings and I could not have asked for more.

To my aunts: **Mrs N Zokufa, Tetani family and the Kenqa family.** From the young age you have shown support towards my studies. Your support increased with the no of years. Thank You. You accompanied me the first day I went to UCT and you have been attending all my graduations I would like to take this opportunity to extend

my highest gratitude for all your sacrifices. They are highly appreciated and God Bless you.

To my uncle. **Mr P Qwebani** Your value of education made me to value more what I was doing. Your motivating words and supporting nature have been highly appreciated. Thank You.

To my family in Cape Town: **Mrs and Mr S Nondlwana** Since I arrived in Cape Town you welcomed me with gladness, you opened your house to be my home. You encouraged motivated and celebrated with me in times of victory. I will forever be grateful to all that you have done, thank You

To My cousins. You are the best cousins a person could ask for and your support and encouragement has added to the achievement of this thesis.

To my friends: **Miss Snawe Pezi, Miss Wendy Tshawe and Miss Khethiwe Cele.** You have been my study partners since undergraduate years. You made studying to be fun and the sleepless nights will always be in my memory as they have added to the success of this day. All the best for the future.

To my mother in-law. **Mrs Oluwasola Ogunleye.** Your prayer, love and caring nature towards me assisted in completing this thesis. Your calls from Nigeria waking me up so that I can complete that which God had started strengthened me and made it to be possible to be submitting this work today. As the saying goes the end of something is more challenging than its beginning and because of your love you made the end to be victorious.

Mr Samuel Olalekan Ogunleye. 'Two are better than one; because they have a good reward for their labour.' (Eccl 4:9). You came to my life when I was in the

climax of the vision but it looked like a dark tunnel. You opened my eyes to see the light shining in front and you assured me that to get there I will not have to walk alone but you will rather **hold my hand and we walk together**. You became a friend, a mentor and a partner. Your faith in me rejuvenated the fire that was dying and made it to be a burning bush. Your leadership qualities, caring nature, support and love made me to rise up, stand and finish victoriously. Forever I will be **grateful**, you make a perfect partner.

Tozama Qwebani

Publications from this thesis are as follows:

"Synthesis and inclusion of *S*-aryl alkylthiosulfinates as stable allicin mimics"

Stellenboom, N.; Hunter, R.; Caira, M. R.; Bourne, S. A.; Cele, K.; Qwebani, T.; le Roex, T. *ARKIVOC* (Gainesville, FL, United States) **2007**, *9*, 53.

''Substituted ajoenes as novel anti-cancer agents''

Roger, Hunter.; Catherine, H. Kaschula.; Iqbal M. Parker.; Mino R. Caira.; Philip, Richards.; Susan, Travis.; Francois, Taute.; Thozama, Qwebani. *Bioorganic and Medicinal Chemistry Letters*. **2008**, *18*, 5277-5279.

Parts of this thesis has been presented as a poster at a conference:

(presenting author underlined)

11th Frank Warren Conference on Organic Chemistry, 2008, Kruger national Park, South Africa.

Poster: Studies on the synthesis, cyclodextrin inclusion and biological activity of ajoene analogues as potentially novel anti-cancer agents.

T. Qwebani, R. Hunter, M. R. Caira.

Chapter 1: Literature review

1.1 Introduction

This chapter will offer an overview of the literature relevant to this research project. First it will include a general overview of garlic together with a history of allicin and ajoene. An overview of cancer and its cell-cycle in humans as well as a description of apoptosis will be followed by a presentation of ajoene and various aspects of its activity with the emphasis on mechanism and cancer. Following this comes the cyclodextrin-inclusion section.

1.2 Overview of Garlic

Garlic, *Allium sativum* L., is a plant belonging to the *Liliaceae* family that is commonly used in cooking worldwide and which has been used as a medicinal agent for many decades.[1] It has generated much interest throughout human history as a food and medicine, and is one of the most researched medicinal plants. Its folklore and therapeutic benefits date back about five thousand years to the Middle and Far East, and probably originated in the advanced civilizations of the Indus valley, from where it was imported to China before spreading to Egypt, Greece and throughout the Roman Empire into Europe.[2-4] In ancient civilizations, garlic was used as a treatment for various ailments including headaches, burns and wounds, colds, worms, stings, bites, tumours, heart disease and ulcers.[5] It possesses potent antibacterial, antifungal and antiparasitic activity against a range of microorganisms.[6,7] Mechanistic investigation over the last few years suggests that by virtue of its strong antioxidant properties garlic may either prevent or decrease the occurrence of major chronic diseases such as cancer, which are mainly due to the abundance of free radicals.[8] In particular, it has been demonstrated that garlic reduces serum cholesterol and triglyceride levels, inhibits platelet aggregation, stimulates immune effector cells and acts on bacteria, viruses and alimentary parasites.[6,7] Other pharmacological activities reported for garlic include hypoglycemic, hypolipidemic, antitumor, antioxidant, antiatherogenic, inhibition of platelet aggregation and also vasolidation. Garlic extracts have also shown to have immunomodulatory and anti-inflammatory properties. The biological activities and health-promoting effects of garlic are attributed to the presence or generation of sulfur-rich compounds. The chemical structures of some of the compounds found

in allium vegetables are shown in Figure 1.[9-11]

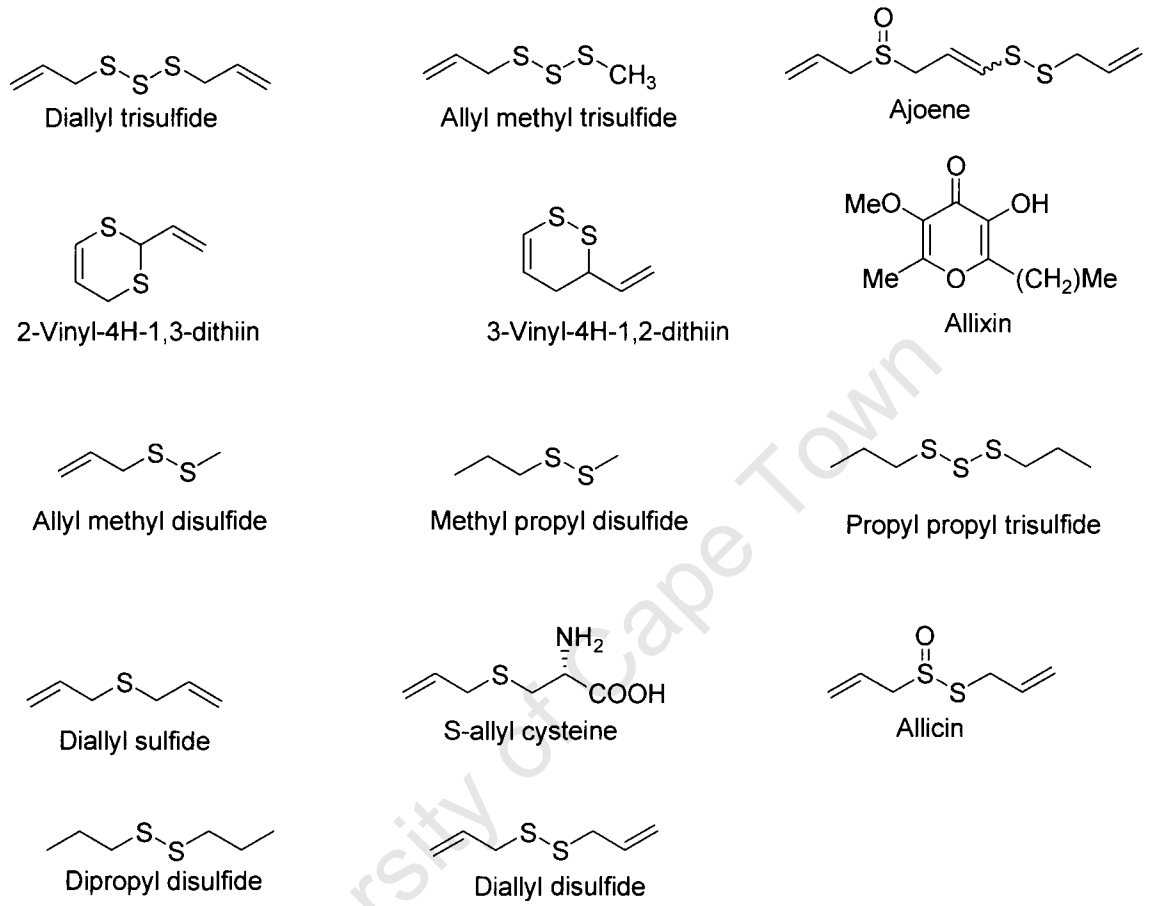

Figure 1: Sulfur compounds present in Allium vegetables.[9-11]

The earliest chemical studies on garlic were reported in 1844 by the German chemist Theodor Wertheim, who studied the steam-distillation of crushed garlic in boiling water, and identified a pungent-smelling oil produced in the steam. He then proposed the name allyl from *allium* for the hydrocarbon groups in the oil.[12] In 1892, another German chemist, F. W Semmler, carried out a steam-distillation on garlic cloves that produced an oil possessing antimicrobial properties.[13,14] He observed that two grams of oil were produced for every kilogram of garlic. A little over five decades later in 1944, Cavallito and Bailey reported the isolation and identification of the component responsible for the antibacterial activity of garlic.[15,16] They observed that different methods of extraction (Figure 2) gave different compounds, which were identified as diallyl disulfide from the ethanol extract, allicin (diallyl thiosulfinate) from the ethanol and water extract and alliin from steam distillation. The ethanol and water extract displayed the most potent antimicrobial properties.[6] Figure 2 below summarizes the structures of the compound from the various extracts.

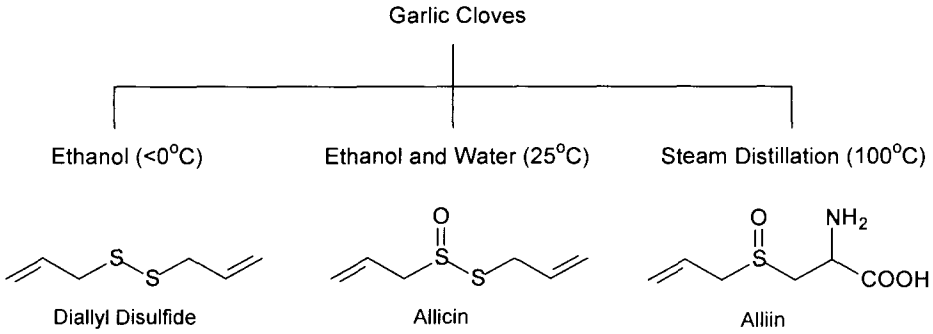

Figure 2: Major organo-sulfur compounds extracted from garlic cloves employing various extraction methods.[15,16]

The final proof of the chemical structure came in 1947 when it was shown that allicin was identical to the compound obtained from selectively oxidizing diallyl disulfide with peracetic acid as shown in Figure 3 below.[17]

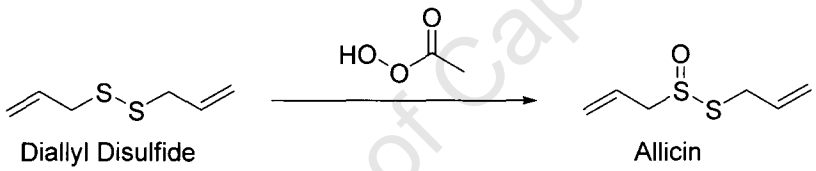

Figure 3: Selective oxidation of diallyl disulfide to allicin.[17]

Hence its structure was assigned as diallyl thiosulfinate or 2-propenyl-2-propenethiosulfinate according to IUPAC nomenclature. In accordance with the literature, 'diallyl thiosulfinate' will be used in this thesis.

1.3 Allicin

1.3.1 Discovery and synthetic aspects of Allicin

Allicin (diallyl thiosulfinate) is a member of a class of unstable and reactive organosulfur compounds known as thiosulfinates and is the most abundant organic compound in freshly-crushed garlic, as well as the principal biologically-active substance. In 1949, Stoll and Seebeck reported the isolation, identification and synthesis of *S*-(allyl)-*L*-cysteine sulfoxide as a substrate from garlic, which they named alliin.[18,19] Alliin is a remarkable molecule in that it was the first natural substance found to display enantiomerism at sulfur, ie one involving two chiral forms due to the asymmetry at sulfur. Nature favours the (+)-*S*-isomer which in itself does not have antimicrobial activity.[20] The enzyme responsible for alliin conversion, allinase, is present in

unusually high amounts in garlic cloves as at least 10% of the total protein content.[19] Allinase has 10 cysteine residues, all of them in S-S bridges, and their reduction and removal of the pyridoxal coenzyme factor renders the enzyme inactive. Cross-section analysis has indicated that the enzyme allinase and the substrate alliin are located in different compartments. This organization suggests a potential defense mechanism against microbial pathogens of the soil, in that invasion of the cloves by fungi and other soil pathogens destroys the membrane that encloses the compartments that contain the enzyme and the substrate, resulting in interaction between allin and allinase to produce allicin, which inactivates the invader. The overall equation and mechanism of formation of allicin is shown in Scheme 1 involving elimination of allin by the enzyme allinase to form allylsulfenic acid, which self condenses to form allicin.

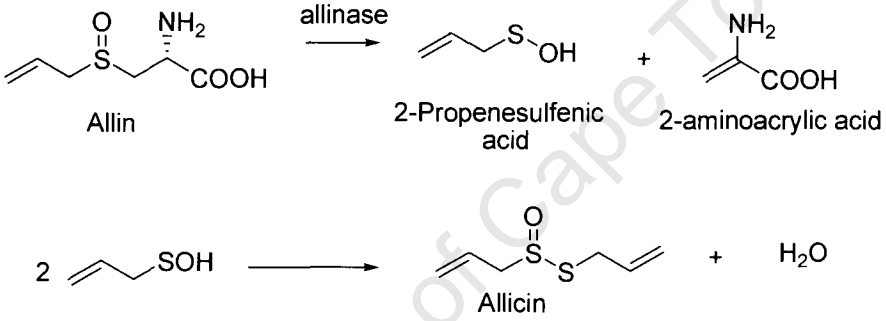

Scheme 1: Generation of allicin from allin in a garlic clove.[6]

Pure allicin is poorly miscible in aqueous solution. It has the typical odor of freshly crushed garlic,[7] and its stability has been investigated in different solvent systems. Although neat allicin decomposes rapidly at 37°C, it is more stable in protic methanol than aprotic polar ethyl acetate. Approximately 90% of the allicin remained after incubation at 37°C for 5 h in water at pH 1.2 and 7.5, while only traces of it could be detected after it was incubated in blood for 5 min.[21-25] Block answered the question of the thermal instability of neat allicin in the 1970's and 1980's by reporting that allicin fragments into thioacrolein and 2-propenesulfenic acid.[26,27] The presence of an allylic hydrogen adjacent to the sulfenyl sulfur is very crucial for this fragmentation, which is shown in Scheme 2 below.[27]

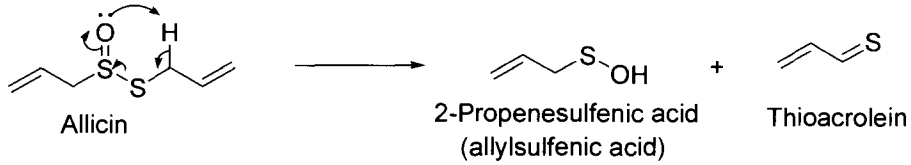

Scheme 2: Mechanism of decomposition of allicin.[27]

The fragmentation products, allylsulfenic acid and thioacrolein themselves undergo further reactions. Thioacrolein dimerizes in a hetero Diels-Alder cycloaddition reaction to form regioisomeric dithiins.[28]

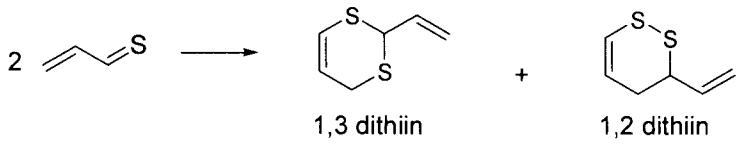

Scheme 3: Heterodimerization of thioacrolein to form dithiins

Alternatively, allicin may participate in a pathway initiated by reaction with itself, with the end-product being the interesting product ajoene as shown in Scheme 4 below. The latter has elicited huge interest as an anti-cancer and anti-thrombotic agent over the last twenty years since its discovery.

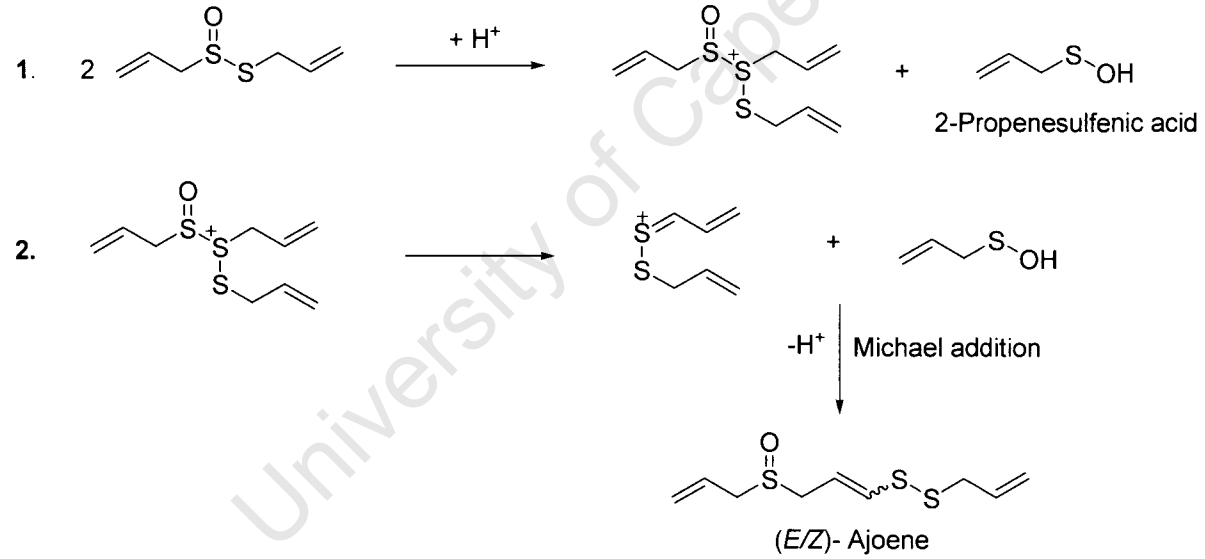

Scheme 4: Rearrangement of allicin to (E/Z)-ajoene[28]

1.4 Ajoene

1.4.1 Discovery of Ajoene

R. Apitz-Castro and M. K Jain of the CSIC (Consejo Superior de Investigaciones Cientificas) in Venezuela together with Professor Eric Block of Albany University, State of New York in the US established the structure of ajoene to be 4, 5, 9-trithiadodeca-1, 6, 11-triene-9-oxide in the early 1980's using spectroscopic methods.[29] They named the compound ajoene from 'ajo' meaning

garlic in Spanish. Studies carried out by Block revealed that ajoene exists as a mixture of *E*- and *Z*-isomers as shown in Figure 4.

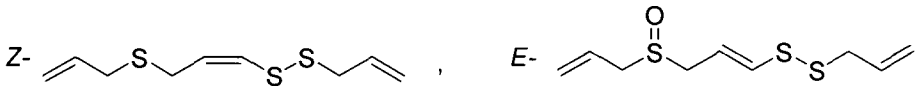

Figure 4: Chemical structures of the isomers of ajoene.[29]

Ajoene is more stable than allicin, and contains a sulfoxide with a very rarely-seen vinyl disulfide functionality.[30] The biological activity of ajoene has been extensively investigated in the past 20 years, and originally the focus was on its anti-thrombotic activity. However, recently it has been demonstrated to posses a range of biological activities including antimicrobial, anti-obesity, antifungal and anti-cancer activity.[31-36] *In vivo* experiments have shown that ajoene prevents platelet loss by inhibition of both the lipoxygenase pathway and tyrosine phosphatase activity in human platelets and that it lowers cholesterol biosynthesis through HMG-CoA-reductase inhibition.[37-39] Ajoene exerts potent inhibitory effects on platelet activation, platelet binding to damaged blood vessel walls as well as thrombus formation.[40-42]

1.4.2 Anti-cancer activity of ajoene

Ajoene has been reported to have therapeutic medicinal benefits, such as anti-cancer,[35,36] anti-fungal,[29] anti-trypanosomal,[34] antithrombotic,[43-46] anti-malaria,[29] antiviral,[44] anti-obesity,[33,47] and anti-inflammatory.[48] Ajoene also lowers triacylglycerol[49] and cholesterol,[50] blood levels and inhibits a number of enzymes such as lipoxygenase,[51,52] cyclooxygenase (COX-2),[53] prostaglandin synthase,[54] inducible nitric oxide synthase,[54] human gastric lipase,[50] glutathione reductase and trypanothione reductase.[55] In this section we will focus on the anti-cancer activity of ajoene of relevance to this thesis and review experiments conducted to unravel this activity. First a review of key aspects of cancer is given.

1.4.3 Cancer

Cancer is a disease that occurs as a result of the suppression of all apoptosis (programmed cell-death) and/or increased cell-proliferation, and proteins that sense cellular damage or growth signals arrest the cell-cycle so that the damage can be repaired or, if that is impossible, apoptosis is induced. Malfunction of this system leads to cancer by allowing cells to proliferate when they should either be repaired or die. Most human carcinogenesis has been shown to have abnormalities in some component of the retinoblastomaprotein (pRb) pathway,[56] in which

mutations of the retinoblastoma gene result in a loss of functioning of the retinoblastoma protein, leading to a wide range of human cancers, including osteosarcomas, small-cell lung cancer, lung cancer and breast cancer. The cell-cycle is controlled by proteins called cyclins and their catalytic partners.[56] The miscoding mutations of a cyclin results in a loss of affinity for its catalytic protein. This can take place due to epigenetic inactivation by methylation in a variety of tumours. Other types of cancers can be due to chromosal rearrangement. In most human cancer cells, the cyclins that have been observed to mutate are CDK4/6 cyclins. For example, it has been observed that a miscoding mutation of CDK4/6 resulted in a loss of P16 binding. By comparison, alterations at CDK2 or cyclin A are rare and mutations at E2F family members have not been identified. The alteration of cell-cycle are possible targets for therapeutic interventions. There have been attempts to exploit this by treating cancer patients with inhibitors that block CDK activity, and indirubicin, flavopiridol and UCN-01 were the first CDK inhibitors tested in clinical trials in which benefits have been noted in some patients.[56]

1.4.4 Cell-Cycle in Human Disease

To ensure a proper progression through the cell-cycle, cells have developed a series of checkpoints that prevent them from entering into a new phase until they have successfully completed the previous one. As previously mentioned, this is controlled by cyclins and their corresponding catalytic enzymes. Figure 5 shows critical regulators and check points of the cell-cycle progression.

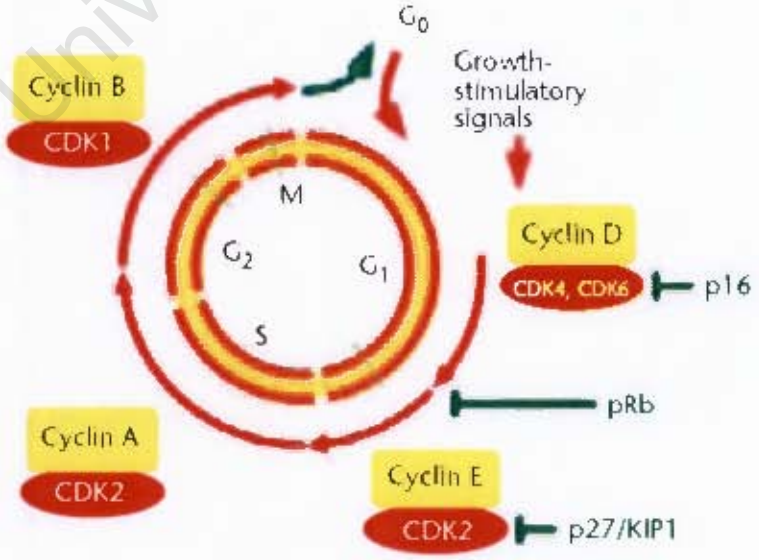

Figure 5: Critical regulaters of a cell-cycle[56]

Growth factor signals stimulate the synthesis of D-type cyclins, which then form active complex with CDK4 and CDK6 active complexes in the early G_1 phase. The primary substrate of CDK4/6 is the retinoblastoma protein (pRb), which in its active, hypophosphorylated form inhibits cell-cycle progression by binding and repressing the activity of the transcription factor E2F.[56] The transcription of several genes takes place in the G_1-to-S transition by hyperphosphorylating the pRb which causes it to disassociate from E2F, and these genes include E-type cyclins. The activation of the cyclin E/CDK2 complex drives progression from the G1 to S phase. The appropriate completion of deoxyribonucleic acid (DNA) synthesis in its S phase requires the activity of A-type cyclins together with CDK2. The B/CDK1 complex regulates entry to mitosis, whereas proteolytic degradation of B-type cyclins regulates the exit from mitosis. Other CDK/ cyclin complexes are regulated as follows: (i) inhibitory or activating phosphorylation; (ii) inhibition by specific CDK inhibitors (CKIs) such as p16, p21/WAF1, p27/KIP1 or (iii) by targeted degradation, mediated for example by the SCF (Skp1 – Cullin – F-boxprotein) ubiquitin ligase. It has been observed that in tumour or cancer cells the cyclin dependent kinase inhibitory proteins are either absent or mediated.[56]

1.4.5 Apoptosis

Apoptosis is an active energy-dependent genetically programmed process that occurs widely during mammalian development. It offers a practical way of getting rid of old, damaged or dangerous cells, and is mediated by 2 major pathways known as mitochondrial and death-receptor pathways respectively. Figure 6 summarizes the various interactions between the two pathways.[56]

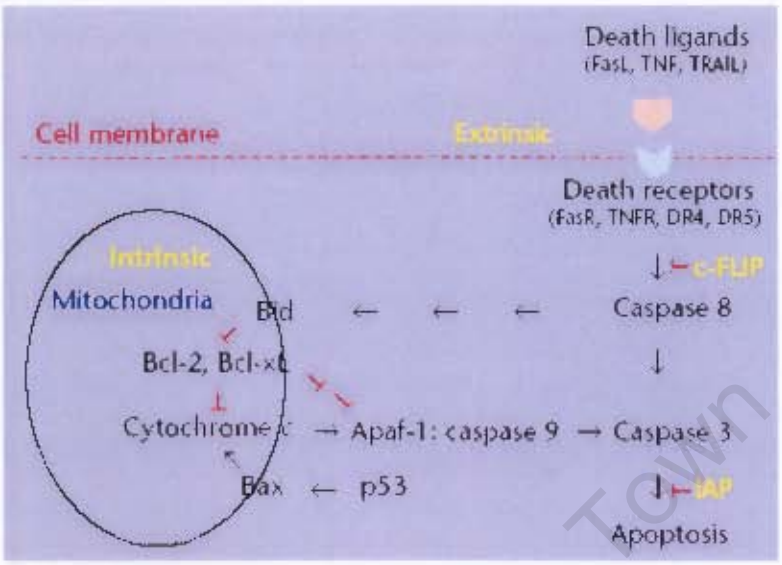

Figure 6: The mitochondrial and death-receptor pathway of apoptosis[56]

Two pathways are intimately connected, and sometimes the death receptor-mediated apoptotic stimulus is amplified by the mitochondrial loop. The death receptor is an extrinsic pathway and is triggered by extracellular cues such as growth factor withdrawal, matrix detachment and cytokine-mediated killing. It begins when a death-ligand such as tumor necrosis factor (TNF), Fas-ligand (FasL) or tumor necrosis factor-related apoptosis-inducing ligand (TRAIL or Apo2L) interacts with its corresponding receptor (TNF receptor, Fas receptor or KILLER/DR4 and DR5 respectively) leading to the activation of a caspase cascade pathway, which results in the cleavage of proteins that are essential to cell viability.[55] The mitochondrial cascade is the intrinsic pathway and might be triggered by intracellular cues such as DNA damage or osmotic stress. The first genetic component of the human cell-death pathway to be identified was the *B-cell CLL/lymphoma 2 (Bcl2)* gene. This pathway is mediated by Bcl-2 family proteins, which consist of 20 members that have been recognised and described in humans.[57] The relative ratios of anti- and pro-apoptotic Bcl-2 family proteins dictate the ultimate sensitivity or resistance of cells to various apoptotic stimuli, including growth factor depletion, hypoxia, radiation and anticancer drugs. In response to apoptotic signals, proapoptotic Bcl-2 family proteins such as Bax translocate and alter the permeability of the mitochondrial membrane, leading to cytochrome C release and activation of the caspase cascade. Anti-apoptotic Bcl-2 family members such as Bcl-2 and Bcl-xL counter these effects.[56] It was then concluded that the apoptotic activity of ajoene is via the mitochondrial pathway.

1.4.6 *In vivo* and *in vitro* studies on ajoene

Early reports on the anti-cancer activity of garlic oils in skin tumourgenesis were carried out by Belman in the early 1980's.[9] A detailed study of ajoene inducing apoptosis in a human promyeolocytic leukemia cell-line HL-60 was reported by Dirsch and coworkers at the Institute of Pharmacology, Toxicology, and Pharmacy in Munich Germany in 1998.[54] The aim of their study was to examine how ajoene is able to induce apoptosis in a human promyeolocytic leukemia cell-line HL-60.[54] This cell-line was chosen since it provides a valid model system for the testing of antileukemic or general antitumoral compounds (Suh *et al.* 1995). A human Promyeolocytic HL-60 cell-line was cultured in a humidified atmosphere (37 °C with 5% CO_2) in order to generate conditions similar to those in the human body.[54] The cell viability of cultured cells was confirmed by an MTT assay involving reduction of 3-(4,5-dimethylthiazol-2-yl)-2,5-diphenyltetrazolium bromide (MTT) to formazan. MTT is a yellow tetrazolium salt which turns to purple in the formation of formazan by metabolic active cells. This cellular mechanism involves the pyridine nucleofactors NADH and NADPH as shown in Scheme 5 below. Destruction of cells shuts off the reduction with retention of the yellow colour. Thus a chemical interference of cells can be followed colourimetrically.

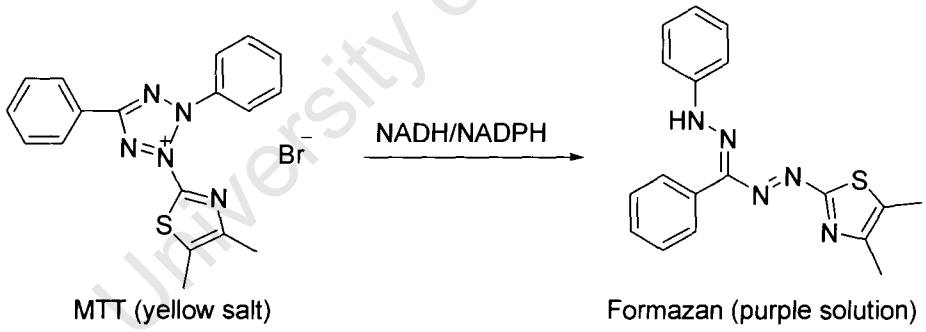

Scheme 5: Reduction of MTT to formazan by NADPH/NADH in active cells

The control of this study was human peripheral mononuclear blood cells of healthy volunteers. *E/Z* ajoene was disolved in less than 0.1% dimethyl sulfoxide and then added to cells in various concentrations (1-80 μM) for different time intervals. Apoptosis was examined by cell morphology, flow cytometry and DNA gel-electrophoresis. The results obtained from these experiments revealed that ajoene induces morphological changes that are characteristic of apoptosis in HL-60 cells. Flow cytometric analysis showed that ajoene-treated cancer cells had a higher side scattering than untreated cells in accordance with the different nucleus

consistency of apoptotic cells as shown in Figure 7. This means that the DNA of ajoene-treated cells fragments.

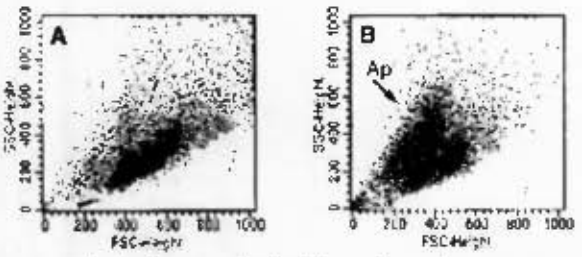

Figure 7: Flow cytometric analysis of apoptosis. **A**. Cell size (Forward scatter) and granuity (side scatter) analysis of untreated cells **B**. Forward and side scatter analysis of ajoene-treated (10μM, 20 hr) cells[54]

Condensation of chromatin and the appearance of apoptotic bodies were also observed. The DNA fluorescence histograms of P_1-stained cells confirmed DNA fragmention in ajoene-treated cells. This was shown by the low DNA stainability of the ajoene-treated cancer cells which resulted in a distinct quantifiable region below the G_1 peak, whereas in untreated cells the G_1 peak predominates as shown in Figure 8C.

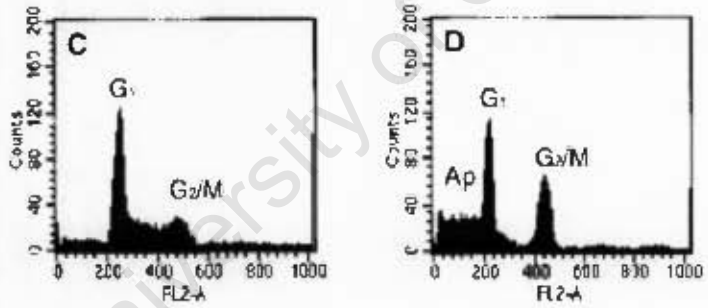

Figure 8: Histograms of P1-Fluorescence. **C**. Untreated HL-60 cells. **D**. Appearance of cells with subdiploid DNA content after treatment with ajoene[54]

In histogram 8D there was appearance of a subdiploid DNA content (Ap means apoptotic) after treatment with ajoene which indicates that apoptosis was taking place. Agarose gel electrophoresis also confirmed that there was a typical DNA fragmentation in ajoene-treated cancer cells (1-40 μm) as shown in Figure 9A.[54] The DNA of the control was intact, whereas that of ajoene-treated cancer cells was fragmented.

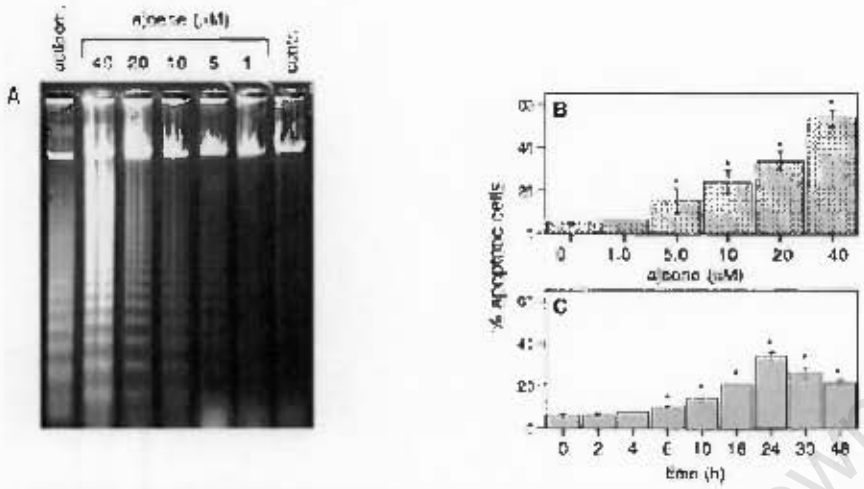

Figure 9: A. Demonstration of apoptosis by gel electrophoresis **B**. Dose-dependent induction of apoptosis of ajoene. C. Time dependency[54]

Quantification of dose dependency was established by monitoring the amount of nuclei with subdiploid DNA content by using flow cytometry. It was found that there was a time-dependent increase of subdiploid DNA, which is shown in Figures 9B and 9C. Ajoene in concentrations higher than 5 μm incubated for 20 h increased the percentage of apoptotic cells up to 60%. They concluded from this study that ajoene does induce apoptosis on a human leukemia cell-line HL-60.

Although Dirsch had proved that ajoene induces apoptosis on human leukemia cell- lines, the mechanism underlying apoptosis induction still needed to be elucidated. The second investigation carried out by Dirsch and coworkers and published in 2002 focused on understanding the mechanism underlying apoptosis induction.[55] Initially they investigated if the ajoene apoptotic activity was due to oxidative stress mediated by the generation of reactive oxygen species, such as peroxide. Previous studies had shown that an important mechanism by which compounds induce apoptosis is through generation of reactive oxygen species (Buttke and Sandstrom, 1994). Therefore, the production of reactive oxygen species was measured by flow cytometry as shown previously by Vollmar *et al* in 1997. Intracellular peroxide production was proved by measuring oxidation of the dye Dihydrorhodamine 123 (DHR-123) in HL-60 cells. DHR 123 is a non-fluorescent mitochondrial dye that is oxidised to the green fluorescent rhodamine 123 as shown below in Scheme 6.

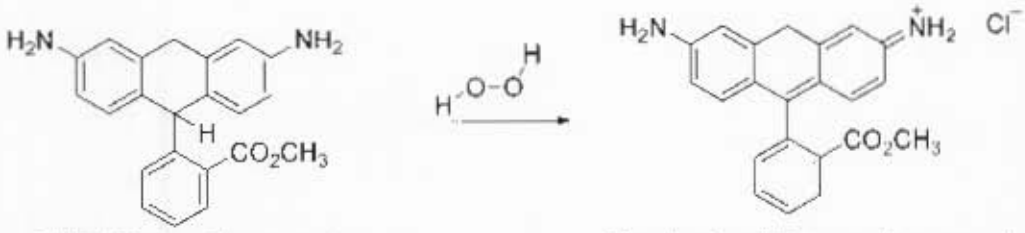

DHR-123 (non fluorescent) Rhodamine 123 (green fluorescent)

Scheme 6: Oxidation of DHR-123 to Rhodamine by peroxide

The results obtained revealed a time-dependent production of peroxides in ajoene-treated cells. This peroxide production was decreased by 50% when an antioxidant *N*-acetylcysteine (NAC) was added, Figure 10B. Previous studies carried out by Grimm *et al* 1996 had shown that the nuclear factor protein NF-κB that is known to induce oxidative stress is also involved in signalling of the apoptotic process. Dirsch and coworkers thus investigated the effect of ajoene in the activation of transcription factor NF- κB. An EMSA experiment (which is a technique used to characterize protein:DNA/RNA interactions) was conducted as previously explained in Boese et al 1996 and they revealed that ajoene (10 μM, 3 h) was able to activate the nuclear translocation of NF-κB.

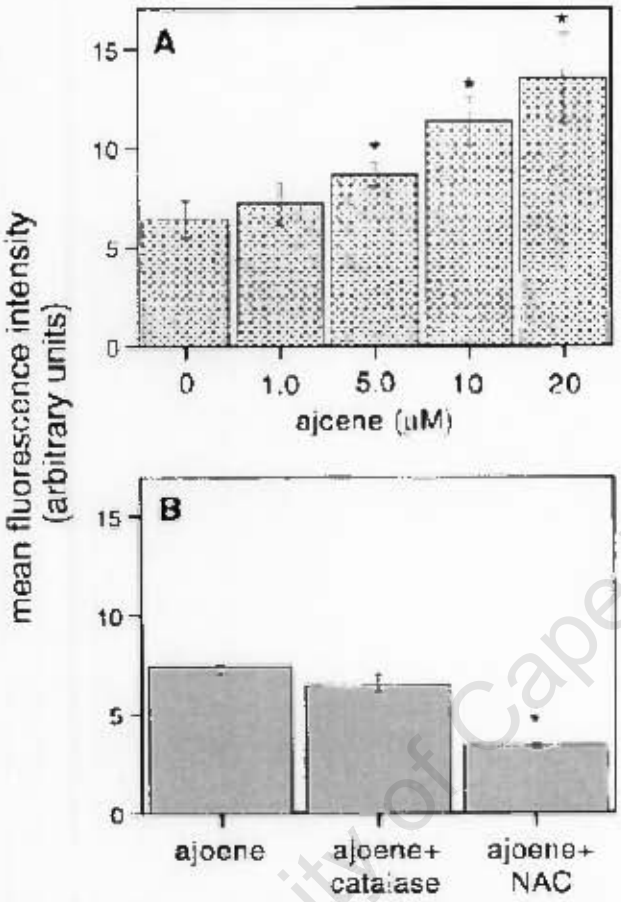

Figure 10: A. DHR 1,2,3-loaded HL-60 cells. **B**. Peroxide levels in three different environments[58]

Similarly, ajoene administered in peripheral mononuclear blood cells (PBMC) of a patient suffering from a chronic myeloid blast crisis with the percentage of myeloblasts (a precursor of leukocytes that normally occurs only in bone marrow) at 70%, confirmed that ajoene induces apoptosis even in chronic leukemia cells. In healthy cells, ajoene did not induce apoptosis in quiescent and proliferating PBMC, and it was found that there was no morphological or DNA fragmentation in these cells. These studies have thus demonstrated that ajoene induces apoptosis in a human acute myeloid leukemia cell-line HL-60 as well as in peripheral blood mononuclear cells (PBMC) isolated from a patient with a chronic myelogeneous leukemia undergoing a myeloid blast crisis but, importantly, not in healthy cells. In addition, ajoene-induced apoptosis in these cells is accompanied by the generation of reactive oxygen species and activation of nuclear factor κB.

Most of the attention on ajoene has been given to the natural product as a mixture of *Z*- and *E*-isomers. Little has been known about the biological activity of separate isomers. However, the

E/Z ajoene (50, 100, and 250 µg respectively) before TPA was applied. Experiments were then monitored over 18 weeks, calculating the percentage of mice bearing tumours and the mean number of tumours per mouse calculated as shown in Table 1 below.

Table 1: Inhibition percentage in different mouse groups[59]

Group	Treatment	Mean no of tumors	Inhibition percentage
1	TPA (positive control)	12.2±1.7	—
2	TPA + 50 µg ajoene	4.0±2.7	67.2
3	TPA + 100 µg ajoene	1.2±1.2	90.2
4	TPA + 250 µg ajoene	0.6±0.4	95.1

It was found that all 5 mice in group 1 bore tumours with a mean of more than 10 tumours per mouse. The results showed that as the percentage of ajoene used increased, the number of tumours decreased. These findings shows that ajoene offers strong protection against TPA-promoted carcinogenesis on the mouse skin, which proves an *in vivo* anti-cancer activity for ajoene.

Min Li of France and co-workers carried out both *in vivo* and *in vitro* studies on the antitumor activity of Z-ajoene in 2002.[60] The first experiment was focused on the effect of Z-ajoene on cell proliferation and cell distribution. Z-ajoene was extracted from a garlic extract using cyclohexane and purified to more than a 98% purity.[60] Seven human cell-lines, namely, breast cancer (MCF-7), nasopharyngeal carcinoma (KB), heptocellular carcinoma (Bel 7402), gastric carcinoma (BGC 823), colon carcinoma (HCT), Hela cells (Hela) and promyeololeukemia cells (HL60) were grown in a humidified environment (37° C; 5% CO_2). The control was a marsupial kidney cell-line (PTK2). Cells were then exposed to an increasing ajoene concentration (1-80 µM) for 48 h before addition of MTT. Plates were read at 570 nm using a Bio-Rad 3500 microplate reader. The concentrations of a compound required to reduce the absorbancy to 50% versus the control cells (IC_{50}), were determined from replicates using linear interpolation between data points.

Table 2: IC_{50} on different human cancer cell lines treated for 48 h[60]

Cell lines	IC_{50}
HL60	5.2
KB	15.8
Hela	17.9
Bel-7402	18.4
HCT	19.6
BGC-823	26.1

It was observed that *Z*-ajoene was the most biologically active in HL60 and the KB cell-lines as indicated by a low IC_{50}. These two cell-lines were then chosen with the control (PTK2) cell-line to determine the cytotoxic activity of *Z*-ajoene. A dose-dependent cytotoxic activity in HL60 and KB cell lines was observed, which is summarised in Figure 12.

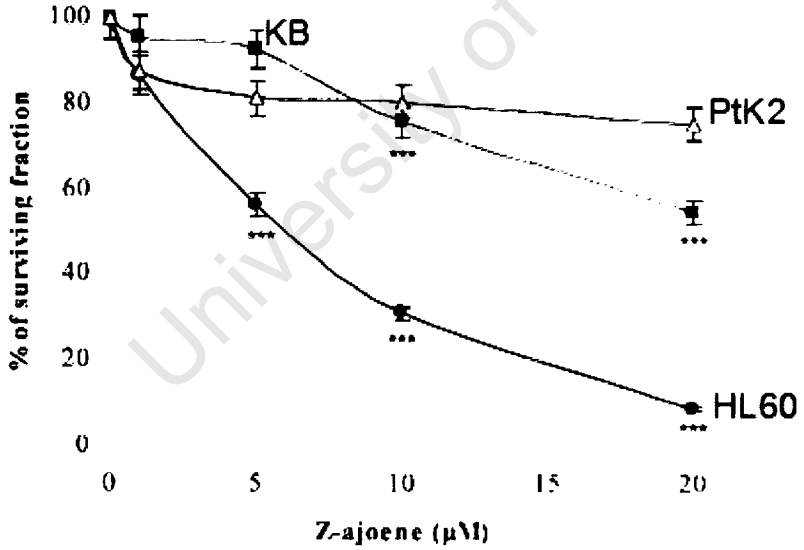

Figure 12: Effect of *Z*-ajoene on cytotoxity. Three cell lines (KB), (PtK2) and (HL60) respectively[60]

The control (PtK2) cell-line was resistant to the cytotoxic activity of ajoene while the KB and HL60 cell-lines showed the cytotoxic effect of ajoene. When the cellular DNA of the HL60 cells was analysed by flow cytometry, it was found that *Z*-ajoene had induced the accumulation of the G_2/M phase of the cell cycle. The G_2/M phase will be fully explained in the cell-cycle section.

study of Yoshida found that the *Z*-isomer exhibits an antimicrobial activity at least twofold higher that of the *E*-isomer.[32] Also, the *Z*-isomer has been previously found to inhibit cell growth and to induce apoptosis with unknown activity on tumour cells. Nishikawa and co-workers then did an *in vivo* investigation of the antitumor effects of *Z*-ajoene in a two-stage carcinogenesis test on a mouse skin.[59] The reason for their study was that they had observed the antimutagenic effects of ajoene against benzo[*a*]pyrene with *Salmonella typhimurium*. Benzo[*a*]pyrene is a potent chemical carcinogen, forming strong and selective adducts in DNA as shown in Figure below 11A.

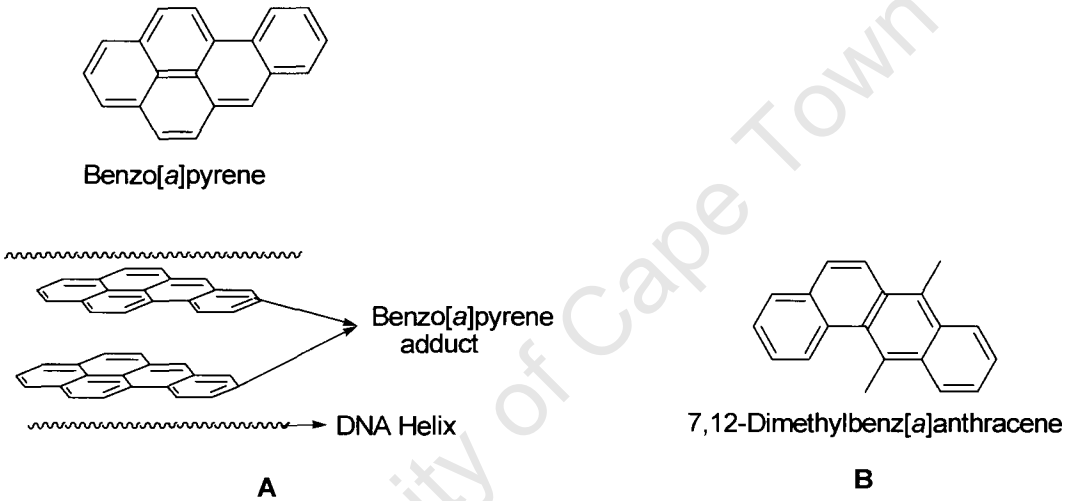

Figure 11: Formation of DNA adducts by pyrene.

Z-Ajoene of more than 98% purity was prepared by the method of Block.[26] Male mice of 7 weeks old, weighing 32-35 g were housed in plastic cages at 23-25 °C individually at a 50% humidity with a 12-h light-dark cycle. Each mouse was provided with water and standard laboratory feeding during the course of the experiment. They were then shaved and applied with 7,12,-Dimethylbenz[*a*]anthracene (DMBA) (50 µg, 190 nmol) as the carcinogenic initiator in acetone. The structure of DMBA resembles that of Benzo[a]pyrene as a polycyclic aromatic, in Figure 11. It thus also intercalates into DNA in the same way as Benzo[a]pyrene. After DMBA was added, a week was allowed to promote tumour growth by adding 12-O-tetradecanoylphorbol-13-acetate (TPA which propagates tumour growth) (1 µg, 1.6 nmol) in acetone in the same place. TPA is a phorbol ester and active component of croton oil. It mimics the second messenger diacylglycerol to activate protein kinase C (PKC) and alter cell signalling pathways (Reviewed in Gottlicher 1999). The mice were then divided into 4 groups of 5 mice each. Group 1, was selected as a control. The remaining groups 2, 3 and 4 were treated with

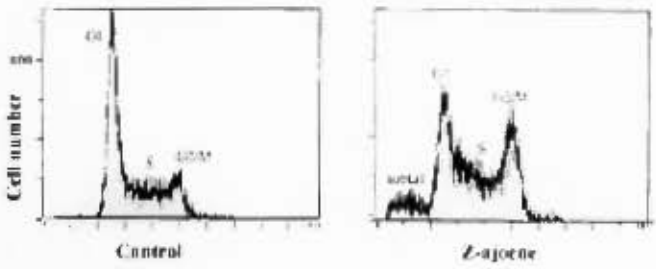

In the control, there is a high content of G1 cells, whereas exposure to 5-80 μM Z-ajoene increases the number of cells blocked in G_2/M phase. The increase of G_2/M phase cells can be explained by the increase of dead cells, which will be explained in the cell-cycle section. Since compounds with antitumour activity have been shown to interact with microtubule or tubulin in order to inhibit cell proliferation and block mitosis,[111] Li then decided to determine the effect of *Z*-ajoene on microtubule cytoskeleton. The PtK2 cell-line was chosen since they are extensive with thinly spreading microtubules. Cells were grown in a humidified environment and then treated with 1-20 μM of *Z*-ajoene for 6h. The cells were then permeabilized at room temperature with a 0.05% Triton solution. Triton (Octyl phenol ethoxylate $(C_{15}H_{26}O_2)_n$ is a non-ionic detergent that removes all cytoplasmic membrane contamination but does not change the cell morphology. After washing with triton, cells were incubated with a mouse monoclonal antibody α-tubulin. A secondary antibody FITC conjugate) which is essential for detecting or analyzing target proteins bound by the primary antibody was also used in this ELISA study. Chromosomes were stained with DAPI (0.2 μg/ml). The control was injected with the antibodies only, and not treated with ajoene. The intensity of the fluorescent (green) network was quantified by the FLUOSTar Galaxy. The results showed a dose-dependent reduction of microtubules in *Z*-ajoene treated cells as shown in Figure 13.

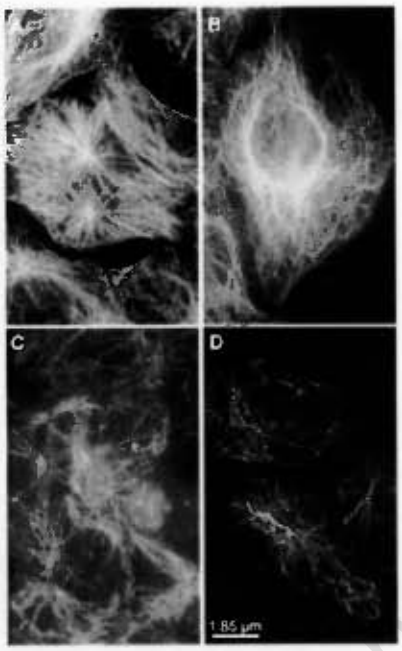

Figure 13: Demonstration of microtubule disassembly[60]

The microtubule cytoskeleton of the control (Figure 13 A) appeared to be intact, whereas that of *Z*-ajoene treated cells (Figures 13 B, C and D) was dose-dependently reduced. This agrees with Nishikawa's findings on the *in vivo* activity of ajoene.[59]

In vitro studies were also conducted on Kunming mice 4-6 weeks old. Kunming mice are the most widely used outbred colony in China. Two transplanted tumors, hepatocarcinoma 22 (H22) and sarcoma 180 (S180) were implanted. In each model, tumour cells were induced in 30 mice by subcutaneous injection of 0.2 ml Phosphate buffer solution (pH 7.4) containing 5 x 10^6 tumor cells, on the right flank at day one. The animals were divided into three groups (10 mice) two for testing and one as a control. On day two, the experimental group injected with hepatocarcinoma 22 received 2 and 4 mg/kg of the *Z*-ajoene every day intraperitoneously. The experimental group injected with sarcoma 180 cells received 4 and 8 mg/kg ajoene under the same conditions. Twelve days later the mice were killed, tumours were weighed and the inhibition rate was calculated in comparison with the control. The results showed that inhibition rates for S180 implanted mice were 10 and 32% while for the H22 transplanted mice, the inhibition rate was 32 and 42%. There was a 0% inhibition rate for the control.

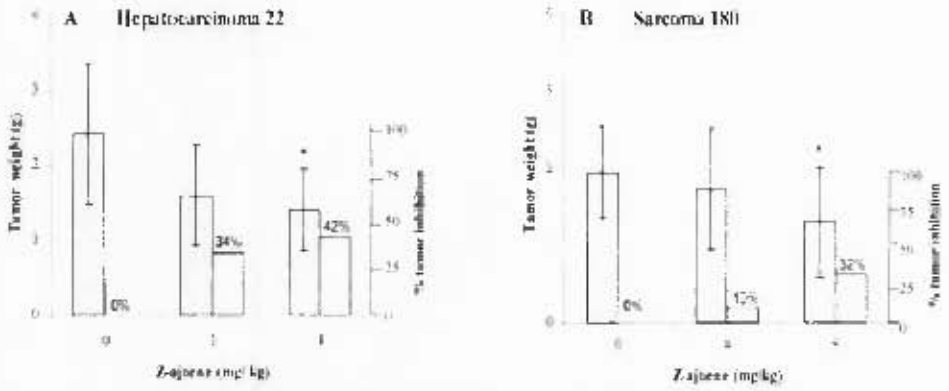

Figure 14: Effect of Z-ajoene in transplanted tumor growth[60]

In conclusion, Li and co-workers successively demonstrated the antitumor activity of Z-ajoene both *in vivo* (on microtubules) and *in vitro* (on mice).

Ajoene has been shown to induce apoptosis in both *in vivo* and *in vitro* in the above discussed studies. However, the mechanism of action of ajoene was not known prior to 2002, when Dirsch and co-workers published the first insight into the molecular events leading to ajoene-triggered apoptosis. The first study was to identify the molecular pathway leading to ajoene-triggered apoptosis in leukemia cells. Two major pathways mediating drug-induced apoptosis have been characterized.[53] One involves the triggering of cell-surface death receptors and the other targets the mitochondria without the involvement of a receptor/ligand system. The cell-surface mediated pathway occurs when a death ligand interacts with the receptor leading to the activation of a caspase cascade, which involves proteins that are essential to cell viability and is further explained in the apoptosis section. The receptor that is involved in apoptosis evoked by chemotherapeutic drugs is the CD95 (APO-1/Fas) receptor system.[63-65] Activation of the CD95 receptor by a death CD95 ligand leads to recruitment of FADD [Fas-associated protein with death domain] and procaspase 8 forming a death-induced signalling complex.[54] Depending on the cell type, large amounts of procaspase leads to the activation of a caspase cascade independent of the mitochondria (type I cells), while small amounts leads to a pathway amplified by the mitochondria-controlled caspase cascade (type II cells).[56] The second pathway occurs in the absence of a CD-95 receptor ligand system.[56] This event is characterised by a mitochondrial membrane permeabilisation which causes loss of the mitochondrial transmembrane potential with the release of cychrome C into the cytosol. This is because the proteins (Bcl-2) that serves as the mitochondrial gateway have lost their activity/function. The first experiment was done to investigate whether ajoene-induced apoptosis is dependent on the activation of caspases. A

human acute myeloid leukemia cells line HL-60 was cultured in a humidified environment, and cells were stimulated with ajoene (20 µM) or Etoposide (10 µg/ml) for different periods of time (0-22 h). Etoposide is a chemotherapeutic drug that is given as a treatment to some types of cancer. Cells were then collected by centrifugation, washed with ice- cold PBS and lysed in 5mM $MgCl_2$; lysates were then stored at -70°C until further analysis. The results showed a time-dependency activity of ajoene that was more detectable after 5 h as shown in Figure 15.

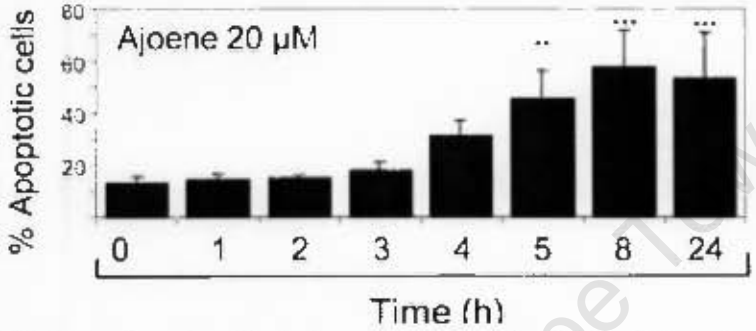

Figure 15: Time-dependent induction of apoptosis in HL-60 cells by ajoene (20 µM)[53]

The activity of caspase was investigated by cleavage of PARP (a nuclear protein involved in DNA repairing, and cleaved by caspase) using western blotting. Results in Figure 16 show a time-dependent activation of caspase-3-like protease.

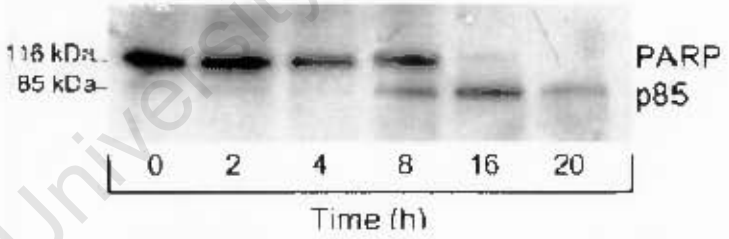

Figure 16: Time-dependent cleavage of PARP[53]

Treatment of HL-60 cells with ajoene (1-24 h) resulted in proteolytic cleavage of caspase-3 to the active p17 subunit as shown in Figure 17A. Caspase 8 is naturally expressed as an inactive precursor in two isoforms, caspase 8a and caspase 8b, which appear as two protein bands of 55 and 53 kDa. When caspase 8 is activated, it cleaves to p43 and p41 as shown in the Figure 17B below.

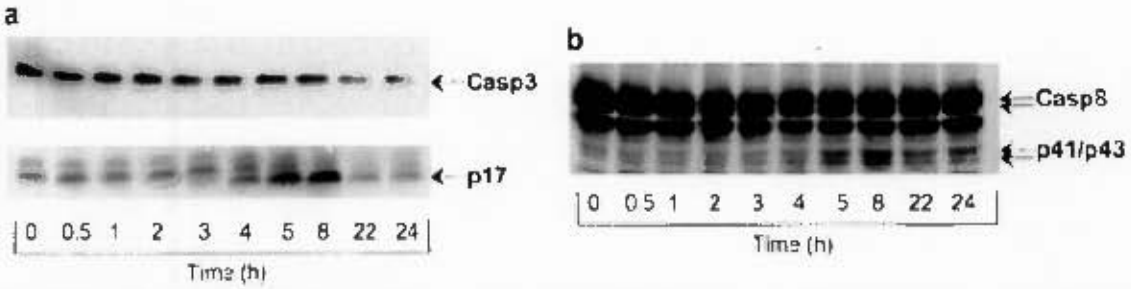

Figure 17: a. Representative of immunoblots showing the time-dependent cleavage of caspase-3 to the active p17 subunit. **b.** Time-dependent cleavage of PARP[53]

Recruitment of both caspase 3 and caspase 8 proves that Ajoene induces apoptosis through the caspase cascade pathway, what was not known was whether this was mitochondrial-mediated or CD-95 receptor mediated. Experiments were conducted to analyse if ajoene-induced apoptosis occurs independently of the CD-95 receptor system. Cells were incubated at 4 °C for 30 min with mouse anti-CD95-body or the isotype control mouse IgG-. CD-95 antibody fluoresces red while the IgG_1 antibody fluoresces green. Cells were then analysed by flow immunofluorescent flow cytometry. It was observed that ajoene-induced apoptosis was independent of a functional CD95 receptor as shown in Figure 18.

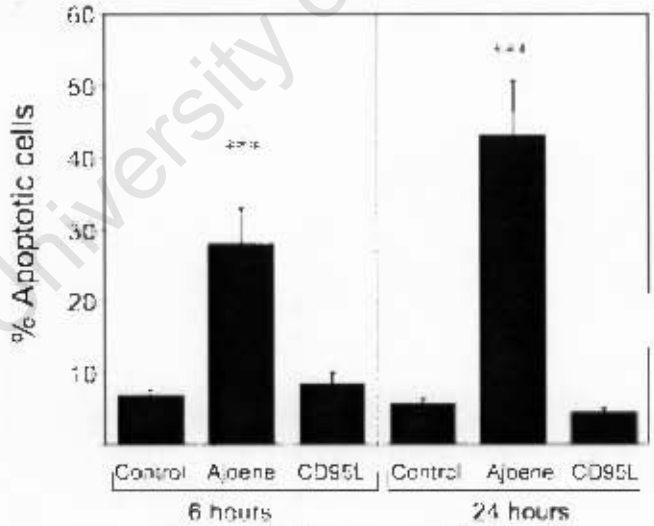

Figure 18: Ajoenes apoptotic effect[53]

Even on addition of the caspase-8 inhibitor ZITD-FMK, this event could not be blocked as shown in Figure 19 below.

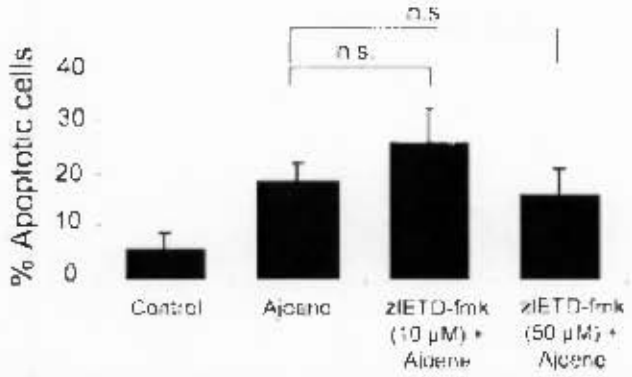

Figure 19: The caspase inhibitor zIETD-fmk unable to abrogate ajoene-induced DNA fragmentation[53]

This study established that ajoene induced apoptosis in a HL60 cell line is not CD95 receptor-mediated. The last experiment was to investigate if this activity is mitochondria mediated. This was done by investigating the selective ability of the mitochondria membrane. HL-60 leukemia cells were treated with ajoene (20 µM) for various time periods (0-24 h) and stained with fluorochrome 5, 5', 6-6' tetrachloro-1,1', 3, 3'-tetraethylbenzamidozol carbocyanine iodide (JC-1; 1.25 µM). JC-1 was used for fluorescence purposes as it fluoresces red. After incubation at 37 °C for 20 min in the dark, the membrane potential was measured by flow cytometry. The mitochondrial membrane permeabilization (MMP) affecting the outer and inner membrane is the key event in mitochondria-controlled cell death.[56] The outer membrane permeabilization involves the release of cytochrome C which is confined to the intermembrane space. The inner membrane permeabilization is then indicated by dissipation of an electrochemical gradient ($\Delta\psi_m$) created by the proteins of the respiratory chain located on the inner mitochochondrial membrane. A time-dependent release of cytochrome C into the cytosol upon addition of ajoene (20 µM) was observed as shown in Figure 20. A significantly increased level of cytochrome C in the cytosol was detectable as early as 4 h which proves that the outer membrane was no longer selective.

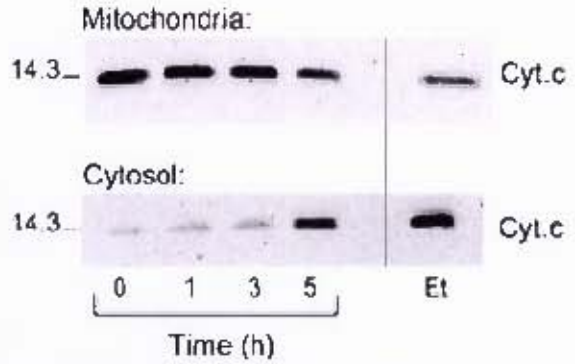

Figure 20: A decrease in mitochondria cytochrome C, followed by an increase of cytochrome C in the cytosol[63]

The selectivity of the inner membrane was assessed indirectly by determining a reduction in ($\Delta\psi_m$). This was achieved by incubating cells with fluorochrome JC-1, which forms aggregates (red) or monomers (green) depending on ($\Delta\psi_m$). Untreated cells loaded with JC-1 displayed red fluorescing mitochondria, referring to intact $\Delta\psi_m$. Cells treated with ajoene exhibited green fluorescing cells corresponding to JC-1 monomer formation and loss of $\Delta\psi_m$ as shown in Figure 21.

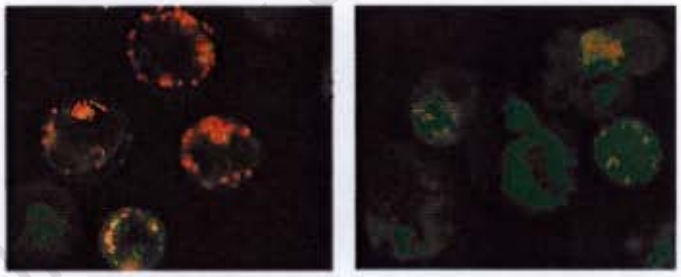

Figure 21: Red fluorescing untreated cells and green fluorescing ajoene treated cells[63]

This shows that the inner membrane was also no longer selective. These studies proved that both inner and outer mitochondria membrane were no longer selective in HL60 ajoene-treated cells. Proteins that guard the mitochondriol gate making it selective belong to the Bcl-2 family.[56] Overexpression of these proteins can block cytochrome C release and thereby the activation of caspases downstream of mitochondria.[56] Dirsch and coworkers observed that ajoene-treated cells showed a low redistribution of cytochrome C and therefore they then investigated whether this was due to the activation occurring downstream of the mitochondria. Two types of cell environments were prepared. The first cell-line prepared involved HL-60 neo cells while the

second one was the HL-60 one that overexpressed Bcl-xL proteins. In HL-60/Bcl-xL cells, ajoene's apoptotic activity was significantly reduced as shown in Figure 22 below.

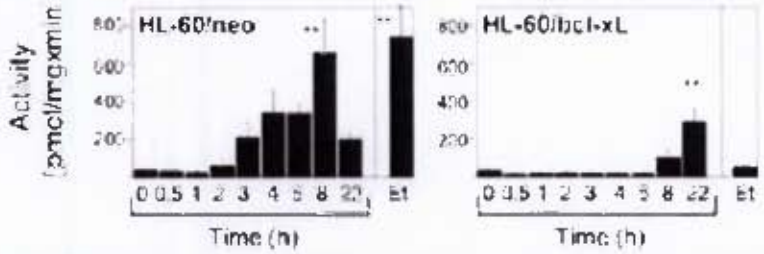

Figure 22: Red fluorescing untreated cells and green fluorescing ajoene treated cells[53]

The cells overexpressed with Bcl-xL did activate caspase-3 and caspase 8 but the rate was significantly lower. In normal leukemia cells it took 3 h to activate caspase 3 to its active subunit p17, while in cells overexpressing Bcl-xL proteins it took 24 h as shown in Figure 22.

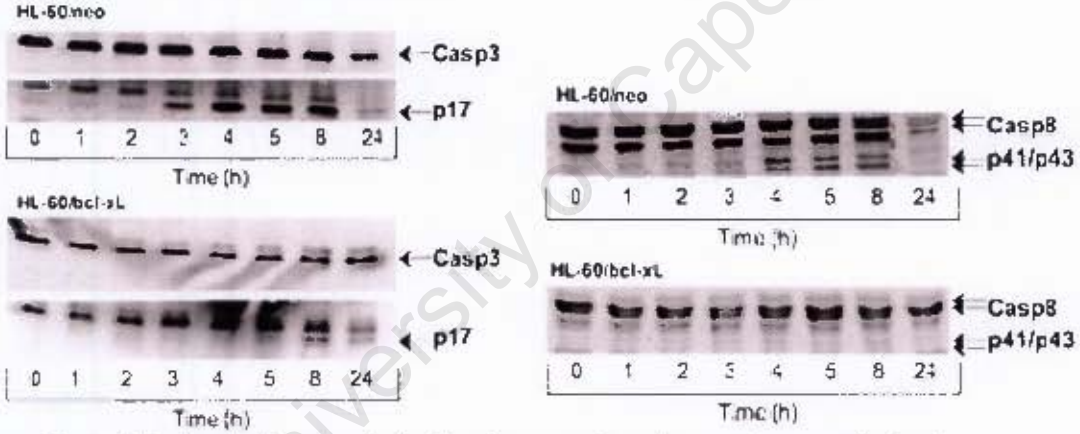

Figure 23: showing the rate of activation of caspase 3 and caspase in normal leukemia cells and leukemia cells overexpressed with Bcl-xL[53]

Caspase 8 was also activated to its p41/p43 active intermediates. From these experiments they concluded that ajoene-treated leukemia cells undergo a time-depenendent reduction in the anti-apoptotic Bcl-2 proteins that promote the release of cytochrome C and the activation of caspase 3. The results provided compelling evidence that ajoene-induced apoptosis in leukemia cells proceeds via a mitochondria-dependent caspase cascade pathway rather than triggering the cell-surface death receptors.

1. 5 Detailed Mechanism of action of Ajoene in human Glutathione Reductase

Ajoene contains a disulphide functional group, which is likely to be involved in its biological activity. Ajoene also contains a sulphoxide and a vinyl group that is conjugated to one of the sulfur atoms of the disulphide rendering it more reactive. Disulphides are considered to be thiol oxidizing agents, as they are able to thiolate cysteine residues on proteins to form mixed disulphides, thereby affecting protein or enzyme activity which leads to cell-death. As previously mentioned, ajoene has been shown to inhibit a number of thiol-containing enzymes such as gastric lipase, glutathione reductase and trypanothione but mechanistic studies have been rare. One exception involves a study of the mechanism of ajoene in inhibiting glutathione reductase. Glutathione reductase (GR) is the enzyme used by human cells to combat oxidative stress, and is a member of the family of disulphide reductases. This family of proteins contain a FAD-redox enzyme that interacts with disulphide substrates. The function of glutathione reductase is to keep the cellular concentration of the reduced form of glutathione (GSH) high and that of its oxidized form (GSSG) low for the body's biological functioning. The glutathione reductase enzyme (E) uses NADPH as a source of its reduction equivalents as in the reaction below.[66]

$$H^{+} + NADPH + E \rightarrow NADP^{+} + EH_2$$

$$EH_2 + GSSG \rightarrow 2GSH + E$$

As shown in the reaction above, GR occurs in two stable forms, E (oxidized) and EH_2 (reduced). The first part in the reaction above is the reduction of the enzyme to its reduced form EH_2. In the oxidized form, the enzyme consists of two subunits which are related to each other by a 2-fold axis and covalently bonded by a single disulphide bond as shown in the Figure 24 below.

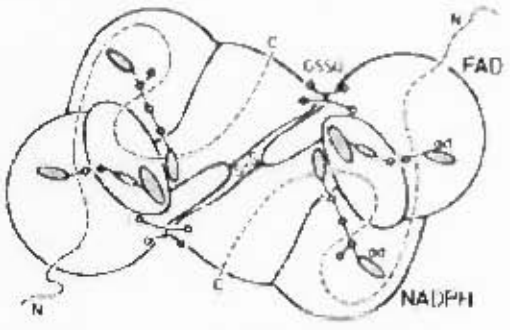

Figure 24: Structure of the dimeric enzyme glutathione reductase as viewed along the molecular 2-fold axis.[66]

The enzyme is divided into four domains, of which the first two domains resemble each other and these bind FAD and NADPH respectively. The N terminal is in close proximity to the FAD without any defined structure in the crystal, whereas the central and interface domain follow on the C-terminal side. The catalytic centre is therefore made up of five different domains, four domains from one subunit and the interface domain of the other subunit. The arm consists of Cys 2 that could possibly reach Cys 58 of the redoxactive disulfide bridge. The catalytic centre can be divided into two parts, the one that binds NADPH and the other binding GSSG. These two parts are separated by a flavin and the redoxactive Cys-58:Cys-63 disulphide bridge as shown in Figure 25 below.

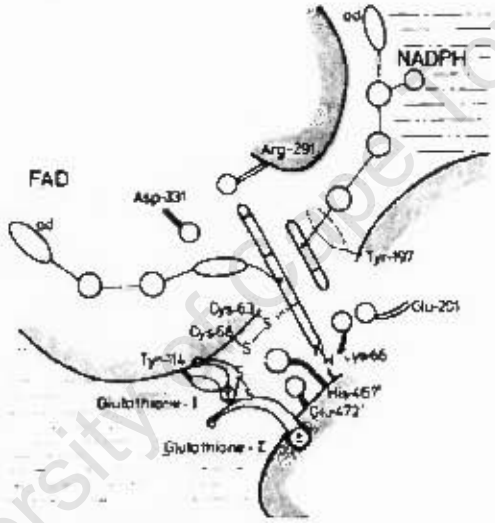

Figure 25: The catalytic centre of glutathione reductase.[66]

The two dinucleotides FAD and NADPH bind in elongated conformation to the protein. The nicotinamide part of the NADPH is in close contact with the flavin part of FAD, while the adenosine moieties of NADPH and FAD are far apart from each other. In the NADPH binding pocket, there is Tyr-197 which covers the nicotinamide binding pocket in the absence of NADPH thereby shielding the flavin against the solvent. When NADPH binds to the protein the phenol (Tyr 197) moves away from the binding pocket allowing the nicotinamide to reach the flavin. Between the flavin and GSSG substrate there is a Cys-58:Cys-63 disulphide bridge. This disulphide bridge contacts the flavin ring near to its C_{11} atoms. On binding of GSSG, Tyr 114 moves by about 0.1 nm. Its phenol ring then fits between the glycine moieties and glutathiones I and II with the hydroxyl group contacting the disulphide bridge of GSSG. In the reduced form of the enzyme the disulphide bridge Cys-58:Cys-63 opens up and the sulphur of Cys58 becomes reduced. The four states of the catalytic reaction cycle of glutathione reductase are summarised by the following, Scheme 7.

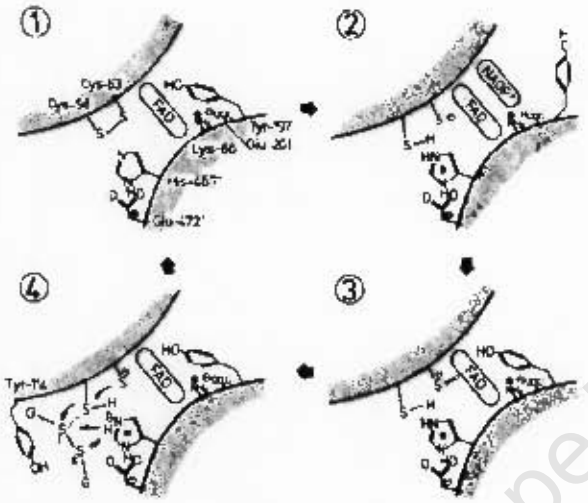

Scheme 7: Four states of the catalytic reaction cycle of glutathione reductase. State **1** is the oxidized enzyme E. State **2** is the complex between $NADP^+$ and the reduced enzyme EH_2. State **3** is the reduced enzyme EH_2, a stable reaction intermediate. State **4** is a combination of the three catalytic steps[60]

It is a big advantage when GSSG is present in high levels and GSH in lower levels in cancer cells as this decreases cell division. A crystallographic study that confirms an increase in the oxidase activity of glutathione reductase upon addition of ajoene was conducted by Helge Gallwitz. Glutathione reductase was incubated with *E*-ajoene in the presence of NADPH at 37°C. The results showed a 50% inhibition within 15 min. No inhibition of GR was observed in the absence of NADPH, which indicated the involvement of NADPH in the active site of the enzyme. The activity of the enzyme was not regained upon addition of the substrate (glutathione) but 70% of its activity could be regained by addition of dithiotreitol. This confirms that ajoene is a competitive inhibitor of glutathione reductase. It was observed that ajoene-modified GR showed a marked increase in oxidase activity. Substrate-independent oxidation of NADPH increases by a factor of about 5 in the ajoene-inactivated enzyme and the rate of cytochrome C reduction is 10-fold higher when compared to the native enzyme. Modification of Cys58 is expected to shift electron density towards the flavin ring and thus to promote the reduction of oxygen at the isoalloxazine ring. This was confirmed by a decrease and a slight hypsochromic shift of $\gamma_{max,vis}$ of flavin spectrum and a concomitant absorbance increase. This is due to the charge-transfer complex formed between Cys63 and the flavin in the reduced enzyme species and is the strong evidence for Cys 58 being the altered protein residue as previously explained. Structural data from X-ray diffraction analysis of ajoene-modified GR

showed the mechanism by which ajoene inhibits glutathione reductase which involves covalent binding to Cys58 to form the modified protein CH_2=CH-CH_2-SO-CH_2-CH=CH-S-Cys58 glutathione reductase.[67] This moiety then does not allow the reduction of GSSG.

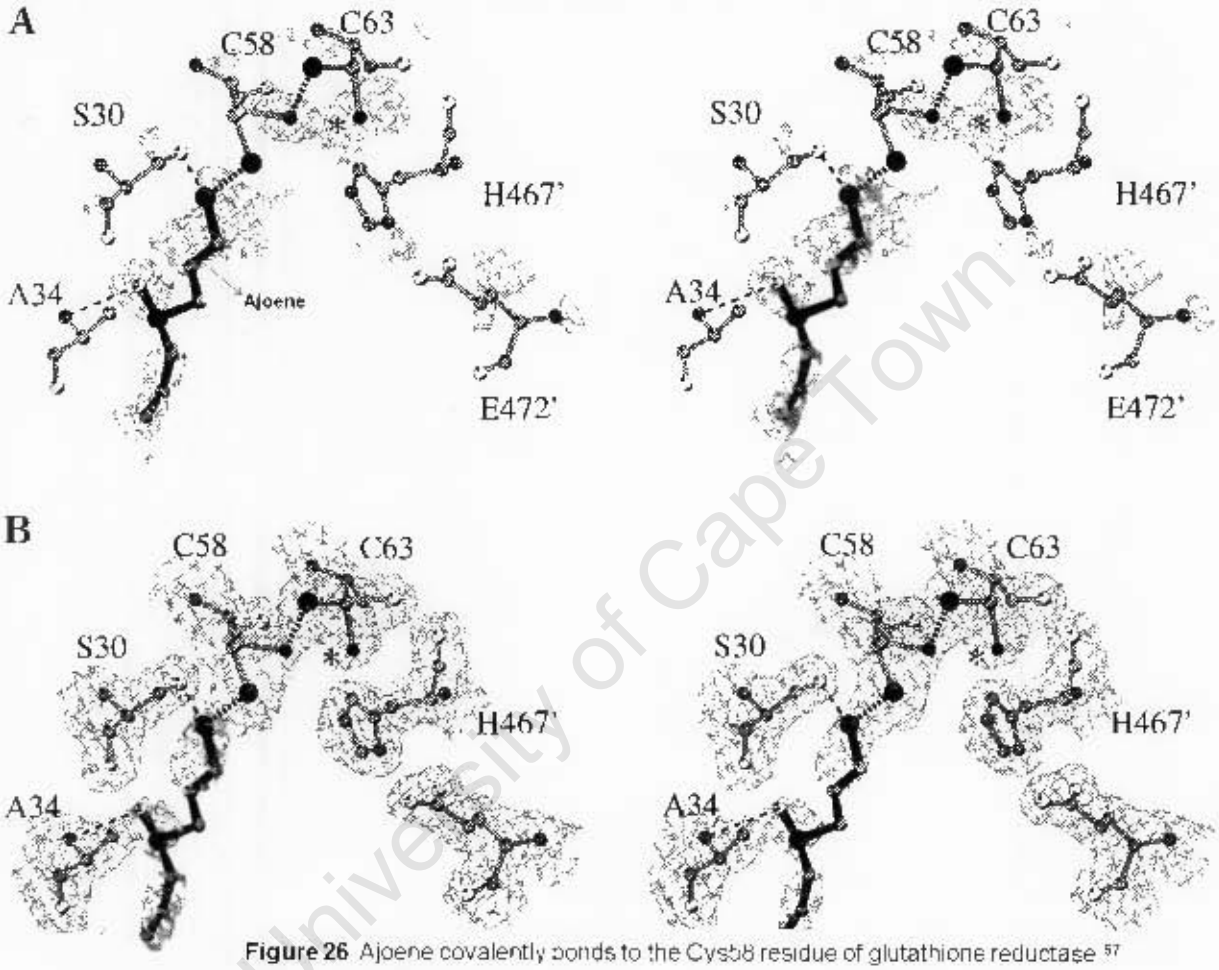

Figure 26 Ajoene covalently bonds to the Cys58 residue of glutathione reductase [57]

Figure 26 show the protein crystal structure co-ordinates of the ajoene-modified Cys58 and Cys63 in their main conformation. The inhibitor fragment (bold lines) is covalently bound to Cys 58 via a disulphide bridge. This type of inhibitor is called a 'turncoat inhibitor' or 'subversive substrate' as it has a strong impact on the redox status of the cell. It lowers the GSH/GSSG by wasting NADPH to produce unharmful oxygen species in cancer cells. The reaction below summarises the reduction of ajoene by GR to produce reduced reactive species.

Chapter 2: Review of synthetic aspects of ajoene

At the beginning of this research, the only published synthesis of ajoene was Block's biomimetic thermal rearrangement of allicin in aqueous acetone.[28] This chapter will present and discuss Block's method in detail, its advantages and disadvantages, potential synthetic strategies for the synthesis of ajoene derivatives and finally the main objectives of this project.

2.1 Block's Biomimetic Synthesis

Block's method is based on the biomimetic rearrangement of allicin as it occurs in nature. In the laboratory, this is achieved by heating allicin in aqueous acetone. Allicin **1,** obtained by peracetic acid mono-oxidation of diallyl disulfide, self-condenses to an intermediate **3** that undergoes a Cope-type elimination to S-allyl vinylthionium ion **4**. This re-adds 2-propenesulfenic **2** acid to give (*E/Z)* ajoene as shown in Scheme.

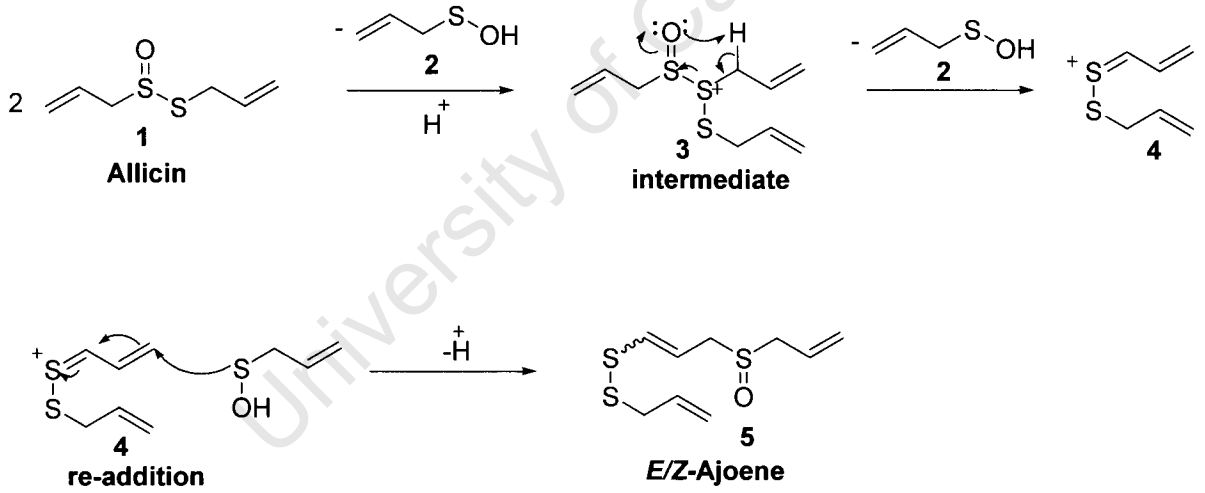

Scheme 8: Thermal rearrangement of allicin **1**[28]

Block reported that flash chromatography of the concentrate of the crude product gave 17% of a mixture of *E/Z*-isomers in a 4:1 molar ratio.[28] The readily available ajoene **5** allowed an *in vivo* study of antithrombotic activity on rabbits to be carried out. Rabbits were each fed 20 mg/kg of (*E/Z*-ajoene) and the results showed a 100% inhibition of collagen-induced platelet aggregation for a period of 24 h after feeding. These findings prompted scientists to explore methods of modifying ajoene for biological evaluation.

2.2 Disadvantages of Block's synthesis

The percentage yield of ajoene using Block's methods is very low (17% = 1.6 g product from 5 kg of garlic bulbs) with the *E*-isomer dominating the *Z*-isomer in a 4:1 ratio.[28] A low percentage yield of the *Z*-isomer is a disadvantage in Block's method, since Yoshida's studies have demonstrated that the *Z*-isomer exhibits at least a two-fold higher antimicrobial activity than its *E*-isomer.[32] A new synthetic strategy that would increase the percentage yield of ajoene with the *Z*-isomer dominating was thus in demand. The literature indicates that the disulfide group is a key motif in chemistry, biology, pharmaceutical and material science.[75-81] Thus, it would be of great advantage if a new synthetic approach could be developed that retains the pharmacophore (vinyl disulfide group) and the sulfoxide group while varying the allyl end groups for generating analogues for biological evaluation. Regarding the scope of Block's synthesis, the sulfenyl allyl group is essential for the rearrangement. Thus, only the group on the sulfoxide side can be varied. This places a serious limitation on Block's method for preparing analogues as the latter can only be obtained varying the one group (R_1) as shown in Figure 27.

Figure 27: Rearrangement of modified allicin

2.3 Potential Synthetic Strategies for Ajoene Synthesis

2.3.1 Introduction

Various synthetic disconnections may be considered for possibly accessing the ajoene derivative target **6** shown in Figure 28 varying both end-groups.

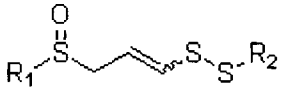

6

Figure 28: General structure of target ajoene

These are discussed separately as cross-coupling, β-hydrogen elimination and radical addition approaches.

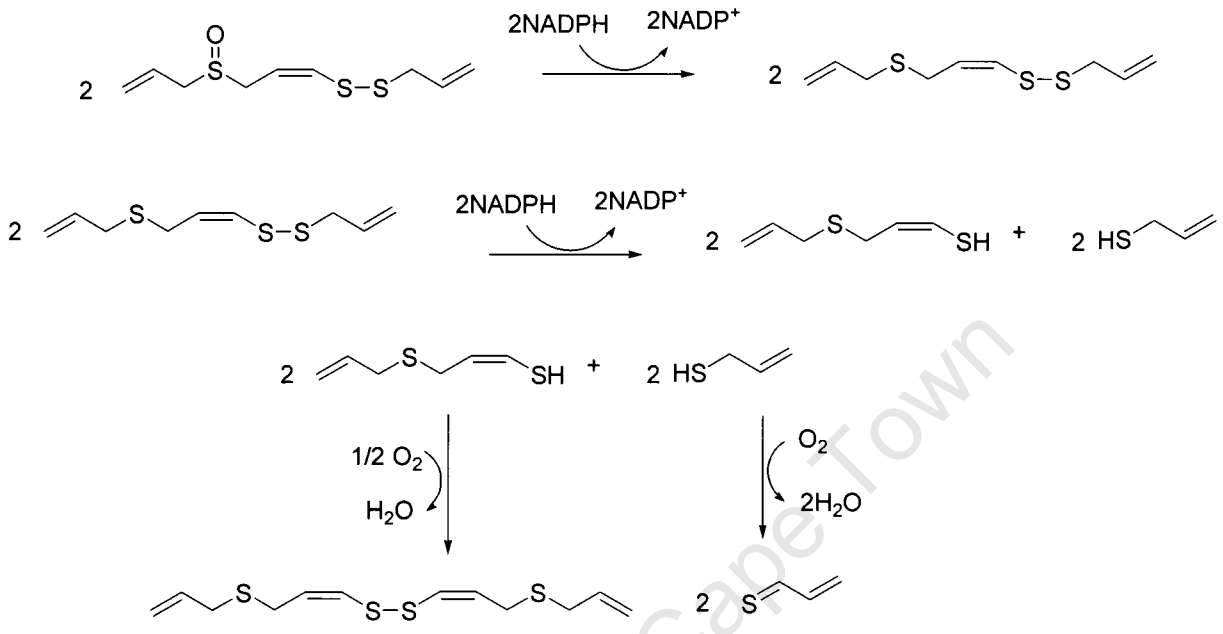

In conclusion, the evidence from this study provides important information on the mechanism by which ajoene inhibits glutathione reductase.

1.6 Summary

In summary, the therapeutic benefits of garlic date back to over 5000 years. These include anti-fungal and prevention of cancer activitites. Modern organic chemistry has played a major role in showing that the compound responsible for biological activity in a garlic clove is a thiosulfinate called allicin. Allicin's instability causes it to rearrange to a stable compound called ajoene. Ajoene posses a variety of biological activities and this chapter has focused more on its apoptotic and anti-cancer activities as they are relevant to this thesis. It has been shown that ajoene induce apoptosis both *in vivo* and *in vitro.* It induced Human Leukaemia Cell-Line (HL-60) and it also offered strong protection against TPA-promoted carcinogenesis of mouse skin. The biological activity of ajoene has been shown to be accompanied by a generation of reactive oxygen species and activation of nuclear factor κB. This prompted scientists to investigate and analyse the biological mechanism of ajoene. It was found that ajoene interferes with glutathione reductase (the enzyme used by humans to combat oxidative stress) and produce reactive oxygen species in cancer cells. In addition it was also found that the apoptotic activity of ajoene is via the mitochondrial-mediated pathway.

2.3.1 Cross-coupling approach

The stereocontrolled synthesis of olefins is of much interest in the synthesis of ajoene as it offers a synthetic method that might access the two *Z*/*E*-ajoene isomers independently. Cross-coupling reactions offer a stereospecific synthesis of alkenes involving the use of a catalyst in the form of Ni(0), Pd (0), Cu(I) or Fe(II), with the most common one involving Pd(0).[68-73] Three major steps are involved in a cross-coupling reaction as oxidative addition, transmetallation and reductive elimination,[74] which are shown in Figure 29 using one of the most common catalysts, $Pd(PPh_3)_4$.

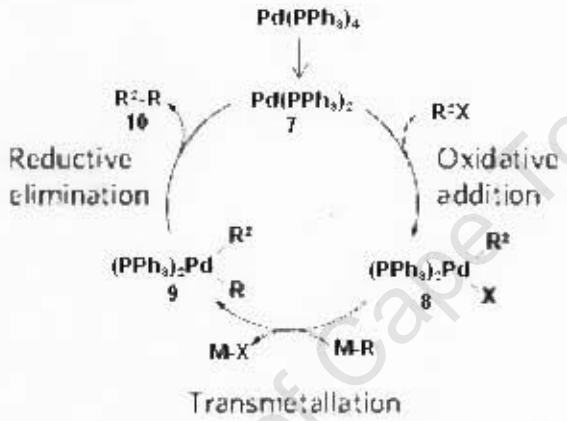

Figure 29: Cross-coupling catalytic cycle using Pd(0)[74]

During the cycle, $Pd(PPh_3)_4$ loses two ligands to form a coordinatively unsaturated form, $Pd(PPh_3)_2$ **7**, which undergoes oxidative addition with the aryl, alkenyl, allyl or benzyl halide R^2X to form complex **8**. This is followed by a transmetallation step with RM in which the R (aryl, alkenyl or some alkyl) group is transferred to the metal catalyst (Pd) centre to form **9**. Different metals M have given rise to different named reactions. Thus, with M = R_3Sn as a stannane the coupling is called a Stille coupling, as a boronic acid ($B(OH)_2$) a Suzuki coupling, and if the metal is ZnX a Negishi coupling. Finally, reductive elimination results in the cross-coupled product **10** with regeneration of $Pd(PPh_3)_2$ for further catalysis. Variations on this general mechanism are in abundant supply in the literature in which both metal and catalyst (via the ligands and oxidation state of the palladium) can be widely varied. Oxidative addition proceeds with retention of stereochemistry with vinyl halides but with inversion of stereochemistry with allylic and benzylic halides.[66,67] The reaction has been extended from C-C bond formation to accommodate C-Het bond formation where Het = N, O or S in order to cover the common heteroatom bonds to carbon. Through the work of Buchwald, Hartwig and others a major advance has been to be able to cross-couple amines, thiols and alcohols directly with aryl and vinyl compounds bearing a leaving group by using more reactive phosphine ligands.[32] This avoids using a Het-M component making the reaction cleaner. An

example is shown in Figure 30 for C-N bond formation, in which the catalytic steps follow the same course as with C-C bond formation.[74]

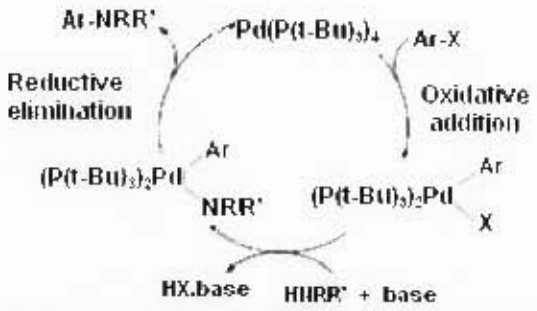

Figure 30 : shows a use of a more reactive catalyst $Pd(P(t\text{-}Bu)_3)_4$.[82]

which allows a cross coupling of an amine directly. Regarding ajoene, the relevant reaction would be a cross-coupling involving a vinyl halide to generate a vinyl sulfide, and recently there has been much interest in developing copper-catalyzed cross-coupling reactions for this purpose, since copper-catalyzed methods are mild, they tolerate a variety of functional groups or substrates and they work extremely well with soft nucleophiles such as sulfur. Venkataraman[83] and co-workers reported a general stereospecific copper-based standard protocol in 2004 for the cross-coupling of vinyl iodides and thiols to form vinyl sulfides, Scheme 9.[53] This protocol involves the use of $[Cu(phen)(PPh_3)_2]NO_3$ as a catalyst and 1.5 equiv K_3PO_4 as a base in toluene at reflux.

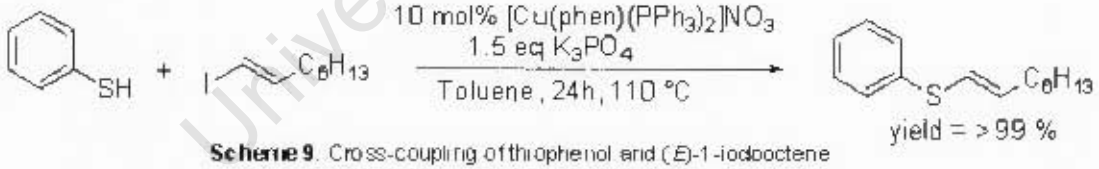

Scheme 9. Cross-coupling of thiophenol and (*E*)-1-iodooctene

Both electron-rich and electron-poor thiols were easily tolerated by this method. This method was also found to be selective for sulfur over oxygen and does not need air-sensitive additives. Although this protocol was a success, there were some disadvantages such as the need to use an air- and moisture-sensitive copper catalyst, which must be used in the glovebox and at a high catalytic load of 10 mol%. It requires the use of harsh conditions in terms of a high temperature which can be sensitive to some labile thiols, as well as long reaction times. This method does not mention tolerance towards protected thiols for preparing vinyl sulfides with SPG (SProtecting Group) for use in the synthesis of ajoene derivatives. Recently, Cook[81] and coworkers improved the reaction conditions that were discovered by Venkataraman[83] by using CuI as an air-stable catalyst that is efficient for vinyl halide coupling reactions. Although the reaction conditions are milder in Cook's method,

there was also no investigation on the success of the protocol for producing protected sulfides.

Regarding applying these findings to a possible ajoene analogue synthesis, Scheme 10 below depicts a possible sequence required for accessing a key synthon **15** for ajoene derivative synthesis using a cross-coupling method. If formed, **15** would need to be deprotected (-PG), sulfenylated to the disulfide and chemoselectively oxidized to target. The example of the catalyst used is palladium which is analogues to a use of a copper catalyst.

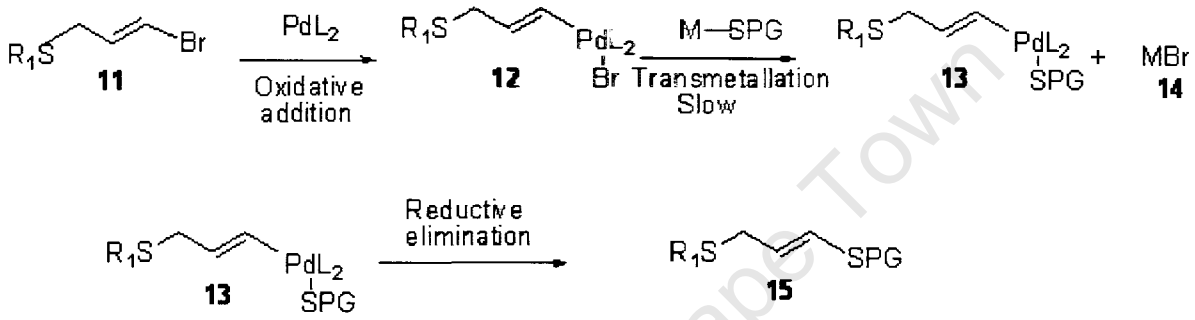

Scheme 10: Stereospecific coupling of a protected thiol

However, there would be some major challenges too. Firstly, stereodefined vinyl halide / allylic sulfide starting materials would need to be accessed. Although there are organometallic methodologies for doing this, the overall synthesis would be rather long. Secondly, a protecting group (SPG) would need to be found that could be deprotected for disulfide bond preparation, while be compatible with the cross-coupling conditions. This is a feature not covered by the reported methods. Alkali metal / liquid ammonia on an S-benzyl group might work to form an enethiolate that could be sulfenylated to generate the disulfide, but such conditions would probably be not compatible with the allyl sulfide. Admittedly, other PG's could be considered to do the job (eg STrityl), but it was felt that several questions remained.

2.3.2 β-Hydrogen elimination of a halide

In the second approach considered, **15** might be formed via an elimination of the type shown in Scheme 11. The starting material would be in principle easy to access via standard substitution chemistry of a 1,3-disubstituted propyl derivative (eg 3-bromopropan-1-ol).

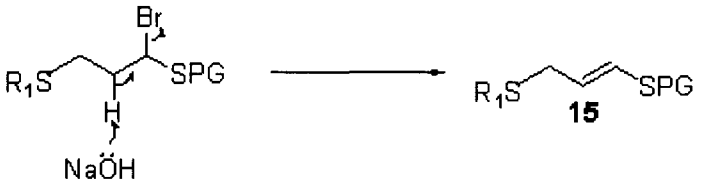

Scheme 11: Elimination of hydrogen halide to form **15**

However. this approach would involve an E-2 elimination that proceeds via an anti-periplanar transition state. Such a stereoelectronically controlled reaction would only render the *E*-isomer, as the SPG and CH_2SR_1 groups would orientate themselves *anti* in the transition state. Thus, the *Z*-ajoene wouldn't be available using this strategy. Olefination strategies also came to mind such as Wittig methodologies, but stereoselectivity and the choice of PG suggested that several reactions might need to be tried out. Thus attention was turned to the final option, the radical addition approach.

2.3.3 Radical addition approach

Radical addition is an important methodology for converting alkynes to alkenes. Early reports of the free-radical addition of thiolacetic acid to alkylacetylenes dates back to the late 1940's by H. Behringer, H Bader and co-workers.[84,86] In mid-1960's, J. A Kampmeier and G Chen proceeded with the study on stereochemistry of the free-radical addition of thiolacetic acid to 1-hexyne.[85] The procedure used was to mix the alkyne with thiolacetic acid at 0°. Initiation by adding an initiator was not needed but it was concluded that the reaction involves radical intermediates. The intermediate acetylthio radical (**17**) adds regioselectively to the alkyne terminus to form a mixture of *E*- and *Z*-stereoisomers of the vinyl thioacetate radicals (**18**, **19**) as shown in Scheme 12.[85]

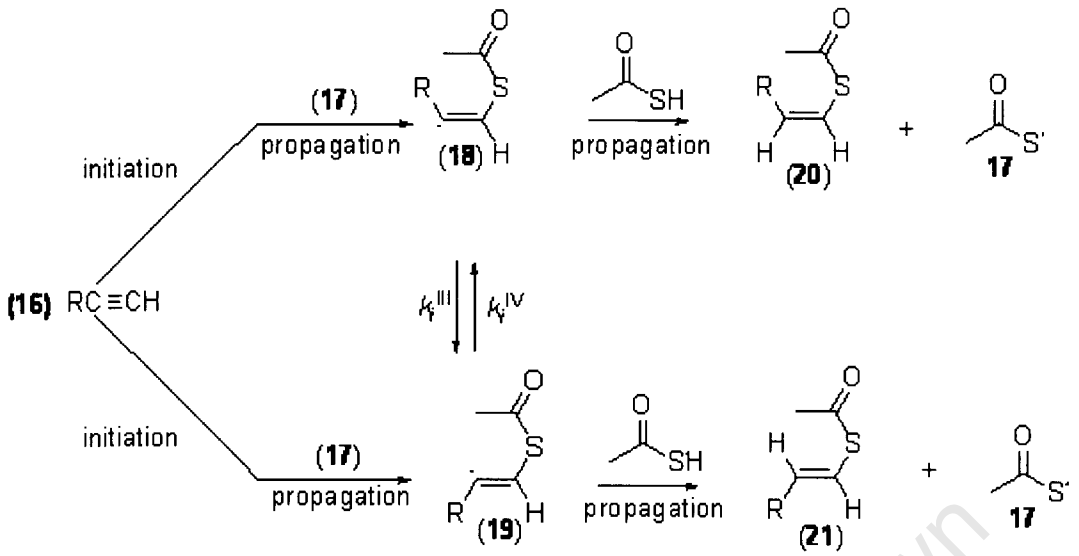

Scheme 12: Radical addition of thiolacetic acid to an alkyne.[85]

The vinyl thioacetate radicals (**18** and **19**) then abstract a hydrogen atom from a second thiolacetic acid to form the mono-adduct as a mixture of *E/Z* geometrical isomers (**20**, **21**) and with regeneration of an acetylthio radical for further propagation. It was established that excess thiolacetic acid promotes the formation of a di-adduct of structure shown in Figure 31.[85] For example, the use of a 1:3 ratio of alkylacetylene : thiolacetic acid instead of a 1:2 ratio facilitates the formation of the diadduct.

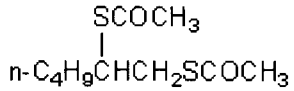

Figure 31: Diadduct of thiolacetic acid

In Kampmeier's study of the addition of thiolacetic acid to 1-hexyne in a 2/1 molar ratio to give a 55% yield of a mixture of pure *cis* and *trans*-1-hexenyl thioacetates after distillation (Figure 32).

Figure 32: *cis/trans* mono-addition adducts

The mono-adduct mixture was isolated by preparative-scale v.p.c (vapour-phase chromatograph) and analysed by ^{1}H NMR in mid-1960's for definitive structural assignments to reveal a 73:27 ratio of *cis*:*trans* isomers by virtue of a higher coupling constant as

expected for the *trans*-isomer ($J_{transA/B}$ = 15.9 Hz, $_{cis}$ = 9.6 Hz). This reaction was noted to form a vinylthio fragment of importance to ajoene synthesis and eventually formed the basis of the UCT synthetic sequence[87a] for substituted ajoene synthesis. Kampmeier compared his findings to those found by Benkeser in the radical addition of trichlorosilane to 1-heptyne, which gave a 75/25 *cis/trans* adduct ratio.[81] In both cases the *cis*-isomer was dominant. A likely explanation for the *cis*-stereoselectivity is that both *Z*- and *E*-vinyl radicals **18** and **19** form and presumably can interconvert, but that the *Z*-radical **18** reacts faster to product in view of lower steric hindrance in the transition state, since the incoming thiolacetic acid delivering an H atom only clashes with a vicinal H in the *Z*-case (**18**) versus a $SCOCH_3$ for the *E*-case (**19**).

2.4 Synthetic analysis of the UCT synthesis

The key mechanistic step in the UCT synthesis thus became the regioselective radical addition of thiolacetic acid to a terminal alkyne to generate a vinyl thioacetate based on the known addition of thiolacetic acid to an alkyne. Retrosynthesis of the target disubstituted ajoene is summarized in Scheme 13.

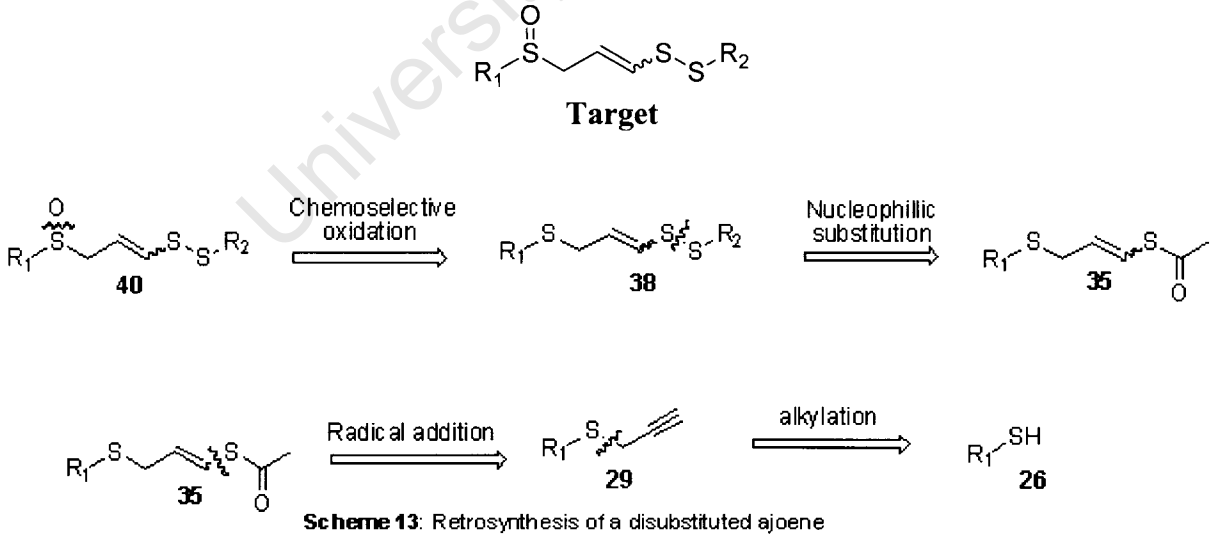

Scheme 13: Retrosynthesis of a disubstituted ajoene

The individual steps will now be discussed. The first step involves propargylation of a thiol, the latter either commercially available or synthesized via thiourea chemistry, which involved reacting thiourea **23** with an alkyl halide **22** to form an isothiouronium salt **24** as shown in Scheme 14.

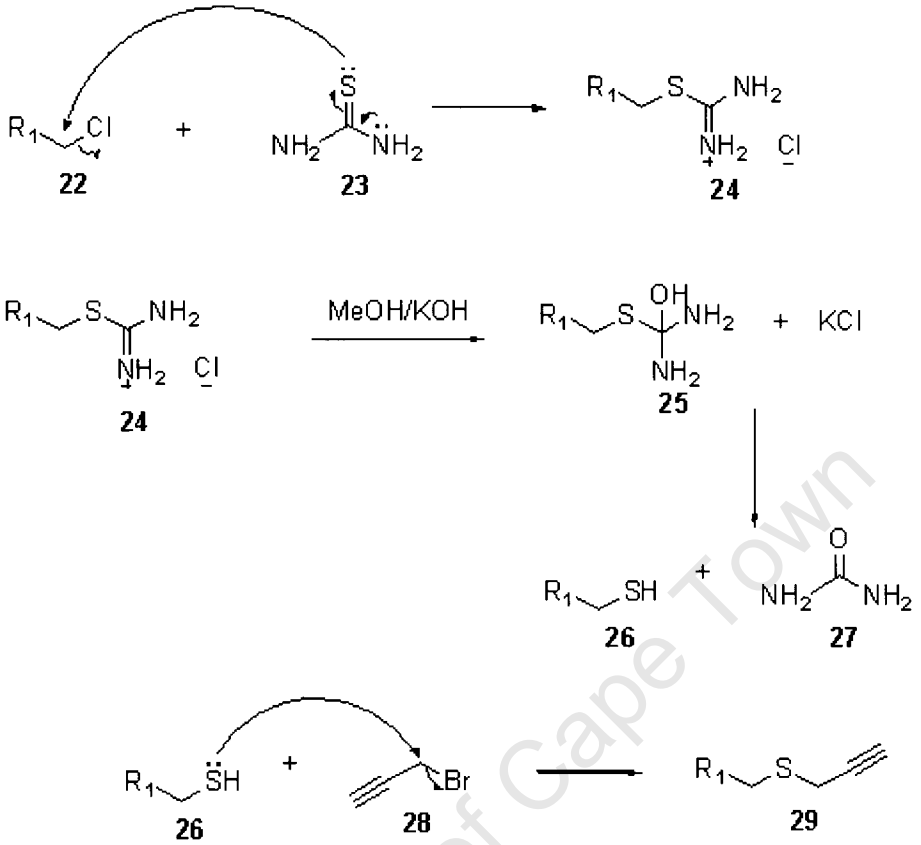

Scheme 14: Preparation of the alkylated thiol

Hydrolysis of the salt **24** occurs with KOH to give an odorous thiol **26** with the formation of potassium chloride and release of urea **27**. Rather than isolate an odorous thiol, it was alkylated *in situ* with propargyl bromide **28** to furnish alkynyl sulphide **29**, which could be isolated via an extractive work-up followed by either distillation or chromatography depending on the nature of R_1. Compound **29** was then reacted with thiolacetic acid using 1,1'-azobis(cyclohexanecarbonitrile) as a radical initiator (catalytic amount). The mechanism of this reaction follows the normal initation, propagation, termination sequence typical of radical reactions, Scheme 15. This mechanism is discussed in detail in the results and discussion section.

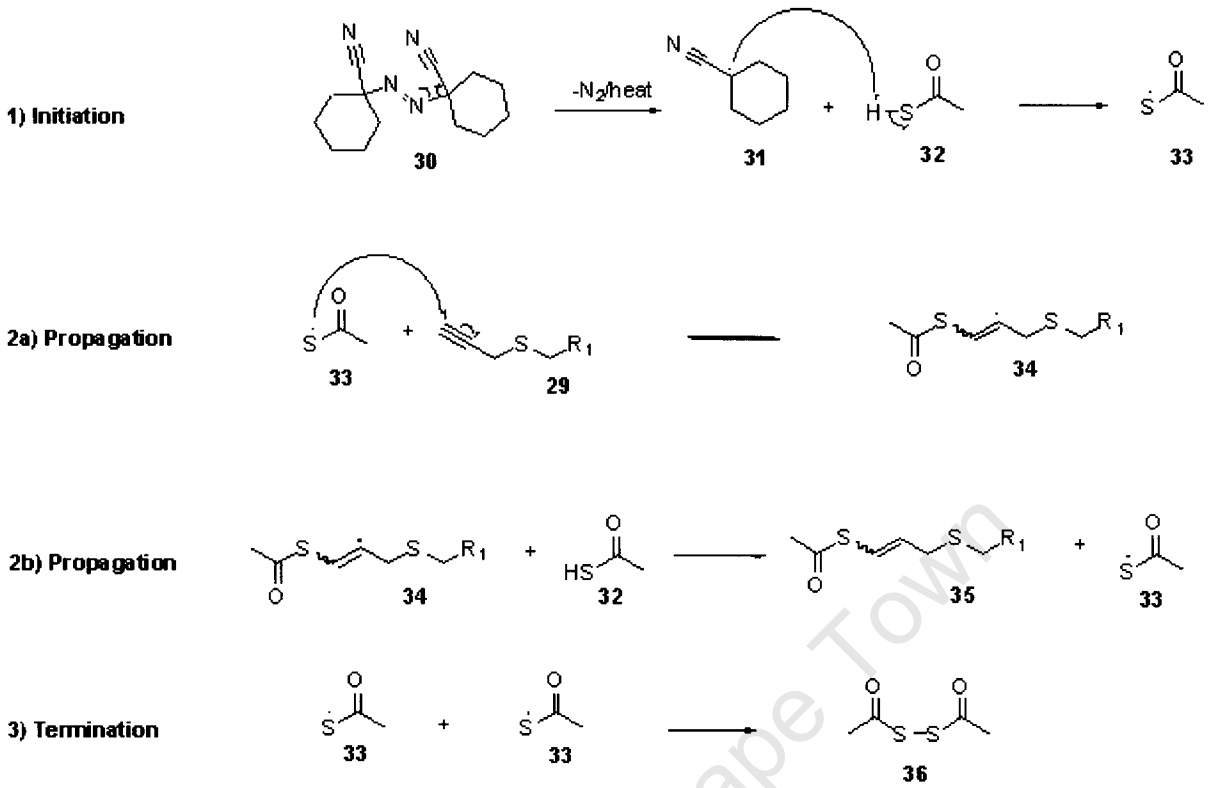

Scheme 15: Mechanism for the radical addition reaction

The vinyl thioacetate **35** is then elaborated by deprotecting it with KOH in methanol at low temperature to form an enethiolate **37**. Subsequent addition of an appropriately substituted thiosulfonate in a sulfenylation reaction affords vinyl disulfide **39**.

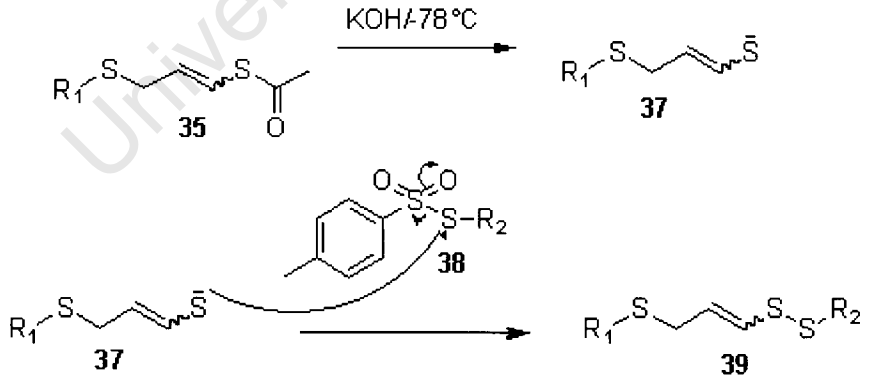

Scheme 16

Thiosulfonate **38** acts as a soft sulfenylating agent towards the enethiolate anion with the expulsion of sulfinate ion.

In the final step of the sequence compound **39** is chemoselectively oxidized to the sulfoxide target **41** with *m*-CPBA (1.2 eq) **40** as the oxidizing agent. *m*-CPBA oxidizes the most

nucleophilic sulfur of the three available, which is the sulfide sulfur. The double bond is also left intact, Scheme 17.

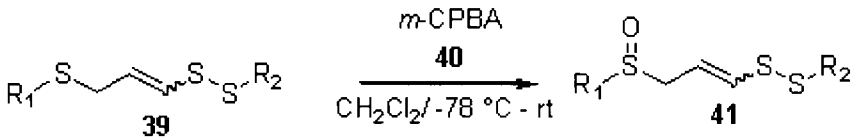

Scheme 17

2.5 Objectives

This project was aimed at synthesizing a small library of ajoene analogues for biological evaluation containing the central vinyl disulphide/sulphoxide core while varying the end groups R_1/R_2 as shown in Figure 33. It was carried out as part of a broader study within the group at UCT.

Figure 33: Structure of disubstituted ajoene target

In conjunction with the broader study, the following four derivatives were targeted for synthesis, inclusion studies into β-cyclodextrin and biological evaluation.

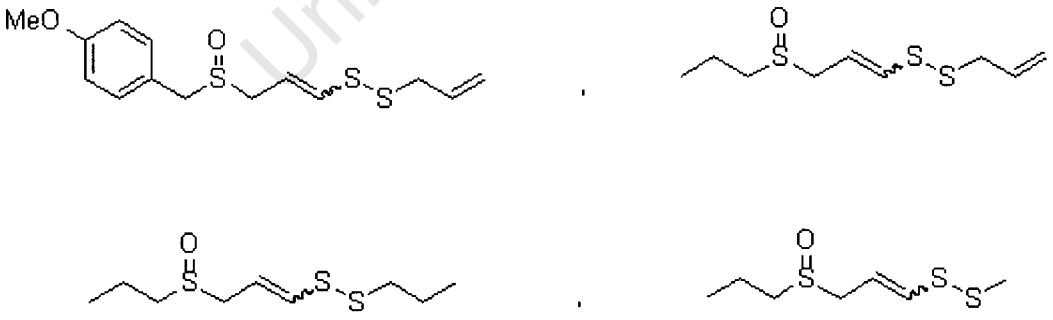

Figure 34: Compounds for study in this thesis

The project was thus divided into three parts:

- The synthesis of substituted ajoene derivatives shown in Figure 34
- Inclusion of the synthesized ajoene derivatives into cyclodextrin

- Biological evaluation of the ajoene derivatives and included derivatives as anti-cancer agents

Chapter 3: Experimental Section

4-Methoxybenzyl-2-propynyl sulfide 8[87a]

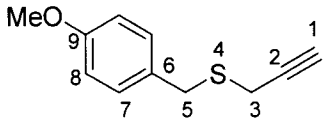

Thiourea (2.67 g, 35.0 mmol) was dissolved in acetonitrile (25 ml), and 4-methoxybenzyl chloride (5.00 g, 31.9 mmol) was then added dropwise. The mixture was subsequently refluxed for 40 min, then cooled in ice and the precipitated product filtered and washed with cold acetonitrile. The washed salt (7.02 g, 30.2 mmol) was then added to a stirred ice-cooled solution of KOH (4.81 g, 67.4 mmol) in methanol (12 ml) to produce an odorous product and a solid (KCl) precipitate. Propargyl bromide (4.82 g, 32.4 mmol, 80% in toluene) was added dropwise to this solution and the reaction allowed to stir at room temperature for 2 h. TLC (3% ethyl acetate in hexane) showed a spot-to-spot conversion to a more polar product that was UV-active. The methanol solvent was removed under vacuum and the residue suspended in CH_2Cl_2, which was shaken with water (20 ml), the organic layer separated and dried ($MgSO_4$), filtered and the solvent evaporated to dryness under reduced pressure to give a light yellow oil. The residue was purified on a silica-gel column using 3% ethyl acetate in petroleum ether as eluent to give **8** as a light-yellow oil (3.86 g, 66%): ν_{max} / cm^{-1} 3282 (HC≡C), 663 (C-S); δ_H (400 MHz, $CDCl_3$) 2.25 (1H, t, *J*, 2.6 Hz, H-1), 3.04 (2H, d, *J* 2.6 Hz, H-3), 3.77 (3H, s, -OMe), 3.80 (2H, s, H-5), 6.84 (2H, d, *J* 8.8 Hz, H-8), 7.24 (2H, d, *J* 8.8 Hz, H-7); δ_C (100 MHz, $CDCl_3$), 18.3 (C-3), 34.6 (C-5), 55.3 (OMe), 71.2 (C-1), 79.9 (C-2), 113.9 (C-8), 129.3 (C-6), 130.1 (C-7), 158.8 (C-9); HRMS (EI): *m/z* 193.0701 $[M+H]^+$, $C_{11}H_{13}OS$ requires 193.0687.

E/Z-S-3-(4-Methoxybenzylthio)-prop-1-enyl ethanethioate 14

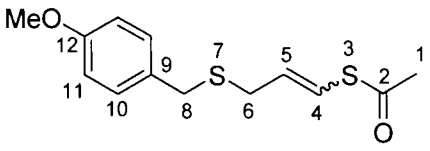

Thiolacetic acid (1.30 g, 17.2 mmol), was added with a dropping funnel to a solution of alkyne **8** (3.00 g, 15.6 mmol) and 1,1'-azobis(cyclohexanecarbonitrile) (190 mg). The mixture was refluxed in toluene at 80 °C over a period of about 2 h under N_2. Toluene was then removed under vacuum and the residue dried on a pump to give a yellow oil which was purified directly on a silica-gel column using 5% ethyl acetate in petroleum ether as eluent to give compound **14** as a 3:2 mixture of *Z/E* stereoisomers (2.32 g, 83% yield based on 991 mg compound **8** recovery): ν_{max} / cm^{-1} 1700 (C=O), 663 (C-S); *Z*-**14** δ_H (400 MHz, $CDCl_3$) 2.36 (3H, s, H-1),

3.09 (2H, dd, *J* 1.0, 7.4 Hz, H-6), 3.63 (2H, s, H-8), 3.78 (3H, s, -OMe), 5.84 (1H, dt, *J* 7.4, 9.5 Hz, H-5), 6.65 (1H, dt, *J* 1.0, 9.5 Hz, H-4), 6.84 (2H, d, *J* 8.3 Hz, H-11), 7.19 (2H, d, *J* 8.3 Hz, H-10); δ_C (100 MHz, $CDCl_3$), 30.8 (C-1), 33.2. (C-6), 35.2 (C-8), 55.4 (-OMe), 113.9 (C-11), 119.3 (C-5), 128.6 (C-4), 130.1 (C-9), 130.2 (C-10), 158.7 (C-12), 191.2 (C-2).

E-**14** δ_H (400 MHz, $CDCl_3$) 2.35 (3H, s, H-1), 3.08 (2H, dd, *J* 1.1, 7.4 Hz, H-6), 3.62 (2H, s, H-8), 3.78 (3H, s, -OMe), 5.80 (1H, td, *J* 7.4, 15.2 Hz, H-5), 6.49 (1H, dt, *J* 1.1, 15.2 Hz, H-4), 6.81 (2H, d, *J* 8.7 Hz, H-11), 7.22 (2H, d, *J* 8.7 Hz, H-10); δ_C (100 MHz, $CDCl_3$), 30.7 (C-6), 30.9 (C-1), 34.4 (C-8), 55.4 (-OMe), 113.9 (C-Ar), 119.6 (C-5), 129.9 (C-9), 130.2 (C-10), 130.4 (C-4), 158.7 (C-12), 191.2 (C-2); HRMS (EI): *m/z* 307.0404 [M+NaO], $C_{13}H_{16}NaO_3S_2$ requires 307.0439.

E/Z-10-(4-Methoxyphenyl)-4,5,9-trithiadeca-1,6-diene 20

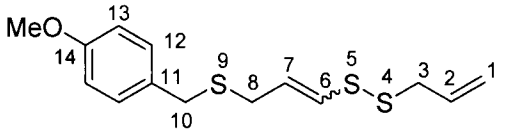

KOH (509 mg, 9.08 mmol) was dissolved in methanol (15 ml) at 0° C and added dropwise to thioate ester **14** (2.00 g, 7.46 mmol) in methanol (5 ml) at -30°C under N_2. The reaction was left stirring for 20 min before cooling to -78°C, whereupon *S*-prop-2-enyl 4-methylbenzenesulfonothioate[87b] (1.74 g, 7.60 mmol) dissolved in MeOH (5.0 ml) was added slowly dropwise. The reaction was allowed to warm to 0°C and left stirring for 3 h before quenching with aqueous ammonium chloride (20 ml). Water (40 ml) was added and the product was then extracted with CH_2Cl_2 (3 x 50 ml). The CH_2Cl_2 layer was washed with saturated NaCl solution (2 x 20 ml), dried and reduced under vacuum. The resultant yellow liquid was purified on a silica-gel column using 5% ethyl acetate in petroleum ether to give compound **20** as a 2:3 mixture of *Z/E* geometrical stereoisomers (1.87 g, 84 % yield): ν_{max} / cm^{-1} 3079 (C-H aromatic), 2913 (C-H aliphatic), 1508 (C=C), 659 (S-C), 470 (S-S); *Z*- **20** δ_H (400 MHz, $CDCl_3$) 3.19 (2H, dd, *J* 1.0, 7.5 Hz, H-8), 3.34 (2H, m , H-3), 3.66 (2H, s, H-10), 3.78 (3H, s, OMe), 5.14 (2H, m, H-1), 5.66 (1H, dt, *J* 7.5, 9.2 Hz, H-7), 5.84 (1H, m, H-2), 6.21 (1H, dt, 1.0, 9.2 Hz, H-6), 6.84 (2H, d, *J* 8.6 Hz, H-Ar), 7.20 (2H, d, *J* 8.6 Hz, H-Ar); δ_C (100 MHz, $CDCl_3$), 32.7 (C-8), 34.6 (C-10), 42.1 (C-3), 55.2 (-OMe), 113.9 (C-Ar), 119.0 (C-1), 128.0 (C-Ar), 128.1 (C-Ar), 130.0 (C-2), 130.1 (C-7), 132.8 (C-6), 158.6 (C-Ar).

E-**20** δ_H 3.06 (2H, dd, *J* 1.0, 7.3 Hz, H-3), 3.34 (2H, m, H-3), 3.62 (2H, s, H-10), 3.79 (3H, s, -OMe), 5.14 (2H, m, H-1), 5.84 (2H, m, H-2, H-7), 6.06 (1H, dt, *J* 1.0, 14.7, Hz, H-6), 6.84 (2H,

d, *J* 8.6 Hz, H-Ar), 7.20 (2H, d, *J* 8.6 Hz, H-Ar); δ_C (100 MHz, $CDCl_3$), 29.4 (C-8), 35.4 (C-10), 41.3 (C-3), 55.2 (-OMe), 114.0 (C-Ar), 119.0 (C-1), 128.0 (C-Ar), 128.1 (C-Ar) 128.2 (C-2), 130.7 (C-7), 132.8 (C-6), 158.6 (C-Ar); HRMS (EI): *m/z* 225.0436 $[M\text{-}C_3H_5S]^+$, $C_{11}H_{13}OS_2$ requires 225.0408.

E/Z-10-(4-Methoxyphenyl)-4,5,9-trithia-deca-1,6-diene 9-oxide 25

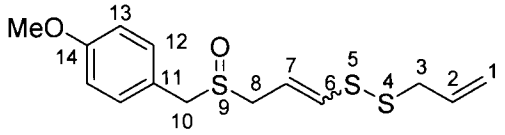

A solution of *m*-CPBA (421 mg, 1.89 mmol) in CH_2Cl_2 (3.0 ml) was added dropwise to compound **20** (535 mg, 1.79 mmol) dissolved in CH_2Cl_2 (5 ml) cooled to -78°C. The reaction was allowed to warm to room temperature and left stirring for 3 h, before quenching with saturated aqueous sodium bicarbonate (20 ml) and extracting with ethyl acetate (3 x 30 ml). The organic extracts were dried with $MgSO_4$ and the solvent evaporated. The residue was then purified on a silica-gel column using 40% ethyl acetate in petroleum ether as eluent to give compound **25** (467 mg, 83%) as a 2:3 mixture of *Z/E* geometrical stereoisomers: ν_{max} / cm 3007 (C-H aromatic), 2826 (C-H aliphatic), 1512 (C=C), 1013 (S=O), 663 (C-S), 450 (S-S); *Z*-**25** δ_H ($CDCl_3$, 400 MHz) 3.34 (2H, d, *J* 7.2 H-3), 3.40(1H, ddd, 1.1, 7.8, 13.3, Hz, H-8a), 3.43 (1H, ddd, 1.1, 7.8, 13.3, Hz, H-8b), 3.78 (3H, s, OMe), 3.90 (2H, s, H-10), 5.14 (2H, m, H-1), 5.80 (2H, m, H-2, H-7), 6.54 (1H, dt, *J* 1.1, 9.8, Hz, H-6), 6.88 (2H, d, *J* 8.8 Hz, H-13), 7.20 (2H, d, *J* 8.8 Hz, H-12); δ_C ($CDCl_3$, 100 MHz) 42.1 (C-3), 49.6 (C-8), 55.3 (OMe), 56.9 (C-10) 114.5 (C-13), 118.4 (C-7), 119.2 (C-1), 121.7 (C-11) 131.2 (C-12), 132.6 (C-2), 138.2 (C-6), 159.8 (C-14).

E-**25** δ_H ($CDCl_3$, 400 MHz) 3.27 (1H, ddd, *J* 1.1, 8.0, 13.2 Hz, H-8a), 3.27 (2H, d, *J* 7.6 Hz H-3), 3.51(1H, ddd, *J* 1.1, 8.0, 13.2, Hz, H-8b), 3.79 (3H, s, -OMe), 3.90 (2H, s, H-10), 5.18 (2H, m, H-1), 5.80 (1H, m, H-2), 5.92 (1H, dt, *J* 8.0, 15.0, H-7), 6.32 (1H, dt, *J* 1.1, 15.0, H-6), 6.88 (2H, d, *J* 8.8, Hz, H-13), 7.21 (2H, d, 8.8 Hz, H-12); δ_C ($CDCl_3$, 100 MHz) 41.3 (C-3), 52.8 (C-8), 55.3 (OMe), 56.3 (C-10) 114.5 (C-13), 117.3 (C-7), 119.2 (C-1), 121.5 (C-11), 131.2 (C-12), 132.5 (C-2), 134.4 (C-6), 159.8 (C-14); HRMS (EI): *m/z* 315.0551 $[M]^+$, $C_{11}H_{16}OS_2$ requires 315.0547.

4-Thia-1-heptyne 28[88]

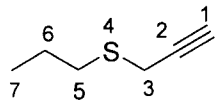

Potassium hydroxide (19.4 g, 340 mmol) was dissolved in degassed methanol (30 ml) and the mixture cooled to 0° C under N_2. 1-Propanethiol (20.0 g, 263 mmol) was added dropwise slowly followed by propargyl bromide (41.0 g, 276 mmol, 80% in toluene) and the reaction allowed to proceed at room temperature for 6 h. TLC (hexane) showed a spot-to-spot conversion to a more polar product that was UV active. The methanol solvent was then removed on the rotoevaporator under water pressure and the residue suspended in diethyl ether (40 ml), which was washed with water (3 x 10 ml). The ether extract was dried with $MgSO_4$, filtered and the solvent removed on the rotorevaporator keeping the bath temperature low. The resultant residue was purified by distillation at 150° C at atmospheric pressure to give **28** (23.9 g, 80 %) as an orange oil: ν_{max} / cm^{-1} 3290 (HC≡C), 2955 (C-H aliphatic), 638 (C-S); δ_H (400 MHz, $CDCl_3$) 1.00 (3H, t, *J* 7.3 Hz, H-7), 1.63 (2H, m, H-6), 2.21 (1H, t, *J* 2.6 Hz, H-1), 2.66 (2H. t, *J* 7.3 Hz, H-5), 3.23 (2H, d, *J* 2.6 Hz, H-3); δ_C (100 MHz, $CDCl_3$) 13.4 (C-7), 19.0 (C-3), 22.3 (C-6), 33.6 (C-5), 70.7 (C-1), 80.1 (C-2).

S-1-(4-Thiahept-1-enyl) ethanethioate 29

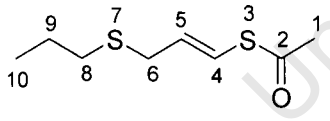

Thiolacetic acid (7.35 g, 96.6 mmol), alkyne **28** (10.0 g, 87.6 mmol) and 1,1'-azobis(cyclohexanecarbonitrile) (2.14 g, 8.76 mmol) were refluxed in toluene at 80°C under N_2 for 2 h. Toluene was then removed under vacuum and the residue dried on a vacuum pump to give an orange oil, which was purified directly on a silica-gel column using neat petroleum ether as eluent to give compound **29 (**9.80 g, 80 % based on recovery of 2.64g of alkyne **28)** as a 3:2 mixture of *Z/E* stereoisomers: ν_{max} / cm^{-1} 2957 (C-H), 1698 (C=O), 634 (C-S); *Z*-**29** δ_H (400 MHz, $CDCl_3$) 0.95 (3H, t, *J* 7.4 Hz, H-10), 1.60 (2H, m, H-9), 2.37 (3H, s, H-1), 2.41 (2H, t, *J* 7.3 Hz, H-8), 3.16 (2H, dd, *J* 1.3, 7.8 Hz, H-6), 5.85 (1H, dt, *J* 7.8, 10.4 Hz, H-5), 6.65 (1H, dd, *J* 1.3, 10.4 Hz, H-4); δ_C (100 MHz, $CDCl_3$), 13.4 (C-10), 22.8 (C-9), 30.8 (C-1), 31.0 (C-6), 33.2 (C-8) , 119.1 (C-4), 130.5 (C-5), 191.2 (C-9).

E-**29** δ_H (400 MHz, $CDCl_3$), 0.96 (3H, t, *J* 7.4 Hz, H-10), 1.60 (2H, m, H-9), 2.32 (3H, s, H-1), 2.41 (2H, t, *J* 7.3 Hz, H-8), 3.21 (2H, dd, *J* 1.3, 7.8 Hz, H-6), 5.80 (1H, dt, *J* 7.8, 15.7 Hz, H-5), 6.52 (1H, dt, *J* 1.3, 15.7 Hz, H-4); δ_C (100 MHz, $CDCl_3$), 13.4 (C-10), 22.6 (C-9), 30.5 (C-1), 33.0 (C-8), 34.0 (C-6), 118.8 (C-4), 130.5 (C-5), 192.8 (C-9); HRMS (EI): *m/z* 190.0485 $[M]^+$, $C_8H_{14}OS_2$ requires 190.0486.

(*E,Z*)-4,5,9-trithia-dodeca-1,6-diene 40

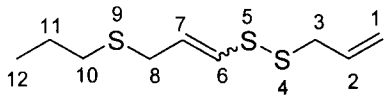

KOH (1.44 g, 25.2 mmol) was dissolved in methanol (20 ml) at 0°C and added dropwise to thioate ester **29** (2.40 g, 12.6 mmol) in methanol (10 ml) at -30°C under N_2. The reaction was left stirring for 20 min before cooling to -78°C, whereupon *S*-prop-2-enyl 4-methylbenzenesulfonothioate[88b] (2.94 g, 12.9 mmol) in methanol (5.0 ml) was added dropwise. The reaction was allowed to warm to 0°C and left stirring for 2 h before quenching with aqueous ammonium chloride (20 ml). Water (40 ml) was added and the product was then extracted with CH_2Cl_2 (3 x 50 ml). The CH_2Cl_2 extracts were washed with saturated brine solution (2 x 20 ml), dried and reduced under vacuum. The resultant orange liquid was purified on a silica-gel column using petroleum ether as eluent to give compound **40** as a 3:2 mixture of *Z/E* geometrical stereoisomers (2.46 g, 89% yield); *Z*-**40** δ_H (400 MHz, $CDCl_3$) 0.99 (3H, t, *J* 7.3 Hz, H-12), 1.63 (2H, m, H-11), 2.48 (2H, t, *J* 7.3 Hz, H-10), 3.27 (2H, dd, *J* 1.1, 7.4 Hz, H-8), 3.37 (2H, m, H-3), 5.18 (2H, m, H-1), 5.69 (1H, dt, *J* 7.4, 9.7 Hz, H-7), 5.87 (1H, m, H-2), 6.23 (1H, dt, *J* 1.1, 9.7 Hz, H-6); δ_C (100 MHz, $CDCl_3$), 13.5 (C-12), 23.0 (C-11), 29.5 (C-8), 33.4 (C-10), 42.1 (C-3), 118.9 (C-1), 128.7 (C-7), 131.7 (C-6), 132.9 (C-2).

E-**40** δ_H (400 MHz, $CDCl_3$), 0.99 (3H, t, *J* 7.3 Hz, H-12), 1.60 (2H, m, H-11), 2.45 (2H, t, *J* 7.3 Hz, H-10), 3.19 (2H, dd, *J* 1.2, 7.7 Hz, H-8), 3.35 (2H, m, H-3), 5.17 (1H, d, *J* 8.9 Hz, H-1 *trans*), 5.29 (1H, d, *J* 16.8 Hz, H-1 cis), 5.86 (2H, m, H-2, H-7), 6.11(1H, dt, *J* 1.2, 14.6 Hz, H-6); δ_C (100 MHz, $CDCl_3$), 13.5 (C-12), 22.7 (C-11), 33.1 (C-10), 33.5 (C-8), 41.3 (C-3), 118.9 (C-1), 127.5 (C-7), 128.6 (C-6), 132.8 (C-2).

(E,Z)- 4,5,9-Trithia-dodeca-1,6-diene 9-oxide 43

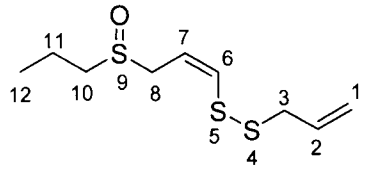

,

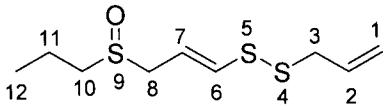

43a **43b**

m-CPBA (396 mg, 2.30 mmol) was dissolved in CH_2Cl_2 (5 ml) and added dropwise to compound **40** (460 mg, 2.09 mmol) in CH_2Cl_2 (5 ml) at -78°C under N_2. The reaction was allowed to warm to room temperature and left stirring for 3 h, before quenching with saturated aq. sodium bicarbonate (15 ml) and extracting with ethyl acetate (3 x 30 ml). The organic extracts were dried with $MgSO_4$, and the solvent removed under vacuum. The resultant residue was then purified on a silica-gel column using 40% ethyl acetate in petroleum ether as eluent to give compound **43** (400 mg, 82%) as a 3:2 mixture of *Z/E* geometrical stereoisomers. These could be separated by slow column chromatography.

Z-**43a** IR ν_{max} (neat) / cm^{-1}, 1368 (C=C), 1018 (S=O), 651 (C-S), 450 (S-S); δ_H (400 MHz, $CDCl_3$) 1.08 (3H, t, *J* 7.3 Hz, H-12), 1.81 (2H, m, H-11), 2.61 (1H, dt, *J* 8.2, 13.7 Hz, H-10a), 2.71 (1H, dt, *J* 8.2, 13.7 Hz, H-10b), 3.37 (2H, m, H-3), 3.56 (1H, dd, *J* 8.1, 13.2, Hz, H-8a), 3.63 (1H, dd, *J* 8.1, 13.2, Hz, H-8b), 5.16 (2H, m, H-1), 5.76 (1H, dt, *J* 8.1, 9.2, Hz, H-7), 5.84 (1H, m, H-2), 6.54 (1H, d, *J* 9.2 Hz, H-6); δ_C (100 MHz, $CDCl_3$), 13.4 (C-12), 16.2 (C-11), 42.1 (C-3), 50.9 (C-8), 53.5 (C-10), 118.5 (C-7), 119.2 (C-1), 132.6 (C-2), 138.2 (C-6).

E-**43b** IR ν_{max} (neat) / cm^{-1} 1400 (C=C), 1018 (S=O), 644 (C-S), (S-S). δ_H (400 MHz, $CDCl_3$), 1.06 (3H, t, *J* 7.3 Hz, H-12), 1.80 (2H, m, H-11), 2.61 (2H, m, H-10), 3.33 (2H, m, H-3), 3.43 (1H, dd, *J* 7.9, 13.2 Hz, H-8a), 3.51 (1H, dd, *J* 7.9, 13.2 Hz, H-8b), 5.15 (2H, m, H-1), 5.82 (1H, m, H-2), 5.91 (1H, dt, *J* 7.9, 14.6 Hz, H-7), 6.34 (1H, d, *J* 14.6, H-6); δ_C (100 MHz, $CDCl_3$), 13.3 (C-12), 16.1 (C-11), 41.2 (C-3), 53.0 (C-10), 54.5 (C-8), 117.1 (C-7), 119.1 (C-1), 132.4 (C-2), 134.2 (C-6)

S-Propyl 4-methylbenzenesulfonothioate 34[88b]

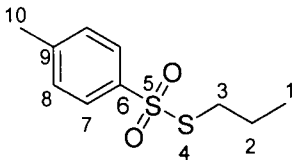

Potassium *p*-toluenethiosulfonate (7.18 g, 31.7 mol) was dissolved in DMF (10 ml) and a solution of 1-bromopropane (3.00 g, 24.4 mmol) added dropwise. The reaction was then left stirring at room temperature for 3 h before quenching with saturated aq. sodium bicarbonate (30 ml) and extracting with CH_2Cl_2 (3 x 30 ml). The extracts were dried with $MgSO_4$ and the solvent reduced under vacuum. The residue was then purified on a silica-gel column using 5% ethyl acetate in petroleum ether as eluent to give compound **34** (7.02 g, 96%). δ_H (400 MHz, $CDCl_3$) 0.93 (3H, t, *J* 7.4 Hz, H-1), 1.64 (2H, m, H-2), 2.45 (3H, s, H-10), 2.97 (2H, t, *J* 7.3 Hz, H-3), 7.34 (2H, d, *J* 8.3 Hz, H-Ar), 7.81 (2H, d, *J* 8.3 Hz, H-Ar); δ_C (100 MHz, $CDCl_3$) 13.1 (C-1), 21.6 (C-10), 22.2 (C-2), 37.9 (C-3), 126.9 (C-Ar), 129.8 (C-Ar), 142.2 (C-Ar), 144.6 (C-Ar).

(*E,Z*)-4,5,9-Trithia-dodeca-6-ene 41

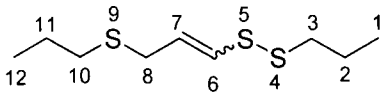

KOH (1.44, 25.2 mmol) was dissolved in methanol (20 ml) at 0°C and added dropwise to thioate ester **29** (4.00 g, 21.0 mmol) in methanol (10 ml) at -30°C under N_2. The reaction was left stirring for 20 min before cooling to -78°C, whereupon sulfenylating agent **34** (4.94 g, 21.4 mmol) in methanol (5.0 ml) was added dropwise. The reaction was allowed to warm to 0°C and left stirring for 4 h before quenching with aqueous ammonium chloride (20 ml). Water (40 ml) was added and the product was then extracted with CH_2Cl_2 (3 x 50 ml). The CH_2Cl_2 layer was washed with saturated brine (2 x 20 ml), dried and reduced under vacuum. The resultant orange liquid was purified on a silica-gel column using petroleum ether as eluent to give compound **41** (2.70 g, 76 % yield based on the recovery of 986 mg of starting material **29**) as a 2:3 *Z/E* mixture of geometrical stereoisomers *Z*-**41** δ_H (400 MHz, $CDCl_3$) 0.97 (3H, t, *J* 7.3 Hz, H-1), 0.99 (3H, t, *J* 7.3 Hz, H-12), 1.61 (2H, m, H-11), 1.69 (2H, m, H-2), 2.47 (2H, t, *J* 7.4 Hz, H-10), 2.70 (2H, t, *J* 7.1 Hz, H-3), 3.26 (2H, dd, *J* 1.3, 7.4 Hz, H-8), 5.66 (1H, dt, *J* 7.4, 9.3 Hz, H-7), 6.23 (1H, dt, *J* 1.3, 9.3 Hz, H-6); δ_C (100 MHz, $CDCl_3$) 12.9 (C-1), 13.4 (C-12), 22.2 (C-2), 22.9 (C-11), 29.4 (C-8), 33.3 (C-10), 41.1 (C-3), 127.9 (C-7), 132.2 (C-6).

E-**41** δ_H (400 MHz, $CDCl_3$) 0.97 (3H, t, *J* 7.3 Hz, H-1), 0.99 (3H, t, *J* 7.3 H-12), 1.61 (2H, m, H-11), 1.69 (2H, m, H-2), 2.43 (2H, t, *J* 7.4 Hz, H-10), 2.68 (2H, t, *J* 7.1 Hz, H-3), 3.17 (2H, dd, *J* 1.3, 7.7 Hz, H-8), 5.86 (1H, dt, *J* 7.7, 14.8 Hz, H-7), 6.11 (1H, dt, *J* 1.3, 14.8 Hz, H-6); δ_C (100 MHz, $CDCl_3$) 13.0 (C-1), 13.4 (C-12), 22.3 (C-2), 22.6 (C-11), 32.9 (C-10), 33.5 (C-8), 40.4 (C-3), 127.8 (C-7), 128.2 (C-6). ; HRMS (EI): *m/z* 222.0566 $[M]^+$, $C_9H_{18}S_3$ requires 225.0571.

(E,Z)- 4,5,9-Trithia-dodeca-6-ene 9-oxide 44

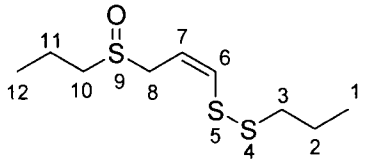

44a

,

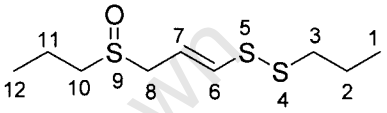

44b

m-CPBA (1.70 g, 9.85 mmol) was dissolved in DCM (5 ml) and added dropwise to compound **41** (2.00 g, 8.94 mmol) at -78°C in DCM (10 ml). The reaction was allowed to warm to room temperature and left stirring for 2 h, before quenching with saturated aq. sodium bicarbonate (15 ml) and extracting with ethyl acetate (3 x 30 ml). The product was dried with $MgSO_4$ and the solvent dried and reduced under vacuum. The residue was then purified on a silica column using 50% ethyl acetate in petroleum ether as eluent to give compound **44** (1.11 g, 52%) as a 2:3 mixture of *Z/E* geometrical stereoisomers; *Z*-**44a** δ_H (400 MHz, $CDCl_3$) 0.99 (3H, t, *J* 7.3 Hz, H-1), 1.08 (3H, t, *J* 7.3 Hz, H-12), 1.70 (2H, m, H-2), 1.80 (2H, m, H-11), 2.65 (4H, m, H-3, H-10), 3.52 (1H, dd, *J* 7.6, 13.4 Hz, H-8a), 3.63 (1H, dd, *J* 7.6, 13.4 Hz, H-8b), 5.75 (1H, dt, *J* 7.6, 9.5 Hz, H-7), 6.56 (1H, d, *J* 9.5 Hz, H-6). δ_C (100 MHz, $CDCl_3$) 12.9 (C-1), 13.4 (C-12), 16.2 (C-2), 22.3 (C-11), 41.3 (C-3), 50.9 (C-8), 53.4 (C-10), 118.0 (C-7), 138.7 (C-6).

E-**44b** δ_H (400 MHz, $CDCl_3$) 0.99 (3H, t, *J* 7.3 Hz, H-1), 1.08 (3H, t, *J* 7.3 Hz, H-12), 1.70 (2H, m, H-2), 1.80 (2H, m, H-11), 2.65 (4H, m, H-3, H-10), 3.45 (1H, dd, *J* 7.8, 13.0 Hz, H-8a), 3.52 (1H, dd, *J* 7.8, 13.0 Hz, H-8b), 5.93 (1H, dt, *J* 7.8, 15.0 Hz, H-7), 6.37 (1H, d, *J* 15.0 Hz, H-6); δ_C (100 MHz, $CDCl_3$), 13.0 (C-12), 13.4 (C-1), 16.2 (C-2), 22.4 (C-11), 40.4 (C-3), 53.1 (C-10), 54.7 (C-8), 116.7 (C-7), 134.6 (C-6); HRMS (EI): *m/z* 146.0211 $[M\text{-}PrSOH]^+$, $C_6H_{10}S_2$ requires 146.0224.

E-**13** δ_H (400 MHz, $CDCl_3$) 0.98 (3H, t, *J* 7.4 Hz, H-10), 1.60 (2H, m, H-9), 2.40 (3H, s, H-1), 2.46 (2H, t, *J* 7.4 Hz, H-8), 3.20 (2H, dd, *J* 1.0, 7.4 Hz, H-6), 5.90 (1H, dt, *J* 7.4, 14.6 Hz, H-5), 6.11 (1H, dt, *J* 1.0, 14.6, Hz, H-4); δ_C (100 MHz, $CDCl_3$) 13.5 (C-10), 22.2 (C-1), 22.7 (C-9), 33.1 (C-8), 33.5 (C-6), 126.4 (C-5), 128.5 (C-4). ; HRMS (EI) *m/z* 194.0248 $[M]^+$, $C_7H_{14}S_3$ requires 194.0258.

(E,Z)-2,3,7-Trithia-deca-4-ene 7-oxide 45

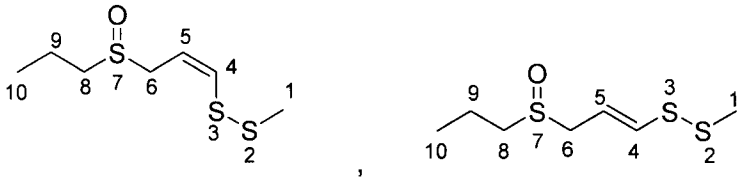

S-Methyl 4-methylbenzenesulfonothioate 35

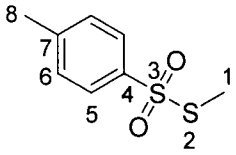

Potassium *p*-toluenethiosulfonate (7.18 g, 31.7 mmol) was dissolved in DMF (10 ml), which was then added dropwise to a solution of iodomethane (3.45 g, 24.4 mmol). The reaction was then left stirring at room temperature for 3 h before quenching with saturated aq. sodium bicarbonate (30 ml) and extracting with CH_2Cl_2 (3 x 30 ml). The organic extracts were dried with $MgSO_4$, and the solvent dried and reduced under vacuum. The residue was then purified on a silica column using 5% ethyl acetate in petroleum ether as eluent to give compound **35** (6.15 g, 96%). δ_H (400 MHz, $CDCl_3$) 2.43 (3H, s, H-1), 2.48 (3H, s, H-8), 7.33 (2H, d, *J* 8.2 Hz, H-Ar), 7.78 (2H, d, *J* 8.4 Hz, H-Ar); δ_C (100 MHz, $CDCl_3$) 17.9 (C-8), 21.5 (C-1), 127.0 (C-Ar), 129.8 (C-Ar), 140.8 (C-Ar), 144,7 (C-Ar)

(*E,Z*)-2,3,7-Trithia-4-decene 42

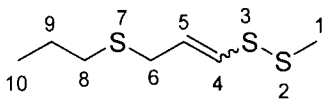

Chapter 4: Results and Discussion

With a versatile synthesis available, the first objective identified was to change just one of the end groups of ajoene, while retaining the other as allyl. The group chosen for change was the one on the sulfoxide end and the studies in this MSc thesis contributed to a broader study of changing that group, Figure 35.

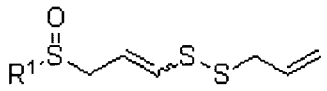

***E/Z*-Ajoene**

Figure 35: General structure of target for structure-activity study

That way, a rational structure-activity study could be undertaken while retaining the vinyl allyl disulfide / sulfoxide core believed to be the main pharmacophore in the molecule. Biological evaluation would involve measuring the anti-cancer activity against CT-1 transformed fibroblast cells as well as an oesophageal cancer cell-line with individual *E*- and *Z*-ajoene isomers as the reference standard. For any drug development it is important to increase the bioavailability of the lead in aqueous media. Thus, inclusion of these derivatives into a cyclodextrin presented itself as a worthwhile objective.

The project was thus divided into three parts:

- The synthesis of suitably modified ajoene derivatives
- inclusion of the synthesized ajoene derivatives into cyclodextrin
- biological evaluation of the ajoene derivatives as anti-cancer agents.

The tools used for purification and separation of these compounds were silica-gel column chromatography and preparative TLC plates. ^{1}H NMR, ^{13}C NMR, IR and mass spectroscopy were used as spectroscopic and analytical tools for confirming the structures of the synthesized intermediates or products.

4.1 Synthesis of Ajoene derivatives

The first target that was envisaged is depicted in Figure 36 as compound **18**.

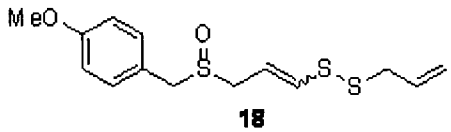

18

Figure 36: structure of the targeted ajoene derivative

The *para*-methoxybenzyl substituent of **18** was chosen due to its lipophilicity as well as for studying the influence of an electron-rich aromatic ring. It was also readily incorporated into the synthetic sequence from a commercial source. Thus, the synthesis of **18** began with propargylation of *p*-methoxybenzyl thiol. Since the latter was not available, its preparation was undertaken using the well-known thiourea chemistry on the commercially available chloride **1**.[87a]

This involved refluxing thiourea **2** (1.1 equivalents) in acetonitrile with *p*-methoxybenzyl chloride to form an isothiouronium salt **3** as shown in Scheme 18.

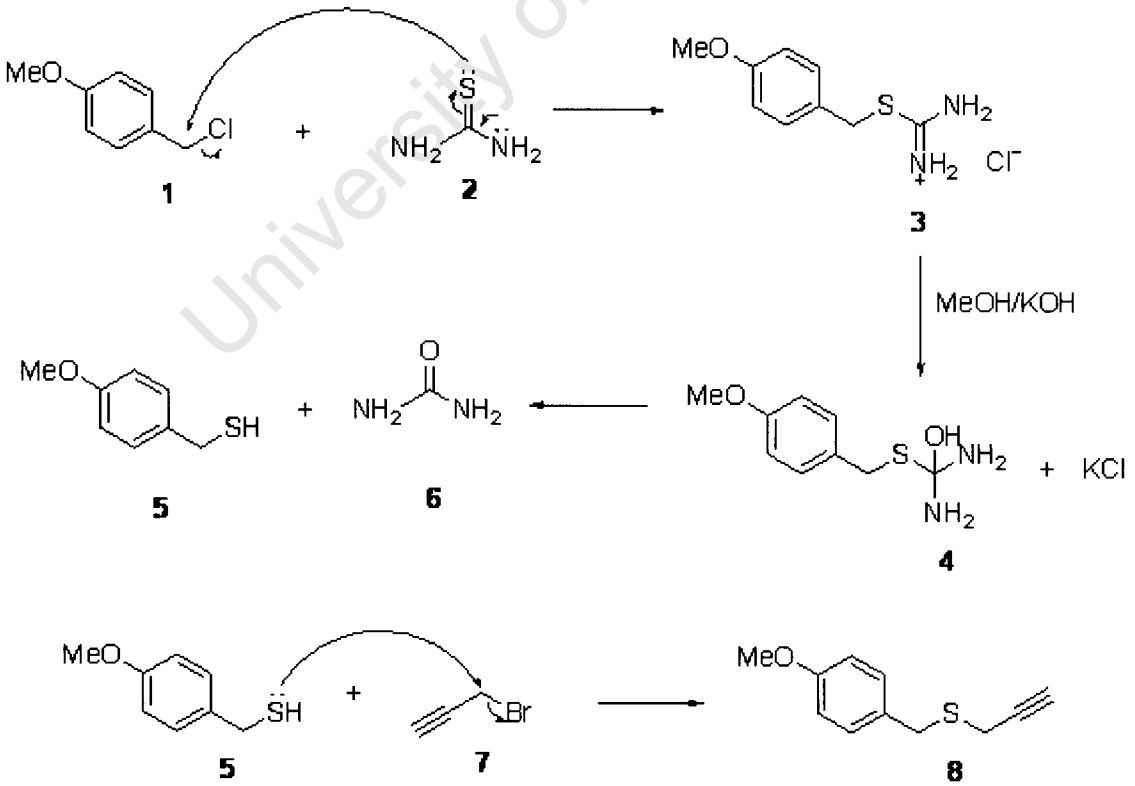

Scheme 18: Preparation of the alkylated salt

The reaction afforded a salt that would only migrate up a tlc plate in very polar mobile systems incorporating a high percentage of ethanol in ethyl acetate. Nevertheless, the reaction could

be followed by the disappearance of chloride **1** and was complete after 40 min. On cooling, the product that crystallised was filtered and then washed with cold acetonitrile. The crystalline salt was then dissolved in methanol and hydrolysed with KOH to the odorous thiol **5** with the formation of potassium chloride and urea **6**. Rather than isolate an odorous thiol, it was decided to alkylate *in situ* with propargyl bromide **7**, which was added directly to the medium. Two equivalents of KOH were added overall, one for the salt hydrolysis and the other for neutralising the HBr from the alkylation. After 2 hrs, tlc indicated the formation of a non-polar sulphide that was isolated by extraction. Column chromatography afforded compound **8** as a yellow oil in 66% yield over the two steps based on chloride **1**. Figure 37 shows the ^{1}H NMR spectrum for compound **8** with all the expected resonances. Traces of ethyl acetate not removed *in vacuo* can be identified.

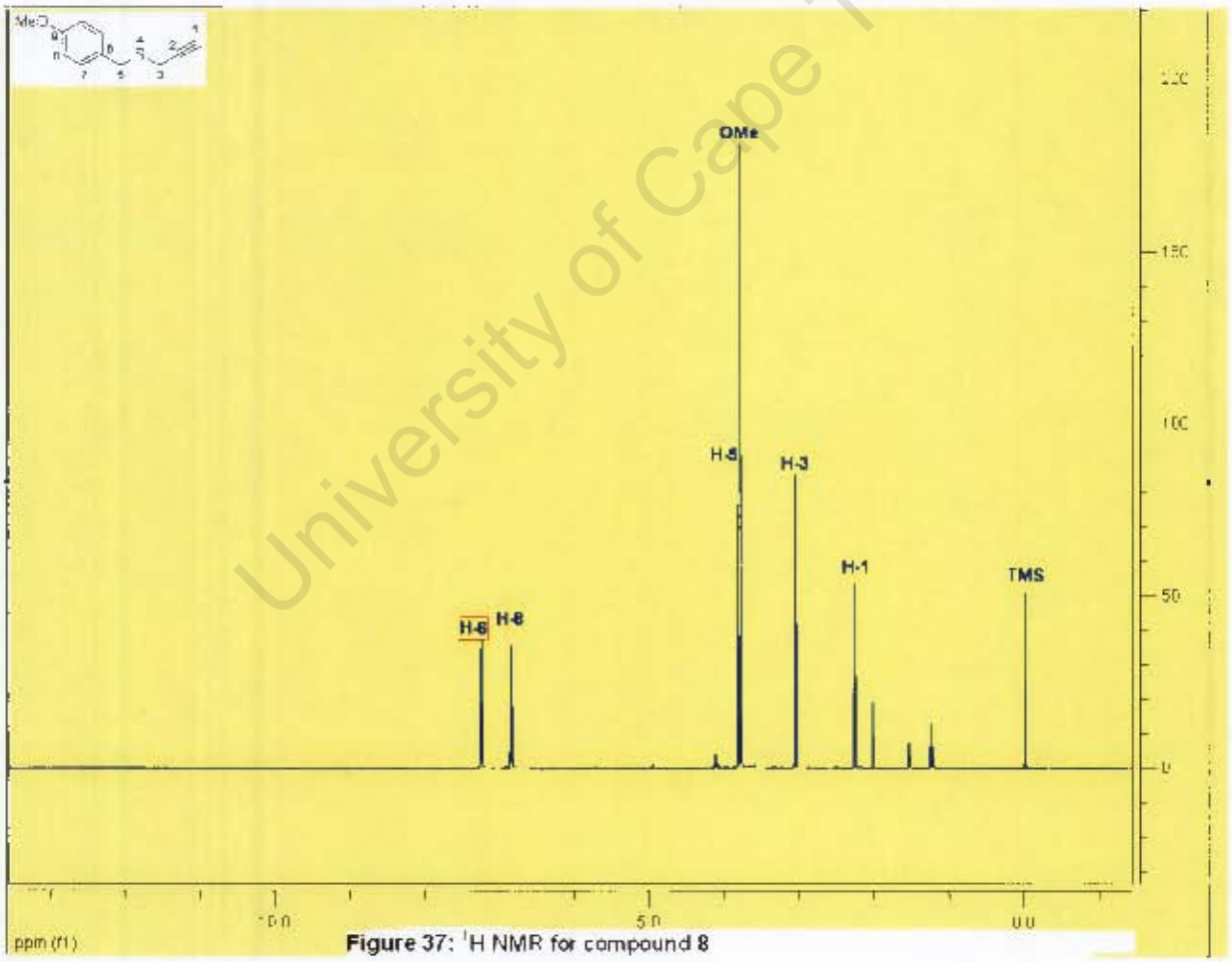

Figure 37: ^{1}H NMR for compound **8**

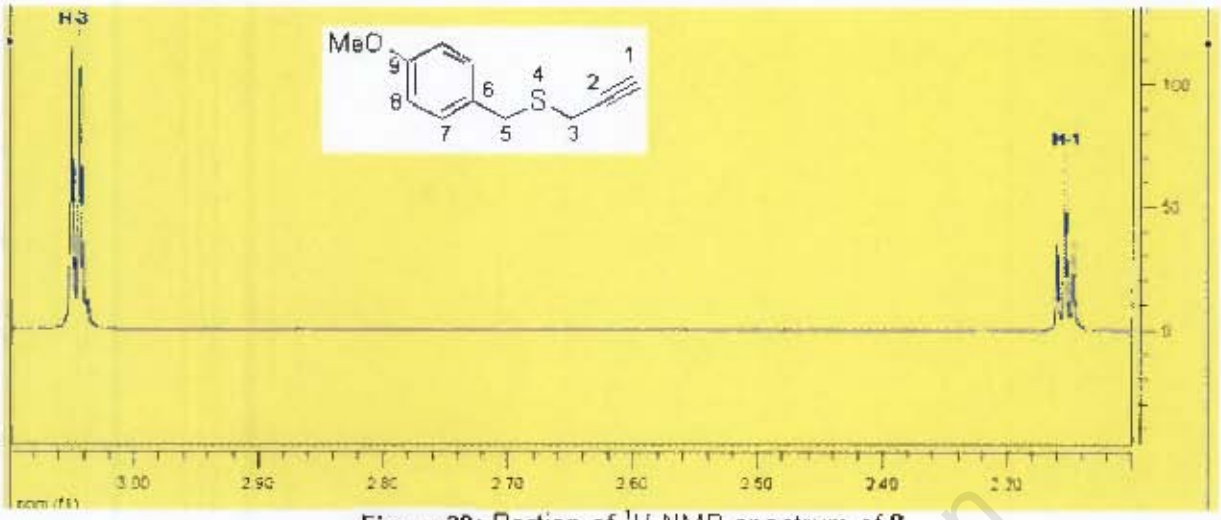

Figure 38: Portion of ^{1}H NMR spectrum of **8**

The structure of compound **8** was confirmed by the presence of an alkyne methine hydrogen triplet in the ^{1}H NMR spectrum at 2.25 ppm due to long-range coupling with the propargylic methylene (H-3). In turn, H-3 was a doublet. Other diagnostic signals included a singlet due to the benzylic methylene allylic H-5 (3.80 ppm) as well as an AB pair for the 1,4-disubstituted phenyl ring (6.84 and 7.24 ppm). Figure 38 show the multiplicities for H-1 and H-3, which serve to confirm the success of the reaction to afford compound **8** (Figure 37).

In addition, two resonances for a triple bond in the ^{13}C NMR spectrum at 71.2 ppm and 79.9 ppm confirmed propargylation. Finally, mass spectrometry was used as a tool to confirm the synthesis of compound **8**. Mass-spectrometry works by using magnetic and electric fields to exert force on charged particles in a vacuum. Therefore, the compounds must be charged or ionized and must be introduced in a gaseous phase. A beam of electrons accelerated from a filament, usually to an energy of about 70eV[31] passes through the sample and an electron collides with a neutral analyte molecule which knocks out an electron resulting in a positively charged ion.[31] This involves the ionization energy and is termed electron-impact ionization. The ionization impact may either produce a molecular ion which will have the same molecular weight and elementary composition as the starting material or it can produce a fragment ion which corresponds to a smaller piece of the analyte. Other ionization techniques involve electrospray (ES) and Fast Atom Bombardment (FAB) techniques. In the FAB technique an analyte is dissolved in a liquid matrix such as glycerol, thioglycerol, *m*-nitrobenzyl alcohol or diethanolamine. A small amount of the solution is placed on a target or emitter. The target is then bombarded with a fast atom beam, for example 6keV Xenon atoms that desorb molecular-like ions and fragments from the analyte. Cluster ions from that liquid matrix are also desorbed to produce a chemical background that varies with the matrix used. By comparison, the electrospray ionization technique works by spraying the sample solution

across a high potential difference from the needle into the orifice in the interface. Heat and gas are used to desolvate the ions existing in the sample solution. This ionization technique can produce multiple charged ions with the number of charges tending to increase as the molecular weight increases.

A high-resolution mass spectrum run using electrospray (ES) gave definitive evidence in support of **8**. The exact mass for compound **8** in a protonated form is 193.0687 and the mass spectrum was in accordance with this value recording a mass of 193.0701 as shown in Figure 39, as an $[M+H]^+$ ion within experimental error (14 in 10,000 is acceptable).

Show more of these in other places

Mass corresponds to $[M+H]^+$, ie

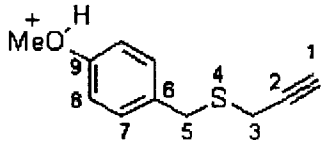

Chemical Formula: $C_{11}H_{13}OS$
Exact Mass: 193.0687
m/z: 193.07 (100.0%), 194.07 (12.9%), 195.06 (4.5%)
Elemental Analysis: C, 68.35, H, 6.78; O, 8.28; S, 16.59

Figure 39

The next step involved a radical addition of thiolacetic acid to the triple bond of compound **8** using 1,1'-azobis(cyclohexanecarbonitrile) **9** as a radical initiator. The latter was added at catalytic levels of about 0.05 equivalents although the fact that it is consumed in the reaction therefore means that it is not a catalyst. The first step was to dissolve alkyne **8** and radical initiator **9** in degassed toluene under N_2. Thiolacetic acid (1.1 eq) was then added dropwise with a dropping funnel to the solution at about 80 °C over a period of about two hours,
which is a high enough temperature for initiation to occur. Thereafter, the mixture was refluxed for 1.5 h with tlc indicating the formation of the more polar vinyl thioacetate product. On completion, no work-up was required; rather the toluene was then removed under vacuum and the residue dried on a pump to give a yellow oil which was purified directly on a silica-gel column using 5% ethyl acetate in petroleum ether as eluent to give compound **14** as a 3:2 mixture of *Z/E* stereoisomers (83% yield based on recovery of about 30% of compound **8**). Evidence for a successful addition came firstly from the ^{1}H NMR spectrum, which revealed a downfield shift for the alkynyl terminal proton of **8** into the vinyl region. Significantly, H-4 (see Figure 40 below) could be discerned as a pair of double triplets in the vinyl region at around δ = 6.5 ppm corresponding to the two geometrical isomers, with the larger vicinal coupling constant corresponding to the *E*-isomer, Figure 40.

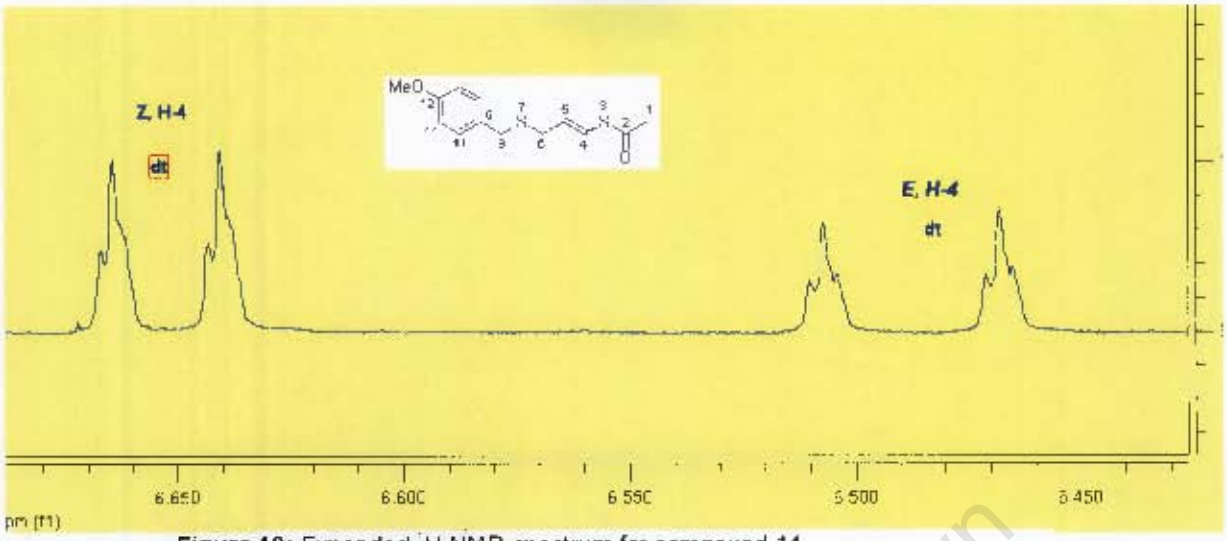

Figure 40: Expanded ^{1}H NMR spectrum for compound **14**

Similarly, the other vinyl signal, H-5 could be readily discerned, also as a pair of double triplets but with a larger *J* value for the triplet part corresponding to the H-5/H-6 coupling. This vinyl vicinal combination also, importantly, confirmed the addition to be regioselective, with the sulphur adding to the terminus of the alkyne rather than the internal carbon, presumably on steric grounds together with the greater stabilization afforded to the more substituted vinyl radical intermediate. Other diagnostic signals included the two methyl acetyl singlets as well as the *p*-methoxybenzyl group signals. Indeed the protons of the S-allylthio group for each isomer could be readily discerned and are given in Table **3**. However, the isomers couldn't be separated by chromatography.

Table 3: Diagnostic peaks for identification of compound **14**

Compound	Chemical Shift	Multiplicity	Coupling Constant (ppm)	Assignment
14 Z	2.36	s	-	H-1
14 E	2.35	s	-	H-1
14 Z	6.65	dt	1.0, 9.5	H-4
E	6.49	dt	1.1, 15.2	H-4

14	**Z**	5.84	dt	7.4, 9.5	H-5
	E	5.80	dt	7.4, 15.2	H-5
14	**Z**	3.09	dd	1.0, 7.4	H-6
	E	3.08	dd	1.1, 7.4	H-6

As expected, H-6 appeared as a pair of double doublets for the two isomers in view of their coupling relationships as well as their enantiotopicity. The ^{1}H NMR spectrum also clearly revealed compound **14** to be obtained as a mixture of isomers by integration, with the *Z*-isomer dominating the *E*- in a ratio of 3:2. The ^{13}C NMR also confirmed the success of the addition by virtue of the appearance of a carbonyl group carbon observed at δ_C 191.2 for the thioester. The mechanism of the radical addition presumably follows the classical radical pathway involving the three steps of initiation, propagation and termination as shown in Scheme 19.

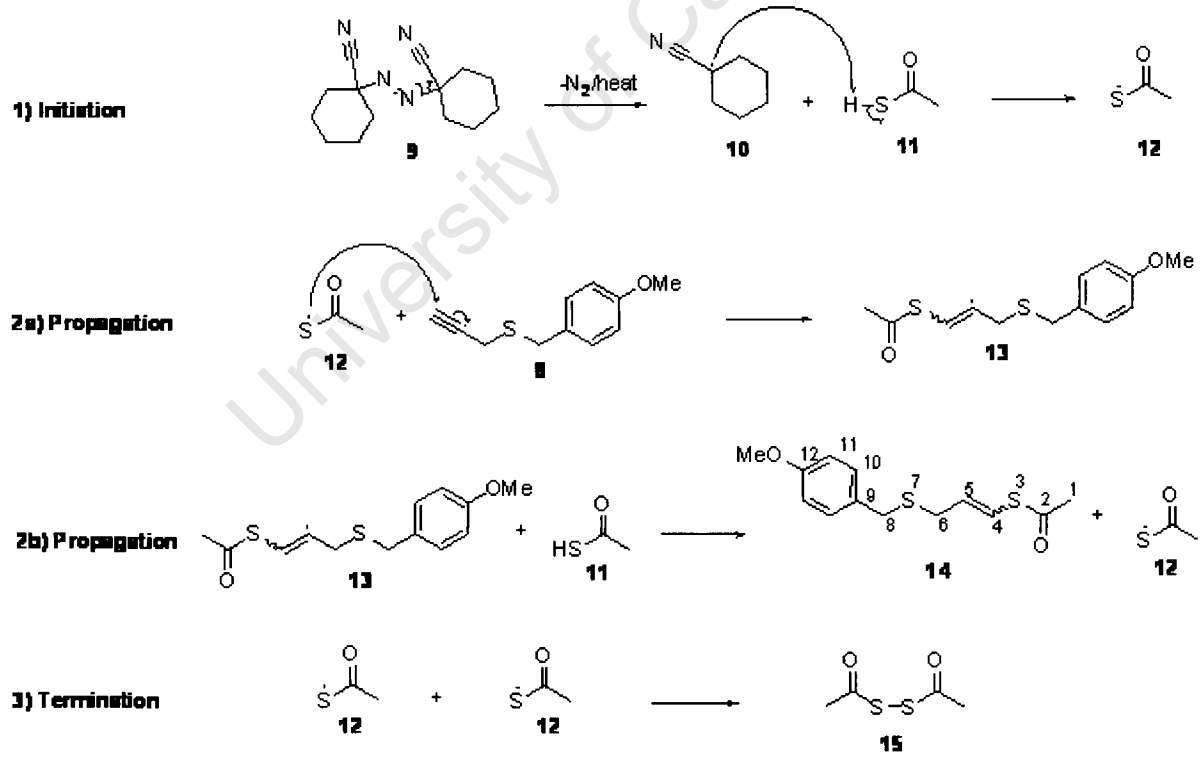

Scheme 19: Mechanism for the radical addition reaction

1) Initiation to give 12

Thus, in the first step 1,1'-azobis(cyclohexanecarbonitrile) **9** undergoes thermal homolytic cleavage resulting in *α*-cyano radical **10**. The thiolacetic acid (1.10 equiv) **11** in the reaction undergoes hydrogen abstraction to generate a thiyl radical **12.**

2) Propagation to give 14 + 12

The thiyl radical **12** then reacts with compound **8** to form a vinyl thioacetate radical **13**. This then abstracts a hydrogen from the second thiolacetic acid to form compound **14** (83%) as a 3:2 ratio of *Z/E-i*somer and radical **12** again, which enters a second cycle of propagation.

3) Termination (dimerisation of 15)

Two thiyl radicals **12** may dimerize to form disulphide diacetate **15**, thus terminating the reaction.

These findings agreed with the 3:2 *Z/E*-isomer ratio found in studies carried out by Kampmeier discussed in Chapter 2. [85]

In the next step, sulfenylating agent **18** was prepared by reacting potassium *p*-toluenesulfonothiate **16**

dissolved in DMF with allyl bromide **17**. The reaction proceeded at room temperature for 3 h before quenching with saturated aq. sodium bicarbonate and extracting with DCM. The extracts were dried with $MgSO_4$ and the solvent reduced under vacuum. The residue was then purified on a silica-gel column using 5% ethyl acetate in petroleum ether as eluent to give thiosulfonate **18** (92%) as shown in Scheme 20. The ^1H NMR spectrum of **18**, a known compound, revealed the required aromatic AB doublet pair integrating correctly against the upfield allyl signals.

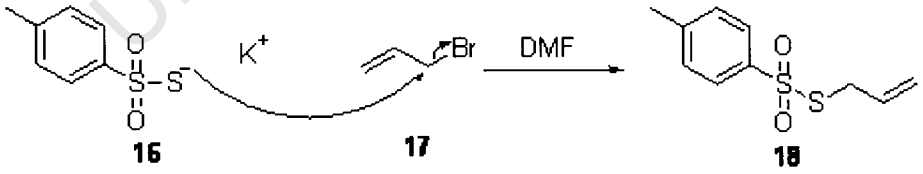

Scheme 20

With the sulfenylating agent in hand, vinyl thioacetate **14** was deprotected by reacting it with KOH in methanol at -78°C to form the enethiolate anion **19**. The low temperature was used to avoid side-reactions of the resultant enethiolate. It also reflects the weakness of the C-S bond of the thioacetyl group. The reaction was allowed to warm to -20°C before addition of thiosulfonate **18**. TLC analysis showed a disappearance of enethiol and a new polar spot after stirring at room temperature for 3 h. This resulted in quenching the reaction with saturated aq. sodium bicarbonate and extracting with DCM. Purification was achieved by column

chromatography using 5% ethyl acetate in petroleum ether to give compound **20** as a 2:3 mixture of *Z/E* stereoisomers (84 % yield). A detailed mechanism is shown in Scheme 21.

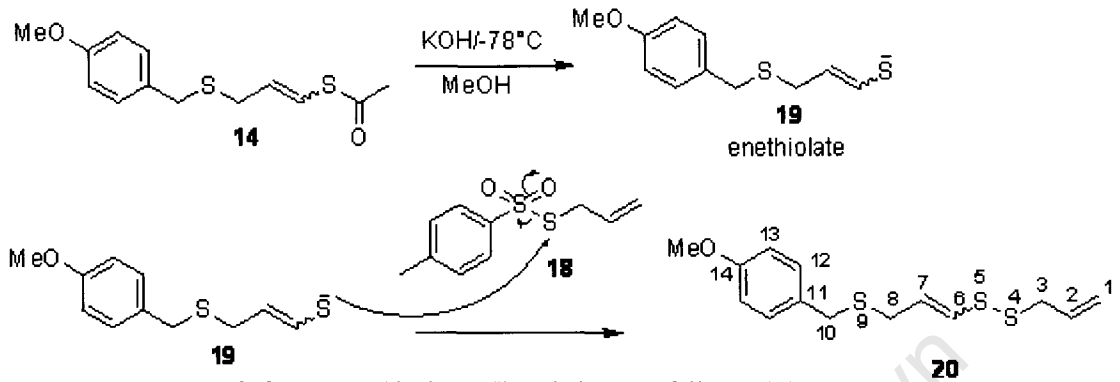

Scheme 21: Nucleophillic substitution of thioacetate

Thiosulfonate **18** can be considered as a -CH_2S-tosylate (Ts) grouping with the important difference compared to the more common -CH_2OTs group that nucleophilic attack occurs at sulfur rather than at carbon. Thus **18** acts as a soft sulfenylating agent towards the enethiolate, which thiates on sulfur. The coupling gives a disulfide bond which is an interesting example of the soft-soft principle. The ^{1}H NMR spectrum of **20** readily revealed a loss of the acetyl group of **14** and the introduction of a new allyl group. Once again, the allyl group of the vinyl disulphide moiety in **20** gave a pair of signals for each of H-6, H-7 and H-8 consistent again with the formation of two geometrical isomers. Also, the coupling relationships, eg dt for H-6 were similar to those of **14**. However, regarding the *E/Z* ratio a change was observed. Instead of a 3:2 *Z/E*-isomer that was observed for compound **14**, there was a change to a 2:3 *Z/E*-isomer ratio. The reason for the shift towards the *E*-isomer suggests a thermodynamic equilibration of sorts that could occur due to protonation by MeOH of *Z*-enethiolate **19** to the enethiol **21** which undergoes tautomerism to form thioaldehyde **22**. This is then followed by rotation of the C-1/C-2 single bond followed by tautomerism to form *E*-enethiol **23** which becomes deprotonated by methoxide to form *E*-enethiolate as shown in Scheme 22. Thereafter, *E*-**19** gets sulfenylated to *E*-**20**.

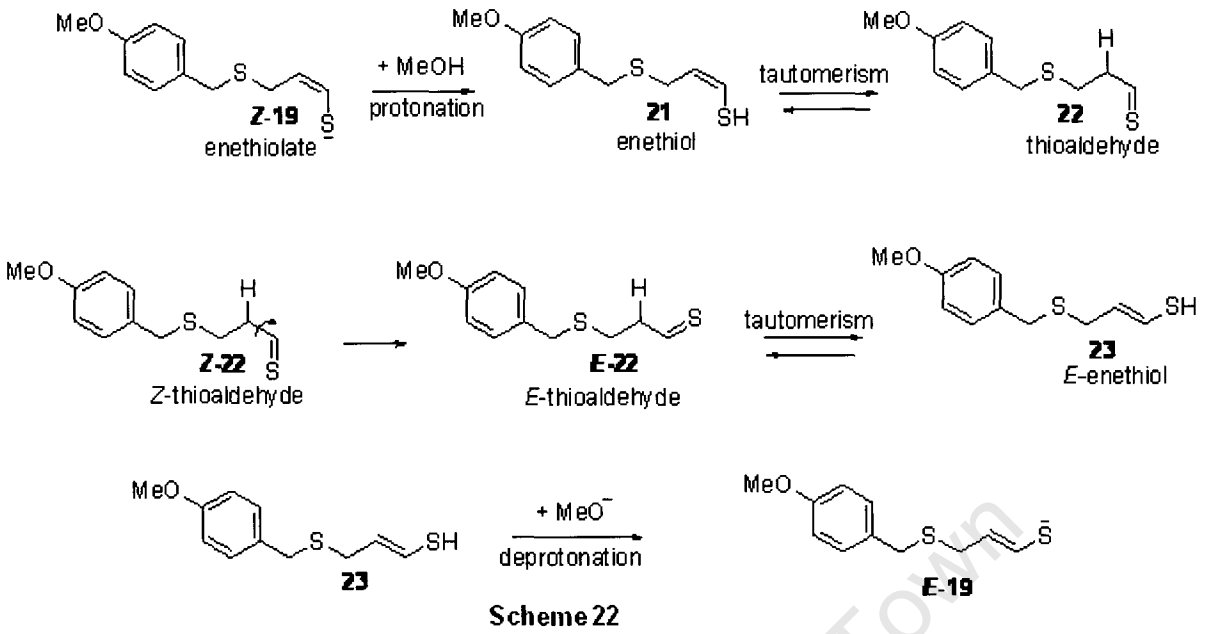

Scheme 22

Compound **20** was also studied by ^{13}C NMR, which returned 12 pairs of signals including four aromatic pairs for the benzene ring. C-6 was observed to be more downfield for both isomers compared to C-7. The reason may be because it is attached to the sulfur atom, which deshields it. 2D-techniques such as HSQC (H to C correlation) were used to assist with assignments given that the proton assignments were trustworthy. Similarly, the IR spectrum of **20** confirmed the presence of a disulfide linkage at 450 cm^{-1}. A high resolution mass spectrum (electrospray) confirmed the formation of compound **20** by showing a peak for disulfide cleavage of the molecular ion [M^+ = $C_{14}H_{18}OS_3^+$] to [M^+ - C_3H_5S] at 225.0436 (expected = 225.0408).

In the final step, compound **20** was chemoselectively oxidized to a sulfoxide with 1 equivalent of *m*-CPBA (*meta*-chloroperbenzoic acid) **24** as the oxidizing agent. This reaction is chemoselective as *m*-CPBA preferentially oxidizes the sulfide S-atom over the sulfurs of the disulfide group, presumably in view of its greater nucleophilicity.

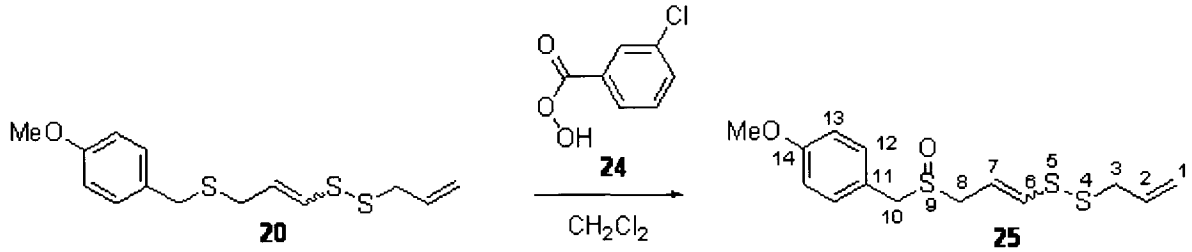

Scheme 23: Chemoselective oxidation of a sulfide

The reaction was conducted at -78° in order to maximise selectivity. Tlc at this temperature via quenching of an aliquot revealed that there was a presence of a new more polar spot with disappearance of compound **20** after 3 h. The reaction was then quenched with aqueous carbonate, the organic product extracted and following the normal isolation and chromatography (using 40% ethyl acetate in petroleum ether as eluent) gave **25** (2:3 *Z/E* 83%). It was noted that the *Z/E*-isomer ratio of **25** did not change when compared to that of its sulfide precursor. The site of oxidation as the sulfide sulfur was indicated by downfield shifts of H-8 and H-10 (α- to the new sulfoxide grouping) relative to those in the sulfide precursor **20**. Thus, H-8 shifted from 3.19 ppm to 3.42 for the *Z*-isomer and 3.06 to 3.27 ppm for the *E*-isomer. By comparison, those for H-3 α- to the disulfide allyl sulfur remained almost the same at 3.34 ppm. Further evidence was provided by the ^{13}C NMR spectrum, which also revealed significant downfield shifts for C-8 and C-10. Table 4 summarises both H and C chemical shifts for all of the positions α- to sulfurs (C-7 included) in both starting trisulfide **20** and sulfoxide product **25**.

Table 4: Diagnostic resonances for identification of compound **20 and 25**

Position	Compounds	^{1}H δ	*Multiplicity; J*	^{13}C δ
3	20	*Z/E*-3.34	m	*Z*-42.1 *E*-41.3
	25	*Z/E*-3.34	d, 7.6	*Z*-42.1 *E*-41.3
6	20	*Z*-6.21 *E*-6.06	dt, 1.0, 9.2 dt, 1.0, 14.7	*Z*-132.8 *E*-132.8
	25	*Z*-6.54 *E*-6.32	dt, 1.1, 9.8 dt, 1.1, 15.0	*Z*-138.2 *E*-134.6
7	20	*Z*-5.66 *E*-5.84	dt, 7.5, 9.2 m	*Z*-130.1 *E*-130.7

	25	*Z*-5.80 *E*-5.92	m dt, 8.0, 15.0	*Z*-118.4 *E*-117.3
8	20	*Z*-3.19 *E*-3.06	dd, 1.0, 7.5 dd, 1.0, 7.3	*Z*-32.7 *E*-29.4
8a 8b	25	*Z*-3.40 *Z*-3.43	ddd, 1.1, 7.8, 13.2 ddd, 1.1, 7.8, 13.2	*Z*-49.6
8a 8b		*E*-3.27 *E*-3.51	ddd, 1.1, 8.0, 13.2 ddd, 1.1, 8.0, 13.2	*E*-52.8
10	20	*Z*-3.66 *E*-3.62	s s	*Z*-34.6 *E*-35.4
	25	*Z/E*-3.90	s	*Z*-56.9 *E*-56.3

A further piece of supporting evidence showing a successful synthesis of compound **25** came from the observation of non-equivalence of the H-8 protons (observed as a pair of resonances for each geometrical isomer) as a result of diastereotopicity due to a chiral sulfoxide. The sulfoxide is chiral because it is asymmetric (one counts the lone pair) and configurationally stable at room temperature. Prior to oxidation, the H-8 protons were enantiotopic showing a single resonance for each geometrical isomer (as a doublet of doublets in each case). Upon oxidation, H-8 splits into two resonances for each stereoisomer, each one as a doublet of doublet of doublets as a result of geminal, vicinal and allylic coupling as shown in Table 8 and Figure 41. The H-10 signal was also expected to split into an AB doublet pair due to the diastereotopic nature of the sulfoxide, but only a singlet was observed for each isomer. The IR spectrum of **25** also showed an absorption due to the sulfoxide 1301cm^{-1}.

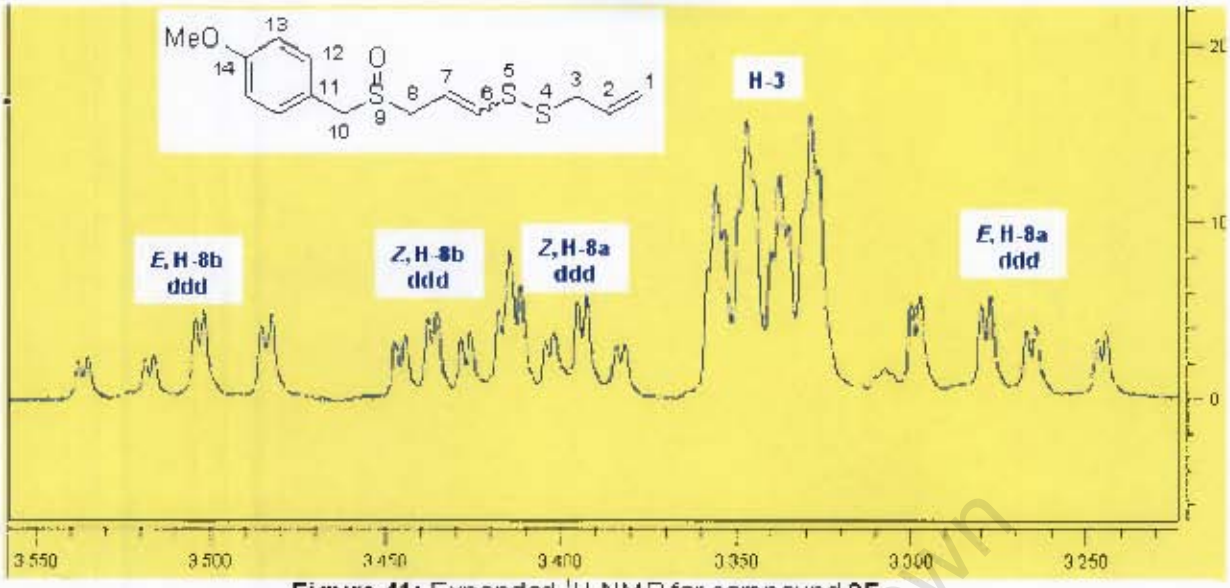

Figure 41: Expanded ^{1}H NMR for compound **25**

Finally, a high resolution mass spectrum (Electrospray) gave definitive evidence in support of **25**.The mass spectrum in Figure 42 shows a molecular ion of 315.0551 g/mol with virtually the same molecular weight as that expected from the formula of 315.0547 g/mol, thus proving the success of the oxidation step.

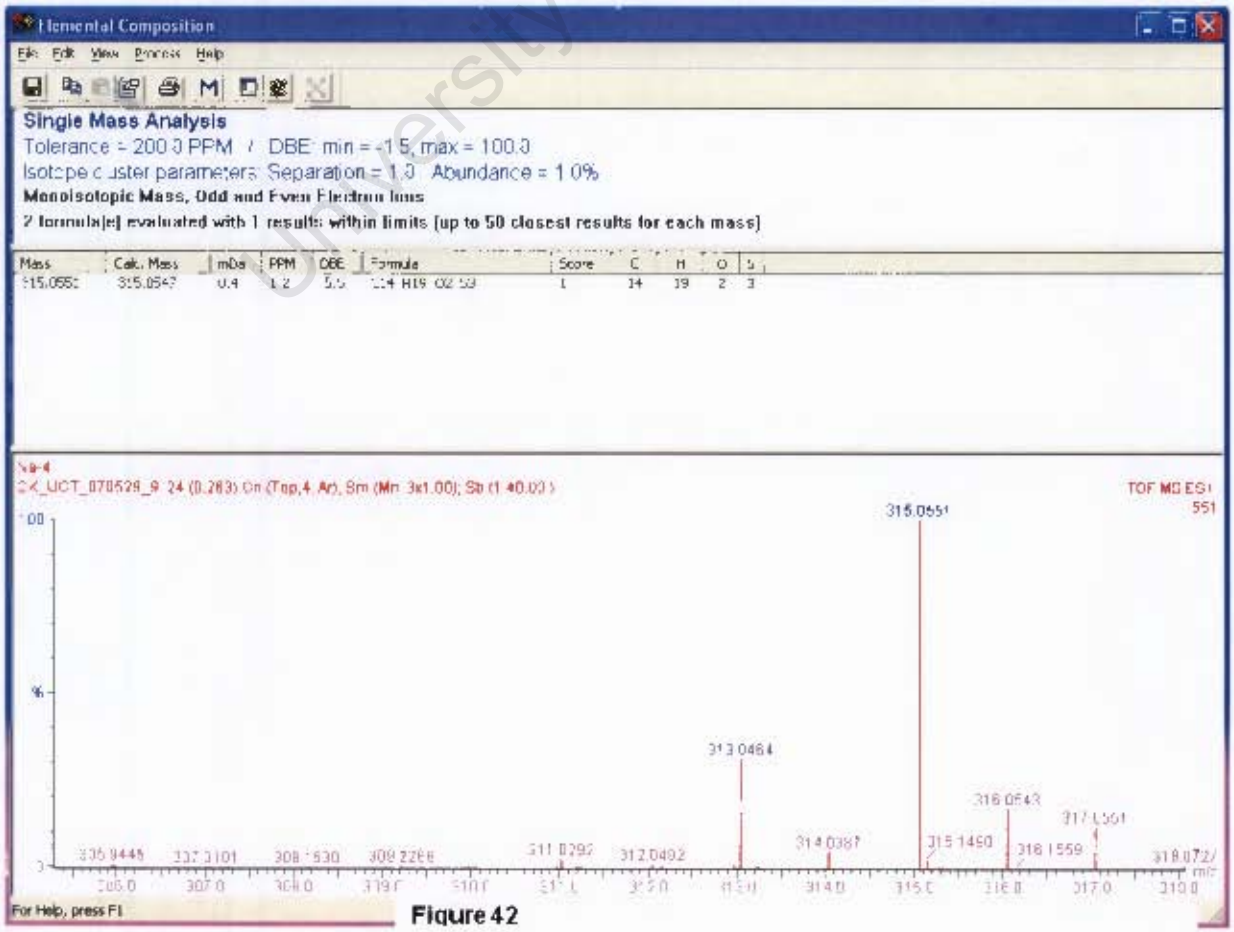

Figure 42

The next set of targets chosen for synthesis were aimed at chemosensitization studies, an issue discussed in Chapter 2. These fell under the following structural type in which the disulfide allyl group was varied and the group at the sulfoxide end was changed from allyl to propyl:

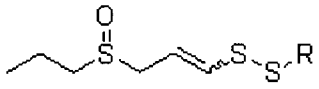

Figure 43

The reasoning behind these changes follow as:

1) Ajoene has been shown to be a potent chemosensitizer in AML for cytarabine, with a mode of action believed to involve suppression of the anti-apoptotic protein bcl-2. Thus, a small library of ajoenes with small end-groups as shown in Figure 44 were chosen for study.

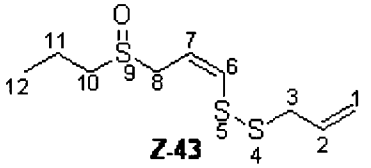
Z-43

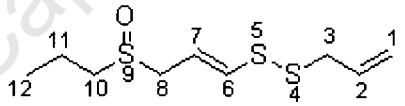
E-43

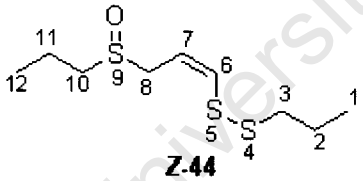
Z-44

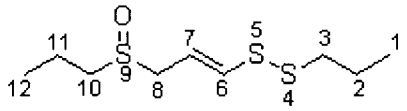
E-44

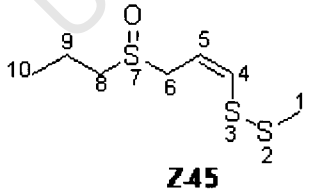
Z-45

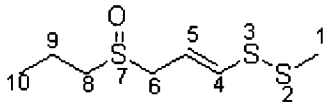
E-45

Figure 44

Changing allyl to propyl at the sulfoxide end agreed with the UCT pilot study in which propyl was shown to have more or less the same activity as ajoene.

2) Varying the allyl group at the disulfide end to another small group made sense for probing structure-activity within chemosensitization in view of the likely role of the disulfide grouping in the process.

Retrosynthetically, all of the targets in Figure 44 above can be derived from the vinyl thioacetate **29** shown in Figure 45.

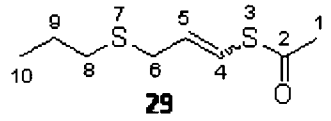

29

Figure 45

Thus, for the synthesis of key intermediate **29**, it was necessary to first synthesize compound **28** from commercially available 1-propanethiol **26**. The latter is very volatile with a boiling point of 65°C. The synthesis began with alkylating 1-propanethiol with propargyl bromide **27** as shown in Scheme 24 using KOH as base to neutralize the HBr formed.

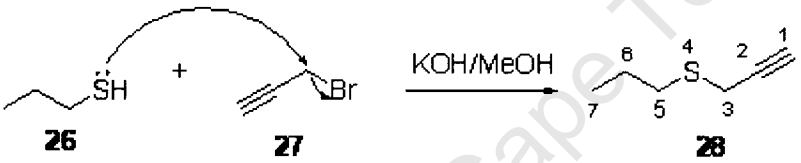

26 **27** **28**

Scheme 24: Alkylation of 1-Propanethiol with Propargyl bromide

For the reaction, potassium hydroxide was dissolved in degassed methanol at 0° C under N_2. 1-Propanethiol **26** was then added dropwise followed by propargyl bromide **27** and the reaction allowed to proceed at room temperature for 2 h, after which time tlc (hexane) indicated the formation of a non-polar spot that was UV active and presumed to be sulfide. The methanol solvent was then removed under vacuum on the rotoevaporator keeping the bath temperature at ambient temperature to minimize product loss and the residue was suspended in diethyl ether (40 ml), which was washed with water (3 x 10 ml). The ether extract was dried with $MgSO_4$ and the solvent removed taking precautions as before with bath temperature. The residue was purified by distillation at 150° C (atmospheric pressure) to give **28** in 80% yield as an orange oil. Its structure was confirmed by the presence of an alkyne methine hydrogen triplet in the ^1H NMR spectrum at 2.21 ppm due to coupling with the propargylic methylene (H-3) as with alkyne **8** previously. Other resonances were as expected and the ^{13}C NMR spectrum returned the six expected resonances with ones at 80.1 (internal) and 70.7 ppm (external) for the triple bond. Furthermore, the IR spectrum gave a stretch at 3290 for the terminal alkyne.

The next step was a radical addition reaction on compound **28** using thiolacetic acid. The same procedure was adopted for the synthesis of **29** as for the conversion of alkyne **8** to *p*-methoxybenzyl vinyl thioacetate **14**. The desired vinyl thioacetate **29** was obtained after 2 hr as a 3:2 mixture of *Z/E*-stereoisomers and in 80% yield based on recovered alkyne **28** (16 %)

after column chromatography, Scheme 25. The ratio of the isomers was consistent with that found for the synthesis of compound **14** and that of Kampmeier,[85] and the mechanism followed that was described in Scheme 19 before.

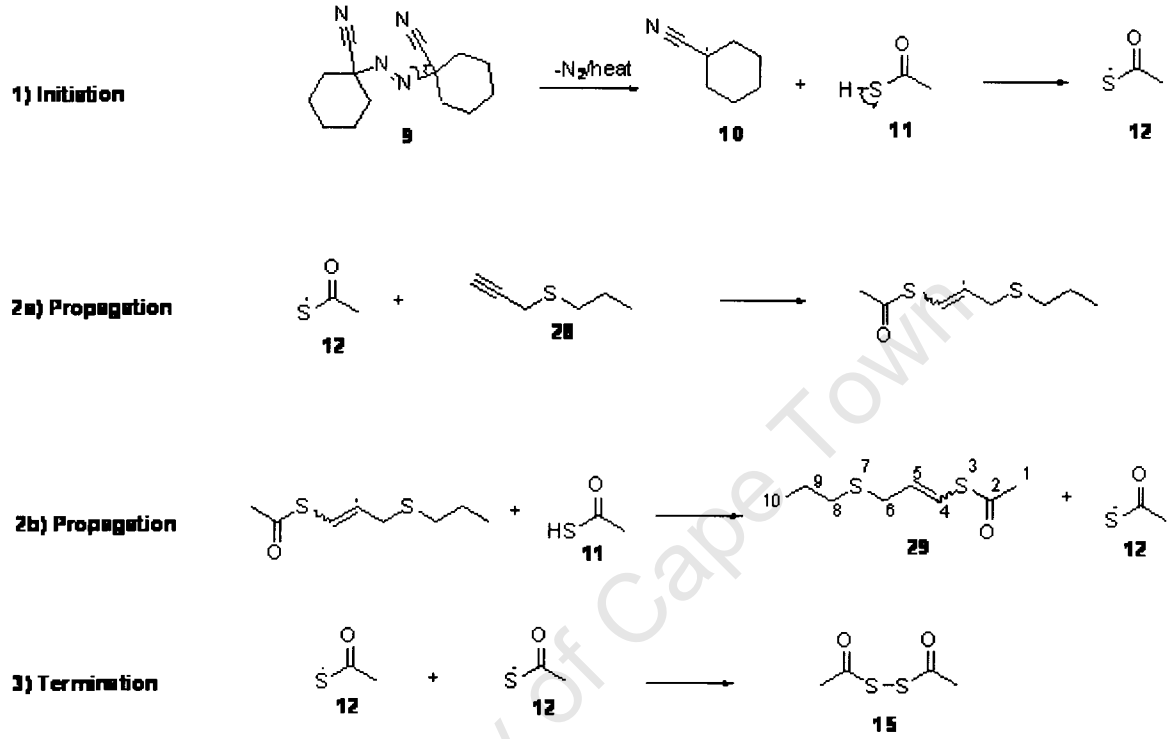

Scheme 25: Mechanism for the radical addition reaction

Once again, evidence for a successful addition of thiolacetic acid came firstly from the ^{1}H NMR spectrum, which revealed a new pair of thioacetyl methyl singlets as well as a downfield shift for the alkynyl terminal proton of **28** (H-1) into the vinyl region (H-4) as shown in Table 5.

Table 5: ^{1}H NMR data for the terminal hydrogens in **28** and **29**

Position	Compounds	$^{1}H\ \delta$	*Multiplicity; J*	$^{13}C\ \delta$
1	**28**	2.21	t, 2.6	70.7
4	**29**	Z-6.65 E-6.52	dd, 1.3, 10.4 dt, 1.3, 15.7	Z-119.1 E-118.8

The ^{13}C NMR spectrum of **29** also confirmed the success of the reaction with resonances due to the presence of carbonyl groups observed at δ_C 191.2 for the *Z*-isomer and 192.8 for the *E*-

isomer. The mass spectrum also confirmed the success of the reaction by showing both the parent ion as well as a fragment ion of M^+ - $COCH_3$ (147.0292 observed; 147.0302 expected) fitting the structure of **29** shown below.

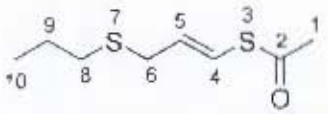

Chemical Formula: $C_8H_{14}OS_2$
Exact Mass: 190.0486
m/z: 190.05 (100.0%), 191.05 (10.5%), 192.04 (9.0%)
Elemental Analysis: C, 50.48; H, 7.41; O, 8.41; S, 33.69

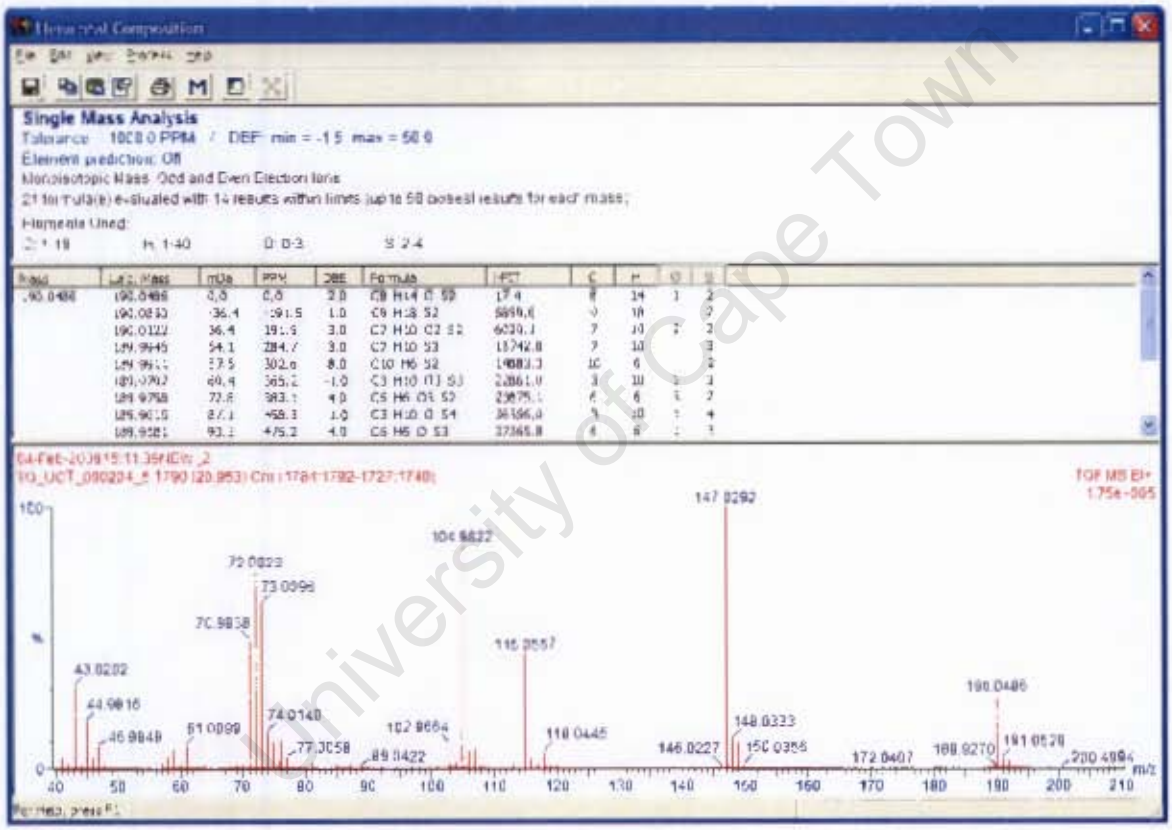

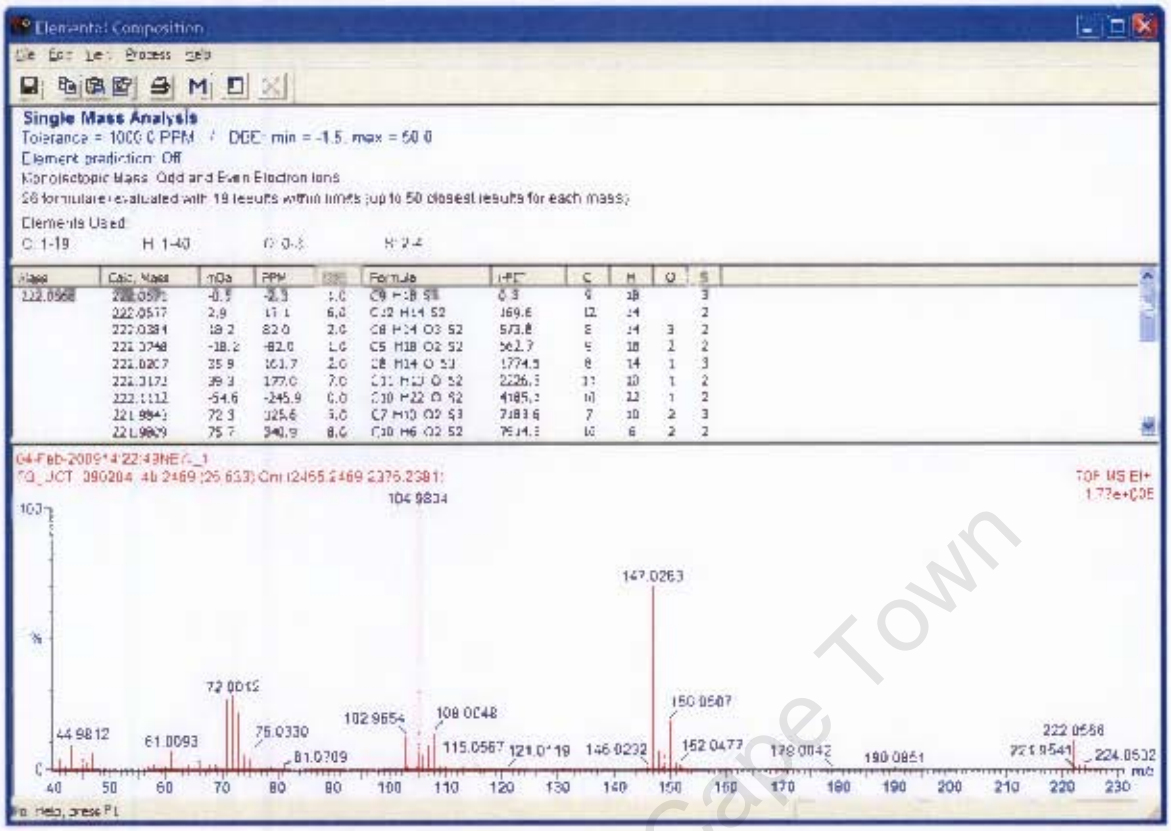

With vinyl thioacetate **29** in hand, the various sulfenylating agents as S-allyl, S-propyl and S-Me could be prepared via nucleophilic substitution of the appropriate alkyl halide with potassium *p*-toluenesulfonothiate **16.**

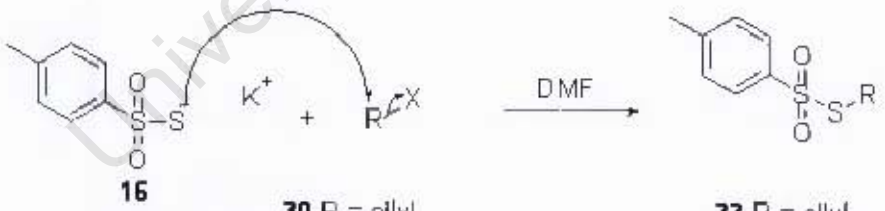

16

30 R = allyl
X = Br

31 R =propyl
X = Br

32 R =Methyl
X = I

33 R = allyl

34 R =propyl

35 R =Methyl

Scheme 26

In each case, **16** was dissolved in DMF and a solution of the appropriate halide as allyl bromide **30**, 1-bromopropane **31** or methyl iodide **32** added dropwise to the mixture. The reactions were then left stirring at room temperature for 3 h. Reactions could each be followed by tlc and at the end were quenched with saturated aq. sodium bicarbonate before extracting

revealed similar resonances for the common propylSallylS- core for each stereoisomer, and data for the various protons and carbons are given in Tables 6 (^{1}H) and 11 (^{13}C) respectively.

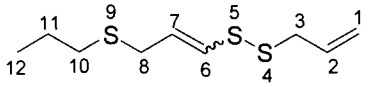

40

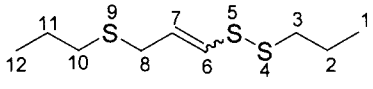

41

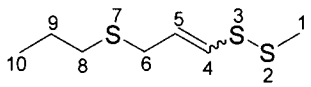

42

Table 6: ^{1}H NMR Diagnostic peaks for characterization of compounds **40, 41 and 42**

Position	Isomer	**40** ^{1}H δ; *Multiplicity; J*	**41** ^{1}H δ; *Multiplicity; J*	**42** ^{1}H δ; *Multiplicity; J*
10/8	*Z*	2.48, t, 7.3	2.47, t, 7.4	2.47, t, 7.4
	E	2.45, t, 7.3	2.43, t, 7.4	2.46, t, 7.4
8/6	*Z*	3.27, dd, 1.1,7.4	3.26, dd, 1.3, 7.4	3.26, dd, 1.0, 7.4
8/6	*E*	3.19, dd, 1.2, 7.7	3.17, dd, 1.3, 7.7	3.20, dd, 1.0, 7.4
7/5	*Z*	5.69, dt, 7.4, 9.7	5.66, dt, 7.4, 9.3	5.74, dt, 7.4, 9.3
	E	5.86, m	5.86, dt, 7.7, 14.8	5.90, dt, 7.4, 14.6
6/4	*Z*	6.23, dt, 1.1, 9.7	6.23, dt, 1.3, 9.3	6.24, dt, 1.0, 9.3
	E	6.11, dt, 1.2, 14.6	6.11, dt, 1.3, 14.8	6.11, dt, 1.0, 14.6
3/1	*Z*	3.37, m	2.70, t, 7.1	2.44, s
	E	3.35, m	2.68, t, 7.1	2.40, s

The ^{13}C NMR spectra for disulfides **40-42** showed a loss of the carbonyl group and the presence of new peaks for the allyl group of **40**, the propyl group for **41** and the methyl group for **42** as shown in Table 7.

Table 7: ^{13}C NMR Diagnostic peaks for identification of compounds **40, 41 and 42**

Position	Isomer	**40**	**41**	**42**
3	*Z*	42.1	41.1	–
	E	41.3	40.4	

Chapter 4 Results and Discussion

with DCM. The extracts were dried with $MgSO_4$ and the solvent reduced under vacuum. The residue in each case was then purified on a silica-gel column using 5% ethyl acetate in petroleum ether as eluent to give sulfenylating agents **33, 34** and **35** in 92, 92 and 96 % yield respectively as shown in Scheme 26. ^1H NMR spectroscopy of **33, 34** and **35** returned satisfactory and similar spectra regarding the aromatic protons. Simple integration of the aliphatic (**34** / **35**) or vinyl (**33**) to aromatic resonances appropriately gave the desired ratios. Similarly, ^{13}C NMR returned four aromatic resonances for each and the aromatic methyl group highfield in each case. The other signals tallied appropriately.

Sulfenylation of **29** with **33, 34** and **35** was carried out using the same set of experimental conditions as for reaction of thioacetate **14** to give compound **20** involving *S*-acetate cleavage at -78°C and sulfenylation up to room temperature as shown in Scheme 27.

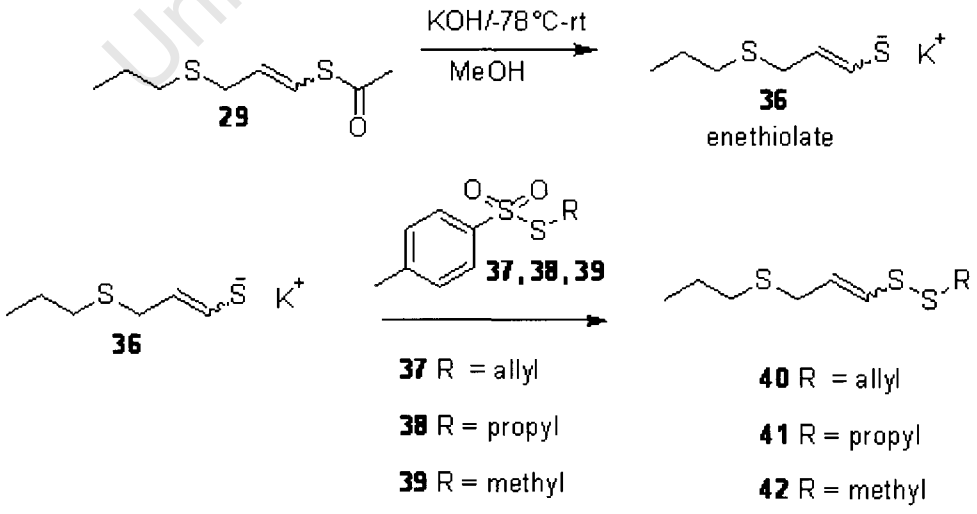

Scheme 27: Nucleophillic substitution of thioacetate

Reactions took 2, 4 and 3 h respectively after addition of the sulfenylating agents to complete and products **40**, **41**, **42** were obtained in 89 %, 76 % and 76% respectively based on

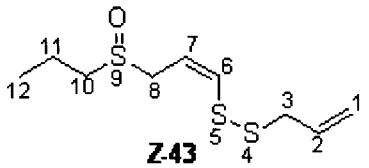

Z-43

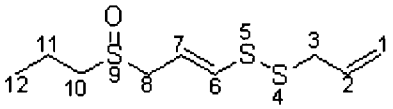

E-43

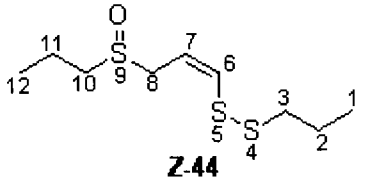

Z-44

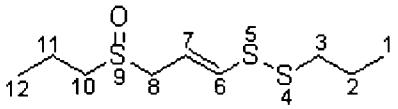

E-44

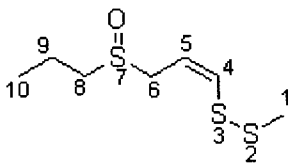

Z-45

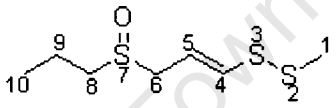

E-45

Figure 46

Each pair of geometric isomers (**43**, **44** and **45**) will be discussed separately highlighting important features that prove that oxidation did occur and that the site of oxidation was at the sulfur of the sulfide not the sulfur of the disulfide group. For compound **43**, the site of oxidation at the sulfide sulfur was indicated by downfield shifts of H-10 and H-8 (α- to the new sulfoxide grouping relative to those in the sulfide precursor **40**). Thus, H-8 shifted from 3.27 ppm to 3.56/3.63 for the *Z*-isomer and 3.19 to 3.43/3.51 ppm for the *E*-isomer. By comparison, those for H-3 α- to one of the disulfide sulfurs remained almost the same at 3.37 ppm and 3.35, Table 8. Secondly, the non-equivalence of the H-8 protons upon oxidation (shown by a split of H-8 hydrogens- a pair of doublet of doublets for each isomer) due to diastereotopicity of the chiral sulfoxide was observed.

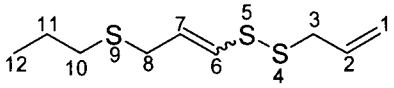

40

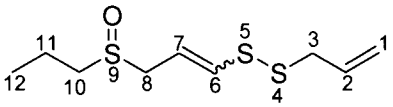

43

Table 8: ^{1}H NMR Comparison of diagnostic peaks of **40** and **43**

Position	Isomer	**40** ^{1}H δ; *Multiplicity; J Hz*	**43** ^{1}H δ; *Multiplicity; J Hz*
10	*Z*	2.48, t, 7.3	2.61/2.67, dt, 8.2, 13.7-Z_{AB}
	E	2.45, t, 7.3	2.61, m
8	*Z*	3.27, dd, 1.1, 7.4	3.56/3.63, dd, 8.1, 13.2 Z_{AB}
8	*E*	3.19, dd, 1.2, 7.7	3.43,/3.51, dd, 7.9, 13.2 E_{AB}
7	*Z*	5.69, dt, 7.4, 9.7	5.76, dt, 8.1, 9.2
	E	5.86, m	5.91, dt, 7.9, 14.6
6	*Z*	6.23, dt, 1.1, 9.7	6.54, d, 9.2
	E	6.11, dt, 1.2, 14.6	6.34, d, 14.6
3	*Z*	3.37, m	3.37, m
	E	3.35, m	3.33, m

The ^{1}H NMR of compound **44** also showed a similar pattern as compound **43**. The hydrogens α-to the sulfoxide both shifted downfield relative to the trisulfide precursor **41** as shown in Table 9. The influence of the chiral sulfur was observed by the splitting of H-8 indeed confirming the success of the chemoselective oxidation step. Prior to oxidation H-8 was enantiotopic showing a single doublet of doublets for each isomer.

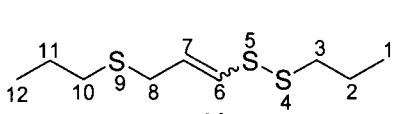

41

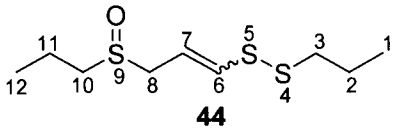

44

Table 9: ^{1}**H** Comparison of diagnostic peaks for **41** and **44**

Position	Isomer	**41** ^{1}H δ; *Multiplicity; J*	**44** ^{1}H δ; *Multiplicity; J*
10	*Z*	2.47, t, 7.4	2.65, m
	E	2.43, t, 7.4	2.65, m
8	*Z*	3.26, dd, 1.3, 7.4	3.52/3.63, dd, 7.46, 13.4 Z_{AB}
8	*E*	3.17, dd, 1.3, 7.7	3.45/3.52, dd, 7.8, 13.0 E_{AB}
7	*Z*	5.66, dt, 7.4, 9.3	5.75, dt, 7.6, 9.5
	E	5.86, dt, 7.7, 14.8	5.93, dt, 7.8, 15.0
6	*Z*	6.23, dt, 1.3, 9.3	6.56, d, 9.5
	E	6.11, dt, 1.3, 14.8	6.37, d, 15.0
3	*Z*	2.70, t, 7.1	2.65, m
	E	2.68, t, 7.1	2.65, m

The ^{1}H NMR of compound **45** also confirmed the success of the chemoselective oxidation of compound **42**. H-6 shifted (α- to the new sulfoxide grouping) from 3.26 ppm to 3.50 ppm. A further piece of supporting evidence came from the observation of non-equivalence of the H-6 protons (observed as a pair of double doublets for each of the geometrical isomers), as a result of diastereotopicity due to a chiral sulfoxide as with **43** and **44**. Prior to oxidation, H-6 was enantiotopic showing a doublet of doublets. Upon oxidation H-6 splits into two doublets of doublets as H-6a and H-6b as a result of geminal and vicinal couplings. This evidence also eliminated the possibility of oxidation at S-3/S-2. In such a case, oxidation of the disulfide to an allicin-like thiosulfinate would have made the molecule very labile. Also, the IR spectra confirmed the presence of an intact S-S grouping via a stretch at around 460 cm^{-1}. The resonances for compound **45** are tabulated in Table 10 in order to compare them with the trisulfide precursor of the previous step.

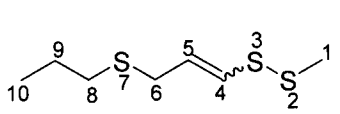

42

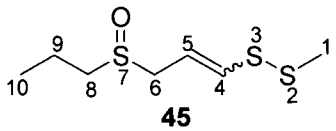

45

Table 10: ^{1}H Comparison of diagnostic peaks for 42 and 45

Position	Isomer	**42** ^{1}H δ; *Multiplicity; J*	**45** ^{1}H δ; *Multiplicity; J*
8	*Z*	2.47, t, 7.4	2.58, m
8	*E*	2.46, t, 7.4	2.65, m
6	*Z*	3.26, dd, 1.0, 7.4	3.50/3.59, dd, 7.7, 13.2 Z_{AB}
	E	3.20, dd, 1.0, 7.4	3.44, m
5	*Z*	5.74, dt, 7.4, 9.3	5.77, dt, 7.7, 9.3
	E	5.90, dt, 7.4, 14.6	5.90, dt, 7.4, 14.8
4	*Z*	6.24, dt, 1.0, 9.3	6.55, d, 9.3
	E	6.11, dt, 1.0, 14.6	6.33, d, 14.7
1	*Z*	2.44, s	2.41, s
	E	2.40, s	2.36, s

Further evidence was provided by the ^{13}C NMR spectra, which also revealed significant downfield shifts for C-8 and C-10 (for compounds **43** and **44**) or C-6 and C8 for compound **45** (Table 11).

Table 11: ^{13}**C** Diagnostic peaks for identification of compound **43, 44 and 45** and their precursors.

Position	Isomer	**40, 43**	**41, 44**	**42, 45**
8/6	*Z*	29.5 , 50.9	29.4, 50.9	29.4, 50.8
	E	33.5 , 54.7	33.5, 54.5	33.5, 54.6
10/8	Z	33.4 , 53.5	33.1, 53.4	33.3 , 53.4
	E	33.1 , 53.0	32.9, 53.1	33.1 54.6

The IR spectra of **43, 44** and **45** also showed a peak due to the sulfoxide 1300 cm^{-1}. Mass spectrometry also showed that the above compounds were synthesized. For instance, the

mass-spectrum for compound **44** showed a dominant peak at 146.0211 consistent with elimination of PrSOH (propylsulfenic acid), [M' - PrSOH; expected mass = 146.0224].

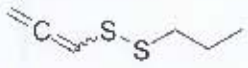

Chemical Formula: $C_6H_{10}S_2$
Exact Mass: 146.0224
m/z: 146.02 (100.0%), 148.02 (9.0%), 147.03 (6.6%), 147.02 (1.6%)
Elemental Analysis: C, 49.27; H, 6.89; S, 43.84 $= C_6H_{10}S_2$]

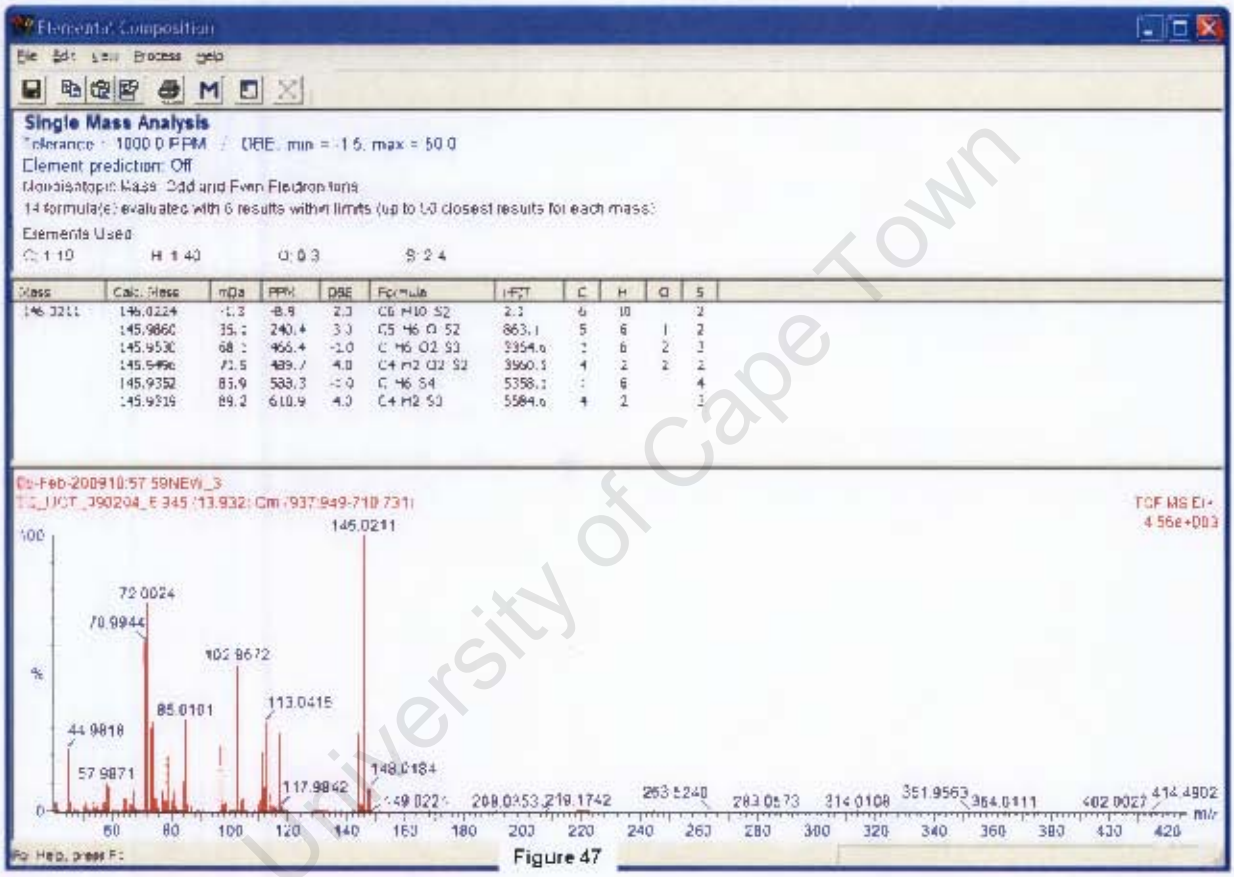

Figure 47

In conclusion, the UCT reaction sequence was successful in the synthesis of a small library of ajoene derivatives. It has been shown that changes can be either in one allyl group or both groups. The vinyl sulfide pharmacophore was not changed for all the derivatives. The overall yield of the four-step sequence for each case was in the range 25-47 %. After a successful synthesis of these derivatives, inclusion of the synthesized ajoene derivatives into cyclodextrin was attempted (Chapter 5). This was then followed by biological evaluation of the ajoene derivatives as anti-cancer agents, which is discussed in Chapter 6.

5.1 Cyclodextrins

5.1 Natural Origins

The enzymatic degradation of starch results in the production of glucose, maltose, maltotriose and other saccharides, that is a long series of linear or branched-chain malto-oligomers known as dextrins.[90] Dextrins are heterogeneous, amorphous and hygroscopic substances which are produced in large quantities in food such as bread or beer or as textile paper.[91] The degradation of such starch is a hydrolytic process and the primary product from this hydrolysis of the glycosidic linkage reacts with water. The enzyme responsible for degradation of the starch is glucosyltransferase enzyme (cGT which is produced by micro-organisms *Bacillus macerans, Klebsiella oxytoca*), and in this enzymatic process the primary product of chain splitting undergoes an intramolecular reaction without the participitation of a water molecule.[90,91] Since these enzymes are not specific the outcome is the formation of variable α-1,4-linked cyclic products called cyclodextins.

5.2 Historical origins

In 1891 Villiers reported the formation of some unidentified crystalline substances during the fermentation of starch in the presence of *Bacillus amylobacter*. He assumed the substance to be cellulose and named it cellulosine.[92] Fifteen years later Franz Schardinger, an Austrian microbiologist, isolated a microorganism named *Bacillus Macerans* which produced two distinct reproducible crystalline substances when cultivated on starch-containing medium.[93] He then named the dextrins α- and β-dextrins. These names were proposed due to the fact that degradation of these substances was similar to degradation of starch products. It was in 1936 that Freudenberg and co-workers determined the structure of these dextrins.[94-96] Freudenberg postulated the crystalline structure to be formed of maltose units joined by α-1,4-glycosidic linkages. In 1950 two groups led by French and Cramer did further analysis on these dextrins. French discovered that there are even larger CDs, while Cramer focused on inclusion work. In 1953 Freudenberg, Cramer and Plieninger obtained a patent on CDs describing application and toxicity in drug formulation.[94] In 1981 the first international symposium was organised where scientists would have the opportunity to summarize the most recent results. Since then symposia have been held every second year and presentations have increased in both quantity and quality.[97-101] Today CDs are relatively inexpensive materials and very important industrial commodities in many ways.

5.3 Structural features of cyclodextrins

The three major native cyclodextrins are α-, β- and γ-cyclodextrins as shown in Figure 48 below. These are macrocyclic oligosaccharides containing 6, 7 and 8 α-1,4-linked D-glucopyranose rings respectively. The shape resembles that of a hollow truncated cone. As a consequence of the $^4C_1$ conformation, the narrow rim is lined with primary hydroxyl groups and the wider rim with twice as many secondary hydroxyl groups.[93]

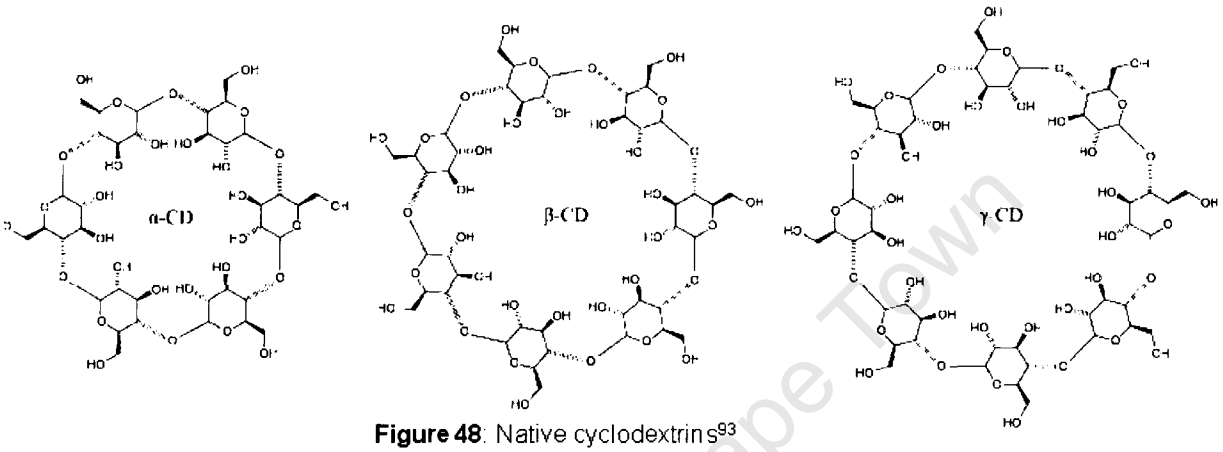

Figure 48: Native cyclodextrins[93]

The cavity is lined with hydrogen atoms and glycosidic oxygen atoms. The nonbonding glycosidic oxygen electron pair is directed towards the cavity; this arrangement increases electron density in the cavity resulting in its Lewis base character.[93] Therefore the internal cavity is hydrophobic relative to the hydrophilic exterior portion.

5.4 Torsion angles and Macrocyclic geometry

French noted a correlation between the O4(n)...O4(n-1) distance and certain endocyclic torsion angles in several pyranoses.[102] Figure 49 shows a three dimensional structure of a β-CD. The conformation is stabilized by C-H...O H-bonds. The average planes of the glucose molecules are not perpendicular to the O(4) plane but incline mostly with the O(6) side towards the inside of the macrocycle. The angle of inclination is referred to as the tilt angle.[102]

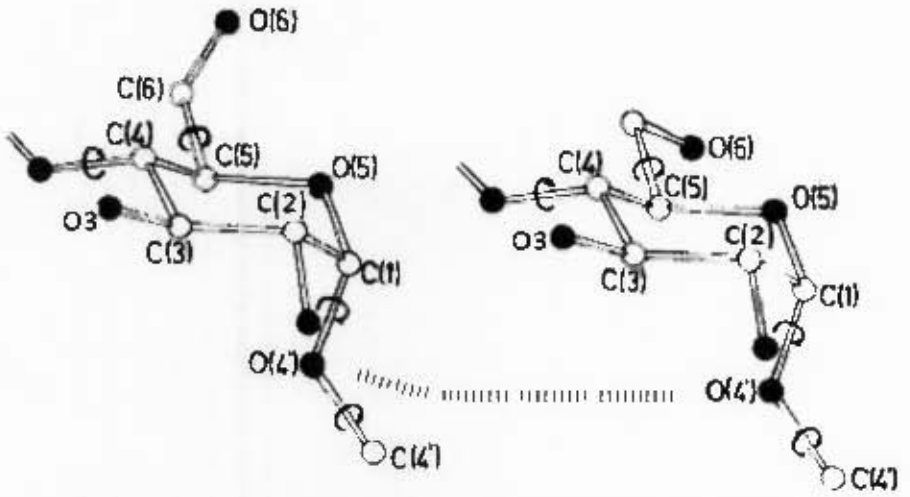

Figure 49:Geometric structure of a pyranose unit of a cyclodextrin, (-)-*gauche* (left), (+)-*gauche* (right) orientations Hydrogen atoms are omitted for clarity[89]

The O4(n)·····O4(n-1) distances are almost the same in all CDs. In line with these observations the distribution of O4(n) ·····O4(n-1) ·····O4(n-2) angles were found to be 120° for α-CDs, 128° for β-CDs and 135° for γ-CDs. In principle there are three orientations of the C6-O6 bonds in glucose units, corresponding to dihedral angles O5-C5-C6-O6 that are (+)-*gauche*, (-)-*gauche* and *trans*-orientation, yet only the first two have been observed thus far as shown in Figure 49. The *trans*-orientation could also be destabilised by the *gauche*-effect operating in the O-C-C-O systems.[102]

5.5 Hydrogen bonding

Structural rigidity of the cyclodextrin macrocycle is primarily due to the presence of a ring of hydrogen bonds. It was found that the intramolecular hydrogen bonding is formed between a C-2-OH group of one glucopyranose unit and a C-3-OH group of the adjacent glucopyranose unit.[89] β-CD forms a complete H-bond belt, whereas α-CD forms an incomplete belt. Therefore, α-CD has four intramolecular hydrogen bonds instead of six. Since β-CD forms a complete belt, this intramolecular H-bonding explains the observation that β-CD has the lowest water solubility of all the CDs. The average O...O distance for hydrogen bonding between cyclodextrins is not constant but decreases from one CD to the next, α-CD (2.98Å), β-CD (2.88 Å) and γ-CD (2.82 Å). This decrease in distances indicates that H-bonds become increasingly stronger as the number of glucopyranose rings increases. The O2(n)·····O3(n-1) hydrogen bonds are the major component of H-bonding, of which the minor component donates to the oxygen of the glycosidic atom.[103] This character contributes to the rigidity as it strengthens the O2(n)·····O3(n-1) hydrogen bonding interactions. The weak intramolecular hydrogen bond O6-H·····O5 represents the minor component of hydrogen bonding

interactions. Sometimes these interactions are mediated by water molecules as in, for example, O6·····W·····O5, where O6 and O5 belong to the same glucose unit.

5.6 Cyclodextrin derivatives

As previously shown, every glucopyranose unit has three free hydroxyl groups which differ both in their functions and reactivity. This is determined by the pH, temperature and solvent. In β-CD there are 21 hydroxyl groups which can be modified by a large variety of substituting groups such as alkyl, hydroxyalkyl, carboxyalkyl and amino as shown in Figure 50 below. These derivatives can be made by either chemical or enzymatic reactions.

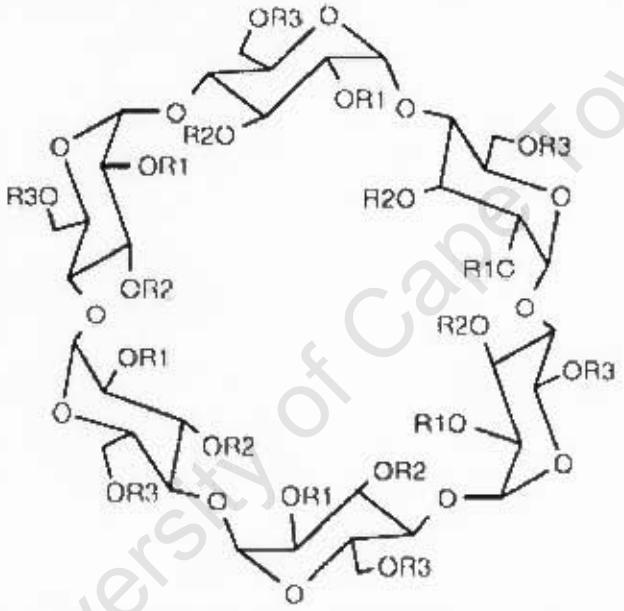

Figure 50: Skeleton of a cyclodextrin derivative

The primary purpose of these modifications is to improve the solubility of CD derivatives, to improve the fitting of a guest molecule, to attach specific (catalytic) groups to the binding site (e.g enzyme modelling) and to form insoluble, immobilised CD-containing structures, polymers e.g for chromatographic purposes. The most important β-CD derivative is the heterogeneous, amorphous and highly water soluble β-CD derivative. This can be methylated or propylated to form methylated β-CD or 2-hydroxypropylated β- CDs. Methylated β-CDs are more hydrophobic than β-CD itself. Therefore they form more stable soluble complexes with cholesterol. Some of these CDs are heptakis (2,6-di-O-methyl)-β-cyclodextrin (DIMEB), heptakis(2,3,6-tri-O-methyl)-β-cyclodextrin (TRIMEB) and randomly methylated-β-cyclodextrin (RAMEB). Of these, RAMEB is the least expensive since it is relatively easily prepared.

5.7 Crystal packing arrangements of Cyclodextrins and their inclusion complexes

For crystallization of an inclusion complex of a CD one has to add the guest molecule in order to form a complex. In crystals, the molecules are arranged in a lattice in either of two modes, described as cage and channel structure according to the overall appearance of the formed cavities.

5.7.1 Channel-type structures

In this motif, cyclodextrins are stacked on top of each other like coins in a roll and linearly aligned cavities form 'infinite channels, in which the guest molecules are embedded, as shown in Figure 51.[103]

Figure 51 Channel-type packing

The stacks are stabilized by hydrogen bonds between the secondary O2-H/O3-H and the O6-H sides producing head-to-tail patterns or between O2-H/O3-H and O2-H/O3-H on one side and between O6-H and O6-H on the other side leading to a head-to-head arrangement.[103] β-CD can be arranged in such a way that the molecules stack to form dimers, hydrogen bonded at their O2-H/O3-H sides. They form basket-like units in which the guest molecules are accommodated. The dimers are then stacked and interact with their O6-H sites to form the channel structure.

5.7.2 Cage-type structures

This type of structure may exist as herringbone or brick motifs. The herringbone motif is packed in such a way that one CD molecule is blocked off on both sides by adjacent CDs thereby leading to isolated cavities in which guest molecules are not in contact with each other, as shown in Fig 52a.

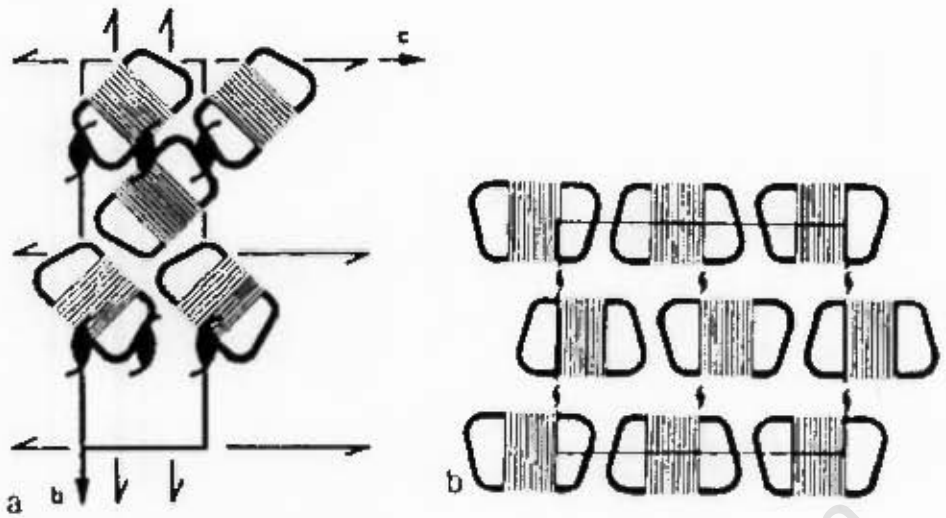

Figure 52:Two Cage-type packing arrangements, **a.** herringbone motif **b.** brick motif[102]

The 'brick' motif is analogous to the stacking of bricks in a wall. The CD molecules are arranged in layers and adjacent layers are laterally displaced so that the cavity of each CD is closed on both sides by molecules in adjacent layers, as shown in Fig 52b.[103] This motif can also assume variations, in which dimer 'baskets' are stabilized intermolecularly by hydrogen bonding between the O2-H/O3-H sides and arranged in layers which are displaced laterally.

5.8 Applications of Cyclodextrins

Cyclodextrins have been used in various industries for a wide range of purposes such as incorporation in items ranging from chewing gums to detergents.[104,105] They are also used in everyday products such as shampoo and toothpaste.[105] The ability of CDs to incorporate guests within their cavity has been advantageous in many applications.[106] They are used to control solubility, mask agents, provide stabilization and also solubilise hydrophobic compounds in aqueous media.[107,108] For example, hespiridin is a compound responsible for both the visible cloudiness and bitter taste in canned oranges. Yasumatsuk and co-workers discovered that the addition of a CD reduced both the cloudiness and bitter taste of hespiridin.[109] An increase in the solubility of a drug generally increases its bioavailability. Itraconazole, an anti-fungal drug, is ineffective when administered alone. However the complex of itraconazole with hydroxypropyl-β-CD shows increased bioavailability due to its increased solubility.[106] Cyclodextrins have also been used to mask unpleasant flavours/smell in deodorants and lotions as well as menstrual products, diapers, tissues and paper towels.[108,110] Reduction of volatility of compounds through complexation has been used in controlled-released applications. When a detergent containing a perfume/CD complex is dissolved in water, some of the detergent molecules, which occupy the CD cavity

preferentially, replace the perfume and release the fragrance. CDs can also incorporate pesticide molecules in order to improve their wettability.[107]

5.9 Inclusion complexation

Inclusion complexation is the largest area of interest in cyclodextrin research. The majority of cyclodextrin complexation studies are performed in aqueous environments in order to prevent competition with a guest molecule in non-aqueous solution. Szejtli and Connors proved that the complexing strength of a cyclodextrin is a result of hydrophobic-hydrophobic interactions between the guest and the host.[107,111,112] Cramer and co-workers were the first to employ CDs as catalysts in synthetic reactions. They explained the mechanism whereby a cyclodextrin acts as an enzymatic model.[94] Since then there has been a tremendous interest in cyclodextrins as biological catalysts, especially as dual phase catalysts and they are also used in the hydrolysis of phosphate esters.[97-104] Phosphate esters are the most toxic esters and there has been tremendous need to use cyclodextrins for their hydrolysis. The paper by Trotta and coworkers reports an investigation of P-O hydrolysis under green chemistry conditions.[116] This was investigated using *p*-nitrophenyldiphenyphosphate (PNPDPP) as a substrate and a membrane reactor with β-CD derivatives as the host.[117] The hydrolysis of PNPDPP to PNP (*p*-nitrophenol) was then investigated. This was made possible by creating two environmental conditions, a homogeneous and a heterogenous environment as described in the paper. For the homogeneous environment, *p*-nitrophenol (PNP) concentration was recorded spectrophotometrically at 401 nm using a 1-cm quartz cell at room temperature. Samples of both the heterogeneous and homogeneous reactions were taken and measured to ascertain PNP concentration. In the homogeneous reaction, it was shown that separation of the product from the catalyst was difficult. This problem has recently been solved by immobilizing cyclodextrins on suitable cross-linked polymers.[118] Heterogeneous-mixture conditions proved that it is not possible to separate the product from the catalyst when using native cyclodextrins, as shown in Figure 53.

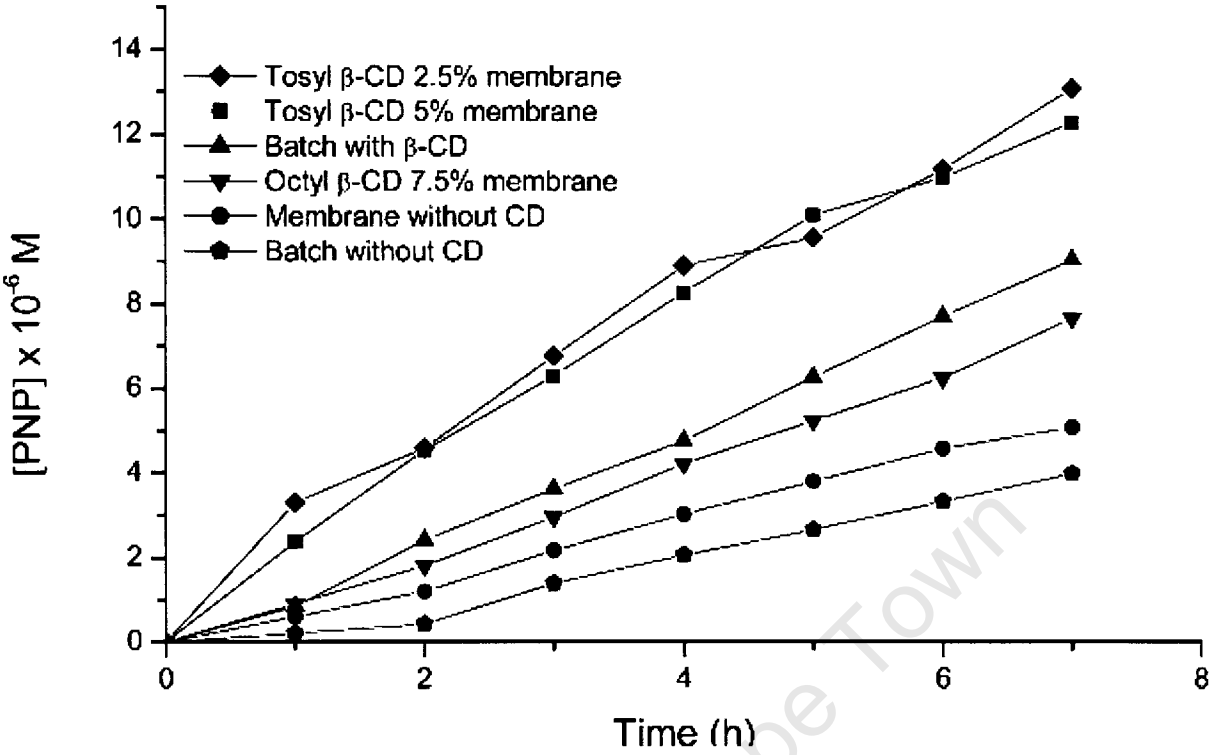

Figure 53: Showing hydrolysis of PNPDPP to PNP with a variety of β-CD derivatives

Figure 53 shows that the hydrolysis of P-O in PNPDPP to PNP is dependent on the nature of the β-CD derivative used and it was also observed that very little hydrolysis occurred in a membrane without cyclodextrin. Inclusion complexation has also been employed to increase guest stability. One example, from our laboratory, is the stabilisation of a derivative of allicin via its inclusion in permethylated β-CD (TRIMEB). Whereas the derivative is chemically unstable at room temperature, when it is included in the TRIMEB molecule it is stable at temperatures higher than 50 °C.

5.10 Complex characterization

Cyclodextrins and cyclodextrin inclusion complex have been characterized by different techniques including NMR analysis, calorimetry and TGA, X-ray diffraction methods, electric field pulse techniques, volumetric techniques, electron microscopy, circular dichroism and electron resonance (ESR and EPR).[100] From NMR spectra it is possible to distinguish protons located on either the exterior or the interior of the truncated cone and those of the guest.[120] Inclusion complex stoichiometries are elucidated either by TGA or NMR analysis. For crystalline CD hosts and their inclusion complexes, powder and single X-ray diffraction techniques yield detailed information concerning the host-guest interaction. Complex stability constants and the dynamics of inclusion are best determined using solution NMR techniques.

6.1 Attempted preparation of inclusion complexes of an ajoene mimic with β-cyclodextrin, γ-cyclodextrin and TRIMEB; physicochemical characterization of the TRIMEB complex

6.1.1 Host compounds

The host compounds β-CD, γ-CD and TRIMEB were obtained from Cyclolab [Budapest, Hungary] and were used as received.

6.1.2 Guest compound

A mixture of *Z/E* 10-(methoxyphenyl)-9-oxo-4,5,9-trithiadeca-1,6-diene stereoisomers was synthesized in Prof Roger Hunter's laboratory using the synthetic procedure developed at the University of Cape Town as described in detail in chapter 2.

6.1.3 Complex preparation and crystal growth

Inclusion complexes of 10-(4-methoxyphenyl)-9-oxo-4,5,9-trithiadeca-1,6-diene with TRIMEB, β-CD and γ-CD were prepared by the co-precipitation method. For the co-precipitation method, a known quantity of TRIMEB (136.40 mg, 0.095 mmol) was dissolved in 2 cm^3 distilled water. An equimolar amount of guest (30.00 mg, 0.095 mmol) was then added and the solution was left stirring at 0°C for 6 h. The cold solution was then filtered into a clean vial using a 0.25 μm Teflon Millex-LCR filter in order to remove dust and debris, thereby reducing nucleation sites. The vial was closed with a lid, two small holes were made on the lid, and the cold solution was placed in the oven at 50°C and left there overnight. The following day, colourless prismatic crystals of the TRIMEB inclusion complex were present at the top and bottom of the vial. The prismatic shape of the crystals was the same throughout. β-CD (123.8 mg, 0.095 mmol) was dissolved in 2 cm^3 distilled water while γ-CD (134.1 mg, 0.095 mmol) was dissolved in 2 cm^3 distilled water at 65 °C. Once all the CD had dissolved, an equimolar amount of the guest (30.00 mg, 0.095 mmol) was added to the solution followed by vigorous stirring for 4 h. The solution was filtered (0.45 μm) and left at room temperature to induce crystallization. However, no evidence of crystalline inclusion complex formation with either of the parent cyclodextrins was found using the above conditions.

6.2. Complex characterization methods

6.2.1 Powder X-ray diffraction

A representative sample of crystals of the TRIMEB inclusion complex from the top and bottom of the vial was removed from the hot mother liquor and dried. This sample was then ground at room temperature for 1 h in an agate mortar in order to compare its PXRD trace with those of

known complexes. This was packed in an aluminium holder and a powder X-ray diffraction pattern was recorded using a Huber Imaging plate Guinier camera 670 with Nickel-filtered $CuK_{\alpha 1}$ radiation (λ = 1.5405981 Å) produced at 40 kV and 20 mA by a Philips PW1120/00 generator fitted with a Huber long fine-focus tube PW 2273/20 and a Huber Guinier Monochromator Series 611/15. The pattern was recorded at steps of 0.005° over the 2Θ range of 5-40°.

6.2.2 Single crystal X-ray diffraction

A single crystal of the TRIMEB inclusion complex of size 0.15 x 0.16 x 0.26 mm was coated with paratone oil (Exxon, USA) and mounted on a Nonius Kappa CCD diffractometer for intensity data-collection with MoKα X-rays (λ = 0.71073 Å). The crystal was cooled to 113 ± 2 K in a stream of nitrogen vapour to enhance diffraction quality and intensity data were collected using Φ- and ω-scans of 1.0° and 1.2 °C (program COLLECT).[113] Unit cell refinement and data reduction were performed with DENZO-SMN[121] and the structure was solved by isomorphous replacement using the rigid skeleton of the host molecule of the TRIMEB·(*Z*)-ajoene complex as a trial model.[114] All remaining non-H atoms of the host and guest were located in successive difference electron density maps. Guest electron density peaks could be interpreted as representing the *E*-isomer only, with the sulfonyl group indicating only one enantiomer. All the non-hydrogen atoms of the host were refined anisotropically while the guest atoms were treated isotropically. H atoms were added in idealized positions in a riding model with isotropic thermal parameters equal to 1.2-1.3 times those of their parent atoms. Full-matrix least-squares refinement on F^2 was performed using the programme SHELXL-97[115] with weights of the form $w = [\sigma^2 (F_0^2) + (aP)^2 + bp]^{-1}$ and $P= [\max(F_0^2, 0) + 2F_0^2]/3$.

6.2.3 Differential Scanning Calorimetry (DSC)

DSC was used to measure the melting point of the TRIMEB complex. This was performed using a Perkin Elmer PC7 system under N_2-purge (flow rate 30 cm^3/min). The instrument was calibrated with high purity indium and zinc standards. A 4.03 mg sample of the inclusion complex was scanned at 10 K/min over a range of 30-300 °C using a vented pan.

6.2.4 Hot Stage Microscopy (HSM)

HSM was used as a visual tool to determine thermal events of the sample during the heating process. Events such as colour or opacity changes in crystals which go undetected by the DSC method are easily detected with HSM. The crystals of the inclusion compound were heated on a Linkam THMS600 hot stage mounted on a Nikon SMZ-10 stereoscopic microscope, on which a Nikon FX-35 camera was mounted for simultaneous photography. The temperature was controlled by a Linkam TP92 temperature controller and was raised manually at a linear rate. The images were captured using a soft Imaging System camera and analysed using analySIS® Image software (Soft Imaging System program analysis).[122]

6.2.5 Nuclear Magnetic Resonance (NMR) Spectroscopy

To obtain a reliable estimate of the host-guest ratio of the TRIMEB inclusion complex, it was decided to use ^{1}H NMR spectroscopy of a sample prepared by dissolving crystals of the inclusion compound in an appropriate solvent. Thus, a sample of crystals was removed from the mother liquor and dried on a filter paper to remove excess solution. It was also necessary to wash the crystals to remove any residual guest material (in the form of an oil) that might not have included in the cyclodextrin host. Cold solvents with different polarities were used. These included acetonitrile, water, hexane and acetone. Hexane was the best solvent for washing as it did not dissolve the complex. The crystals were weighed before washing and reweighed after washing and there was a noticeable mass loss due to the surface guest being removed. The washed product (5.00 mg) was dried on a filter paper and dissolved in $CDCl_3$ and this solution was then submitted for ^{1}H NMR analysis. TRIMEB (5.00 mg) and the guest (10.0 mg) were also submitted separately for ^{1}H NMR analysis for comparison.

Chapter 7: Results and discussion

This chapter discusses visual and analytical methods used to confirm complex formation. These methods included Powder X-ray diffraction (PXRD), Hot Stage Microscopy (HSM), Differential scanning calorimetry (DSC), and Single Crystal X-ray diffraction methods. The results from the analysis revealed that inclusion of the guest was only possible with TRIMEB.

7.1 Powder X-ray Diffraction Studies

Complex Preparation

Co-precipitation method: β-CD was dissolved in 2 cm^3 distilled water and γ-CD was also dissolved in 2 cm^3 distilled water at 65 °C. Once all the CD had dissolved, an equimolar amount of the guest as a mixture of E/Z-isomer was added to the solution followed by vigorous stirring for 6 h at 65 °C. Table 12 shows the amounts of guest and host used in the co-precipitation method. The solution was filtered (0.45 μm) and left at room temperature to induce crystallisation. However, the permethylated host TRIMEB was dissolved in 2 cm^3 distilled water at 0° C, and an equimolar amount of the guest as a mixture of E/Z-isomer was added and left stirring vigorously at 0° C for 6 h. The solution was then filtered (0.45 μm) and incubated at 50° C to induce crystallization.

Table 12: Molar quantities for complex preparation

Guest (mg, mmol)	β-CD (mg, mmol)	γ-CD (mg, mmol)	TRIMEB (mg, mmol)
10-(4-Methoxyphenyl)-9-oxo-4,5,9-trithiadeca1,6-diene (30.0, 0.095)	123.8, 0.095	134.1, 0.095	136.4, 0.095

Suitable crystals of an inclusion complex were obtained only with the host TRIMEB. A batch of crystals was scooped out of the crystallization vial, dried and ground for 1 h for comparison of its PXRD trace with those of known complexes The PXRD pattern of the crystalline product was compared with PXRD patterns of the crystalline host (TRIMEB, existing in three distinct crystal forms) and those of the isostructural reference patterns for known TRIMEB complexes. This revealed that the product was not the host compound. However, an acceptable match of the PXRD trace with that of a known isostructural TRIMEB complex series (BD 3) was obtained, as shown in Figure 54.

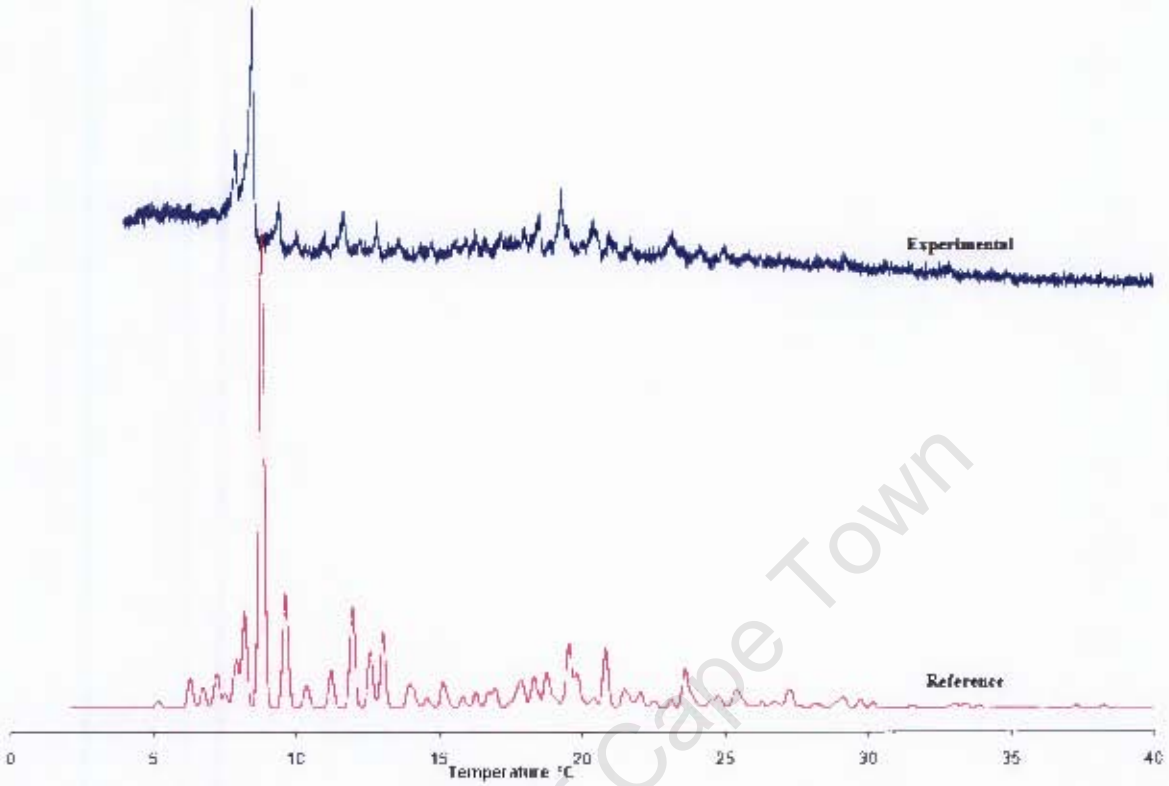

Figure 54: Experimental PXRD trace for the product of co-precipitation of TRIMEB and the guest (top) and a computed reference pattern for a known isostructural complex series (bottom).

This agreement reveals the isostructural relationship between the complex and those of series BD3. Isostructurality refers to two or more crystalline phases sharing the same three-dimensional packing arrays, with similar unit cell dimensions and internal molecular arrangements.[123] As observed from the PXRD traces, the experimental and reference peak positions and intensities are not identical. This is due to the fact that the reference trace is the average pattern for a series of complexes with different crystal water contents, types of guest present, size and orientation of the guest molecules as well as the temperatures at which the respective data were collected. However, using this technique of crystal characterization the level of agreement, especially as regards peak angular positions are concerned, is good. The predicted space group and unit cell dimensions, based on the PXRD match that indicates isostructurality, are shown in Table 13 below.

Table 13: Estimated unit cell data for the TRIMEB complex based on isostructural analogy

Space Group	Isostruc. Class	a (Å)	b (Å)	c (Å)	α (°)	β (°)	γ (°)
$P2_12_12$	BD3	14.8	21.5	27.9	90.0	90.0	90.0

7.2 ^{1}H NMR Analysis

Representative complex crystals were scooped from the vial and washed with cold acetonitrile before dissolving them in chloroform and submitting them for ^{1}H NMR analysis. TRIMEB was also dissolved in chloroform and submitted for ^{1}H NMR analysis. All the diagnostic peaks for TRIMEB (112 hydrogens) were observed in the NMR spectrum, as shown in Figure 55.

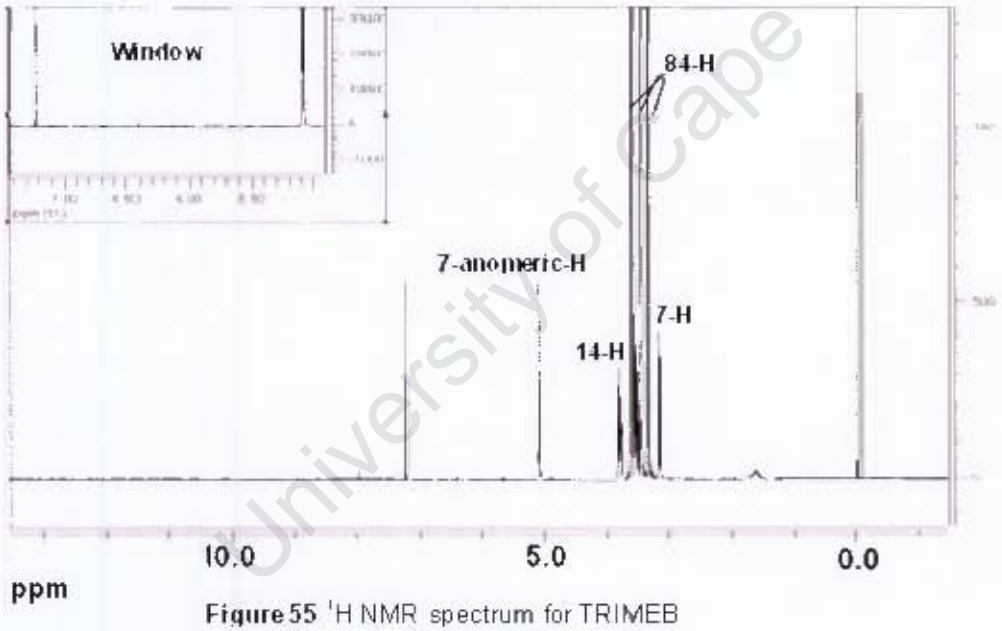

Figure 55 ^{1}H NMR spectrum for TRIMEB

A window-like area was observed between 5.0 ppm and 7.2 ppm which was not found in the batch of the complex as shown in Figure 56.

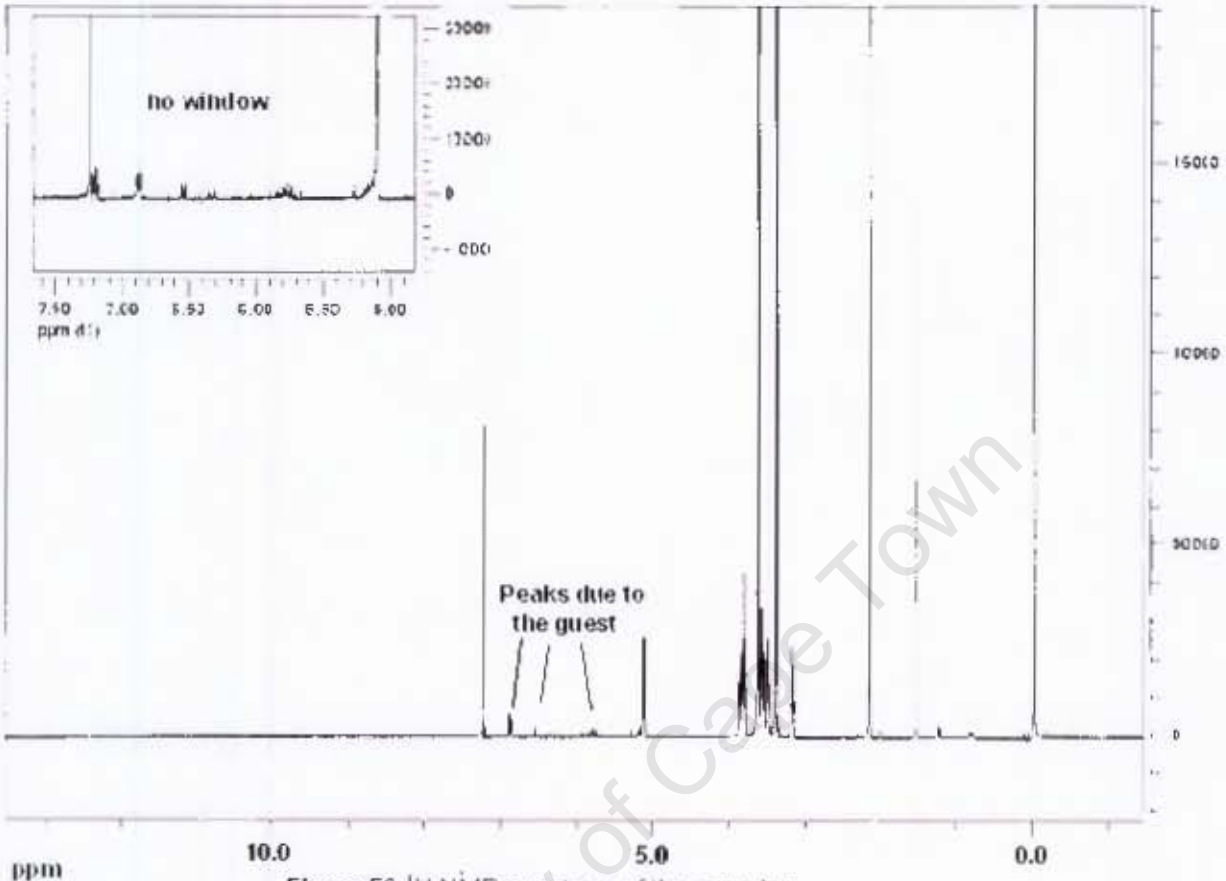

Figure 56: ^{1}H NMR spectrum of the complex

Both guest and host peaks were observed in Figure 56 confirming that the guest was successfully included in TRIMEB. The ^{1}H NMR was consistent with results from the synthesis that showed a 2:3 *Z/E*-isomer ratio, although the single crystal that was selected for the X-ray diffraction study was the *Z*-isomer.

7.3 HSM Analysis

HSM is used as a visual tool to study the morphology and physical changes of a crystal as it is heated over a given temperature range. Changes detected can be related to physicochemical events such as guest release (and/or dehydration in the case of hydrated complexes), melting, and complex decomposition. Crystals were dried, immersed in silicone oil and heated at a scanning rate of 10 K min^{-1}. The clear, prismatic crystal did not show any morphological changes between room temperature and 150 °C. In the range 154.5-155.1 °C the crystal melted as shown in Figure 57 below

Figure 57: HSM-behaviour of a crystal of the TRIMEB inclusion complex during heating. The crystal is immersed in silicone oil.

The HSM findings are in agreement with the conclusions from the DSC analysis (below) that the crystal is unsolvated and that the melting point is about 154°C.

7.4 DSC Analysis

For DSC analysis, the sample was crushed, the excess water being removed by drying the sample on filter paper. The scan is shown in Figure 58 below.

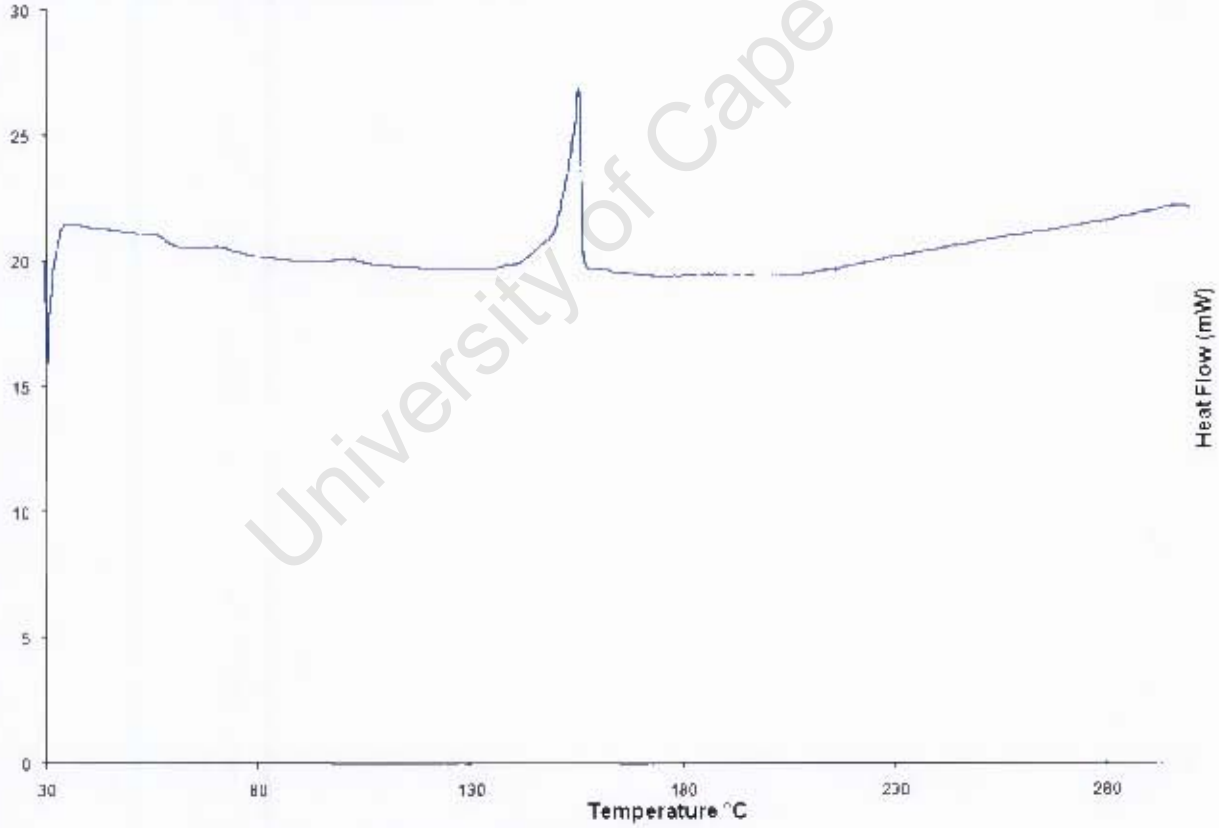

Figure 58: DSC trace of the TRIMEB inclusion complex

From the DSC trace, the only endotherm observed occurred at 155.4 °C and was attributed to melting. The lack of significant endotherms prior to fusion shows that the crystal is unsolvated.

7.5

Complex Formula	$(C_{63}H_{112}O_{35}).(C_{14}H_{18}S_3O_2)$

Crystal Structure Analysis

7.5.1 Space Group Determination, Structure Solution and Refinement

Preliminary unit cell parameters and the space group were obtained form intensity data measured on a Nonius Kappa CCD diffractometer. Identification of the Laue symmetry of the reciprocal lattice as *mmm* indicated the orthorhombic system while the systematically absent reflections revealed that the space group of the complex is $P2_12_12_1$, as predicted from the PXRD trace (Section 7.1). The structure of the complex was solved by isomorphous replacement using published co-ordinates of the host molecule in the known TRIMEB·(Z)-ajoene complex.[99] Refinement of the host molecule followed and the atoms of the guest were located in subsequent difference Fourier syntheses. Anisotropic thermal parameters were employed for the host atoms. Bond length constraints were applied to the guest molecule to maintain reasonable geometry and the guest atoms were refined with a global isotropic thermal parameter. The structural solution confirmed that the crystal is unsolvated, as inferred from the HSM and DSC analyses. Crystal data and refinement parameters are shown in Table 14 below.

Formula weight	1743.89 g/mol
Temperature / K	113(2)
Crystal system	Orthorhombic
Space group	$P2_12_12_1$
a / Å	14.7900(2)
b / Å	21.4857(2)
c / Å	27.9036(4)
Volume / $Å^3$	8867.0(2)
Z	4
Density (calc.) / g cm^{-3}	1.306
Radiation, wavelength MoKα / Å	0.71073
Absorption coefficient / mm^{-1}	0.17
F(000)	3744
Theta range /°	1.00-25.03
Index ranges	-17=<h=<17, -25=<k=<25, -33=<l=<33
Reflections collected	108965
Observed reflections [I>2σ(I)]	94897
Data/restraints/parameters	15583/2/892
Final R indices [I>2σ(I)]	0.1023
R indices (all data)	0.1946
Largest diff. peak and hole/ $eÅ^{-3}$	-0.60, 0.79

Table 14: Crystal Data, Data Collection Parameters and Refinement Details for the complex

7.5.2.2 Mode of Guest Inclusion

A perspective view of the complex structure is shown in Figure 59, with the host in ball-and-stick mode and the guest in space-filling representation. The guest molecule adopts a hairpin conformation with the sulfoxide moiety located near the cavity 'roof' and the methoxyphenyl and allyl residues directed towards the secondary rim of the host molecule. The guest molecule, with H atoms removed, is drawn separately on the right in the Figure below. It is evident that in the crystal selected, the inclusion complex comprises one host molecule and one guest molecule, the latter being the *R*-enantiomer of the two enantiomers of the *Z*-isomer.

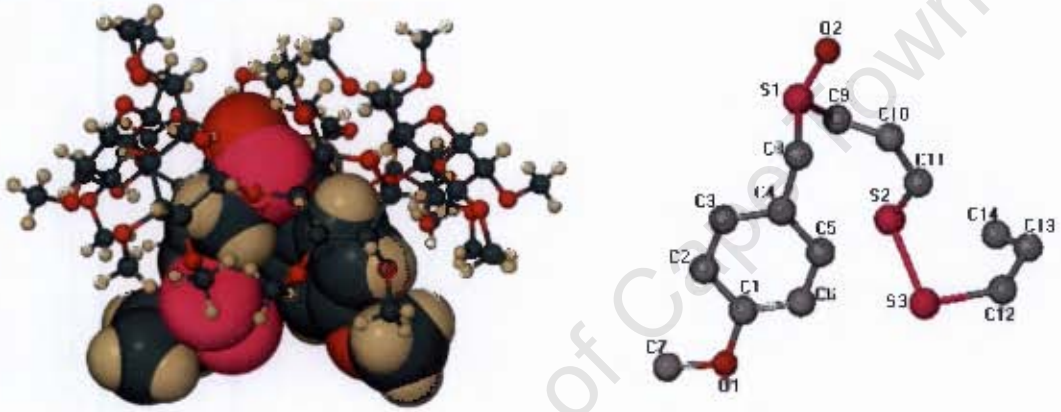

Figure 59: The 1:1 inclusion complex (left) and an enlarged view of the guest molecule (right). H atoms have been omitted for clarity.

There is no significant molecular disorder in the complex (a somewhat unusual feature for an inclusion complex of this type) and no evidence was found for included water molecules. No hydrogen bonding between host and guest was indicated from a detailed analysis of the host-guest interactions and it is thus concluded that the guest is exclusively stabilized in the host cavity by hydrophobic interactions.

7.5.2.3 Crystal Packing Arrangement

Figure 60 is a stereoview showing the crystal packing viewed along [100]. There are no hydrogen bonds between adjacent complex units. Water molecules are also not included in the complex. This then confirms that the only interaction present is due to van der Waals forces.

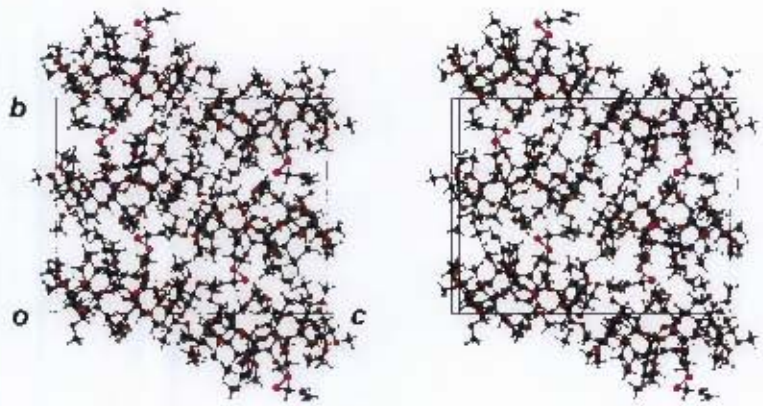

Figure 60: Crystal packing diagram: stereoview along the [100] direction

The guest residues that protrude from the secondary side of the host fill spaces surrounded by symmetry-related complex units. Interestingly, when this complex is compared with the complexes TRIMEB•(*Z*)-Ajoene and TRIMEB•(*E*)-Ajoene, a disordered arrangement, comprising both the *R*- and *S*-enantiomers of the guest, was identified within the host cavity, a situation that is not observed here.[119]

8.1.2 Growth of WHCO1 cells

All work on the cells was performed in a sterile tissue culture hood. Cancer cells used for this study were WHCO1 oesophageal cancer cells established from surgical biopsies. The cells were cultured in DMEM containing 10% fetal calf serum and 1% penicillin and streptomycin at 37°C in a humidified atmosphere of 5% CO_2. Cells were grown on 150 mm sterile tissue culture plates and split 1:12 every four days. Briefly, the media was first removed and the cells were washed with PBS (10 ml). Trypsin (10 ml) was then added and the cells were incubated with trypsin at 37°C for 2 min. The detached cells were then transferred to a sterile 12 ml conical tube and centrifuged at 1000 x g for 3 min. The cell pellet was then re-suspended in DMEM (8 ml) and the cells split 1:12. DMEM is Dulbecco's Modified Eagle Medium which is a solution of salts and other nutrients that are used to keep mammalian cells in culture alive. PBS is phosphate buffered saline.

8.1.3 The MTT assay

WHCO1 cells were rinsed and detached from the bottom of the plate with trypsin and counted using haemocytometer. 3 x 10^3 cells were then planted in sterile CellStar 96 well plates in 90 µL DMEM per well. After 24 hours, the cells had attached to the bottom of the plates and the compounds solubilized in DMEM + 1% DMSO (10 µl) were added to the wells and DMEM + 1% DMSO. (10 µl) alone was added to the control (no drug) to give a final concentration of 0 – 200 µM compound and 0.1% DMSO. After 48 hours incubation period, 10 µL of the MTT labeling reagent (final concentration 0.45 mg / ml) was added to each well and incubated for 4 hours in a humidified atmosphere at 37°C. One hundred microlitres of the solubilization solution (10% SLS in 0.01M HCl) was then added to each well and the plates were incubated overnight at 37°C. The spectrophotometric absorbance of the wells was then measured at 595 nm using a microtiter plate reader. The absorbance of the blank (media alone) was subtracted from the readings and the data were plotted using the software package Graphpad Prism 4 using the dose-response curve (variable slope) to fit the data. The half maximal inhibitory concentration (IC_{50}) is generated from the software. Independent experiments were performed between four and twelve times and the average is reported. The 95 % confidence interval is reported for the data as a measure of the error. The plots are displayed in Figure 63 and the IC_{50} values are reported in Table 15.

8.2 Analysis and Results

The chemical structures of the compounds used in the study are displayed in Figure 47. Unfortunately, the *Z*-isomers for the propyl / propyl and propyl / methyl analogues could not be obtained in sufficiently pure form. Also, the allyl / propyl (allyl on the sulfoxide side) derivative

was not accessible from the radical cyclization route used in view of likely addition of the vinyl radical onto the allyl double bond during the radical addition step. However, enough data were generated overall in order to be able to draw some preliminary conclusions on structure-activity relationships. The IC_{50} data generated on WHCO1 cells are displayed in Table 15, while the representative plots of the raw data obtained are displayed in Figure 63.

8.2.1 Structure-Activity analysis of ajoene

From the data, it can be seen that both *E*- and *Z*-ajoene are equally potent at inhibiting cell growth of WHCO1 cancer cells. This implies that for ajoene, the stereochemistry about the double bond is not important for inducing cancer cell death. This is in contrast to ajoene's anti-thrombotic activity where the *Z*-isomer is reported to be 1.3 times more active than the *E*-isomer at inhibiting platelet aggregation.[27] In contrast to what was found for ajoene, for the propyl / allyl isomers, the *Z*-isomer was found to be 1.7 times more active than the *E*-isomer at inhibiting the cell growth of WHCO1 cancer cells. It can be seen that substituting allyl for propyl on the sulfoxide end is tolerated without a change in anti-cancer activity for the *Z*-isomer (21.6 vs 20.5 μM for Z-propyl/allyl and Z-ajoene resp.), but causes a reduction in activity for the *E*-isomer series (35.8 μM vs 20.5 μM for *E*-propyl / allyl and *E*-ajoene resp.). Converting allyl / propyl to propyl / propyl does not affect the anti-cancer activity of the *E*-isomers (35.8 μM vs 33.8 μM for *E*-propyl / allyl and *E*-propy / propyl respectively), but substitution of the propyl group at the disulfide end for a methyl group decreases the activity (33.8 μM vs 47.4 μM for *E*-propyl / propyl and *E*-propyl / methyl respectively).

In summary, end-group changes appear to reduce the activity more for the *E*-isomer than the *Z*-. However, the data suggest that the pharmacophore of ajoene resides in the sulfoxide - vinyl disulphide core and not with the terminal groups. From a drug-discovery perspective, this is important as it opens up an avenue to generate more potent ajoene analogues by varying the physical characteristics of the groups at either end of the molecule but retaining the central active core.

8.2.2 Inclusion of PMB into a cyclodextrin

The most active analogue in the series, the *p*-methoxybenzyl analogue, was included into the cyclodextrin TRIMEB in an attempt to improve its bioavailability. The ajoene analogues are water insoluble and the inclusion methodology is used to solubilize the drug within the core of a soluble cyclodextrin. To our surprise, the inclusion complex was seven-fold less active at inhibiting WHCO1 cancer cell growth than the non-included compound (IC_{50} = 51.6 vs 7.1 μM for inclusion vs non-included PMB). This may likely be due to the fact that the PMB compound may be tightly bound within the cyclodextrin and unable to readily dissociate from the complex

to gain entry through the lipophilic membrane into the cell. From a bioavailability perspective, the inclusion complex may be important but in our in vitro assay system, this method of delivery is not favourable. TRIMEB itself was not toxic to the cells.

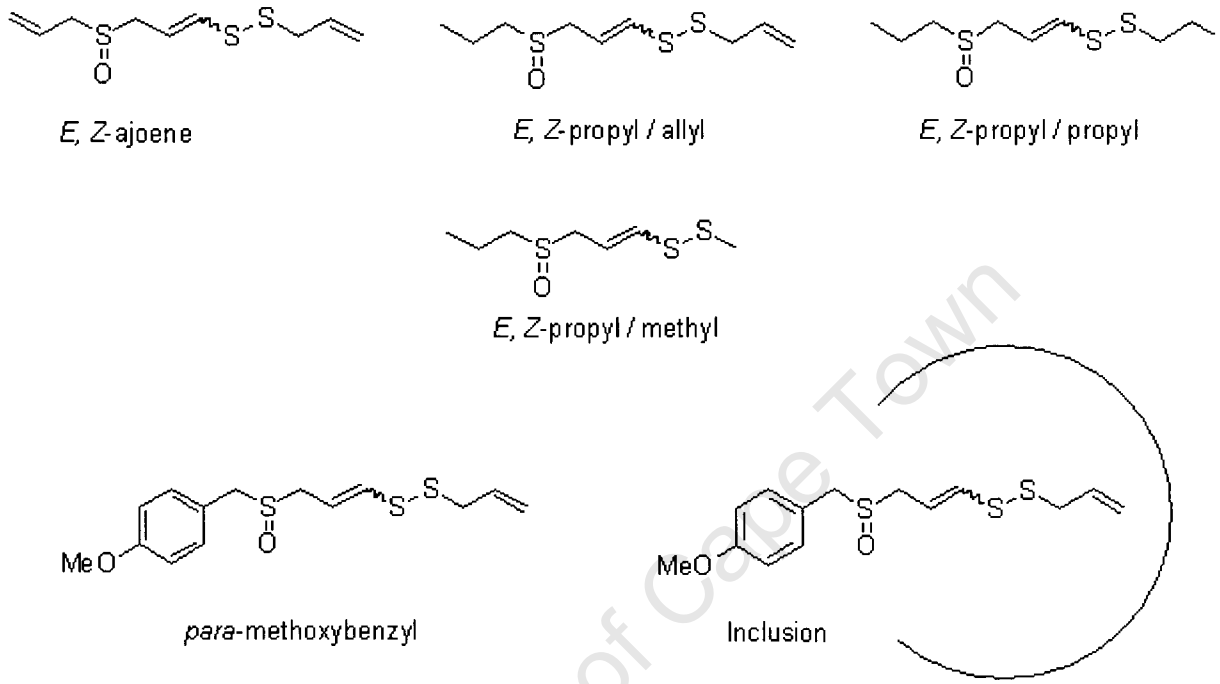

Figure 62: Chemical structures of the ajoene analogues synthesized for the study

Table 15: IC_{50} values of the tested compounds on WHCO1 cells

Compound	N	IC_{50} / µM	95% CI
E-ajoene	6	20.9	20.7 – 21.1
Z-ajoene	6	20.5	20.2 – 20.8
Z-propyl / allyl	12	21.6	21.5 – 21.7
E-propyl / allyl	10	35.8	35.5 – 36.0
E-propyl / propyl	4	33.8	34.2 – 33.4
E-propyl / methyl	5	47.4	47.1 – 47.7
TRIMEB	4	none	None
para-methoxbenzyl	6	7.1	7.1 – 7.20
Inclusion	4	51.6	51.2 – 52.0

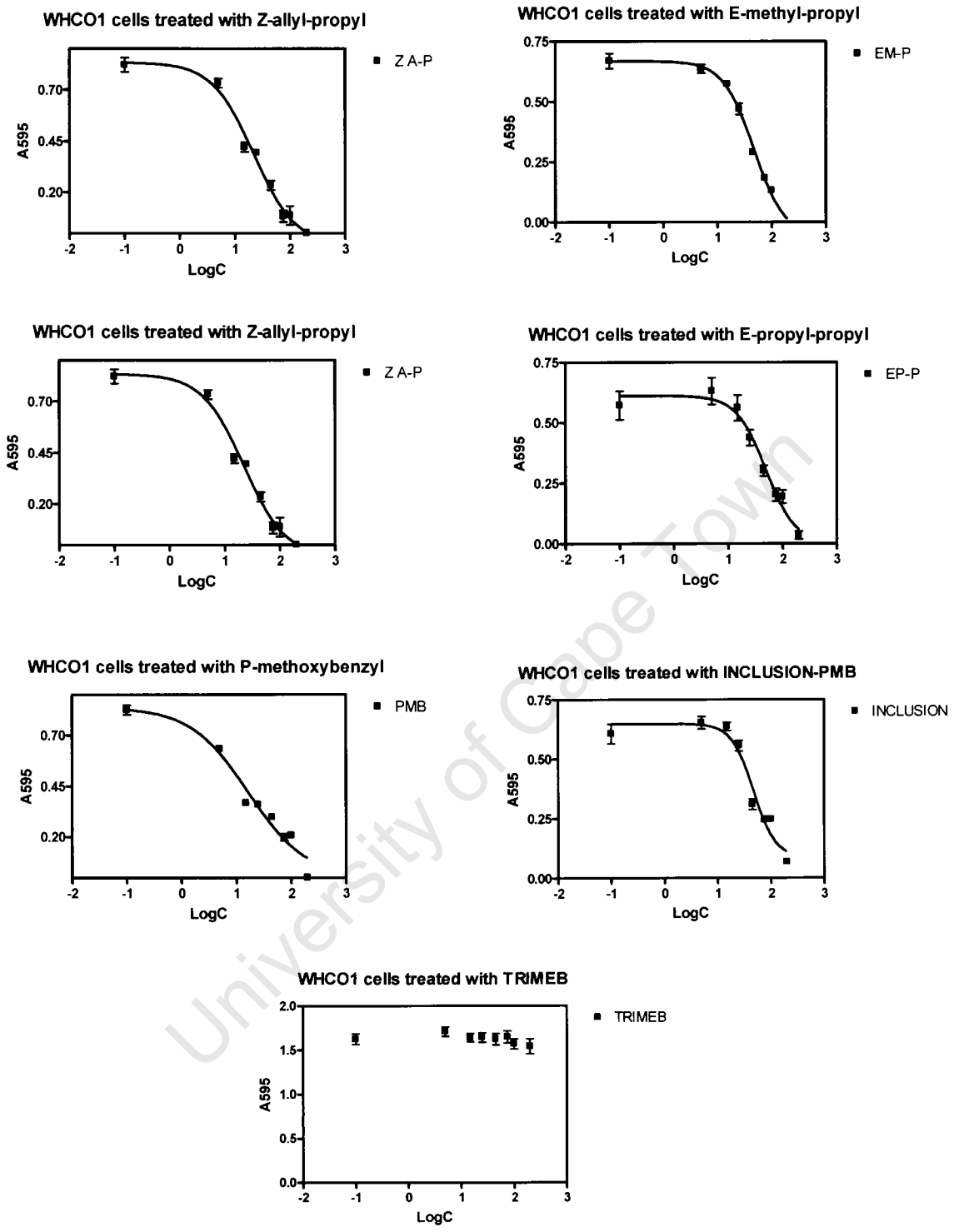

Figure 63: Plots of MTT data: absorbance obtained at 595 nm vs log of the drug concentration. Data analyzed using Graphpad prism 4 software, fitted to the dose response curve (variable slope).

8.2.3 Dependence of the IC_{50} on the lipophilicity of the compound

The Log P values of the compounds as a measure of compound lipophilicity were calculated using a free online software package and the IC_{50} for the compounds in the *E*-series was plotted against the Log P. We did not plot similar data for the Z-series as some of the analogues in this series were missing as mentioned before. A good correlation between Log P and the IC_{50} was observed (Figure 64). This implies that the lipophilicity of the compound is important for anti-cancer activity on WHCO1 cells. This may be related to the compound's ability to rapidly diffuse across membranes or may be related to a specific binding interaction between the compound and a specific protein at the target site. Since the target of ajoene in

Chapter 8 Biological Studies

Chapter 8: Biological studies

8.1. Measurement of anti-cancer activity

The synthesized ajoene analogues were tested for their ability to inhibit cell growth of WHCO1 cancer cells using the MTT assay.[125,126] The WHCO1 cell-line is an oesophageal cancer cell-line of South African origin which was originally established from surgical biopsies of primary oesophageal squamous cell carcinomas.[127] In this assay, different concentrations of the ajoene analogue are added to WHCO1 cancer cells that have been grown in a 96-well plate. The analogues are incubated with the cells for 48 hours and then MTT {3-(4,5-dimethylthiazol-2-yl)-2,5-diphenyltetazolium bromide} in PBS is added to each well and incubated with the cells for 4 hr. Metabolically active (or living cells) contain an intact mitochondrial reductase which metabolizes the soluble yellow MTT reagent into a crystalline blue formazan precipitate (see Figure 61 below). Dead cells therefore cannot metabolize MTT. The crystalline MTT is then solubilized with detergent and the absorbance at 595 nm is measured for each well. The intensity of the blue colour (absorbance) gives a measure of cell viability from which a dose-response curve can be generated. The IC_{50} is defined as the concentration which inhibits the growth of 50 % of the cell population. Therefore, the lower the IC_{50}, the more active the compound at inducing cell death.

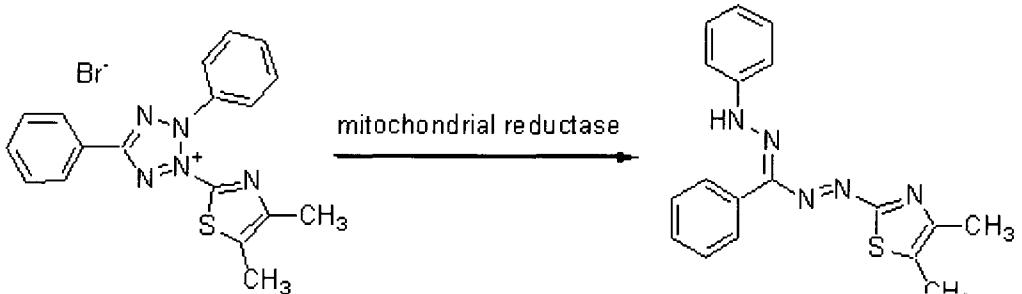

more active than ajoene and the most potent analogue of the set with an IC_{50} below 10 μM. The enhanced activity of this analogue relative to the other analogues may be due to the fact that it still retains the central sulfoxide-vinyl disulfide pharmacophore but has increased lipophilic character relative to ajoene.

Chapter 9: Conclusion

In conclusion, a new synthetic sequence that is concise and cost-effective has been successfully developed for the synthesis of a small library of ajoene analogues. The synthesized analogues were biologically active at inhibiting the cancer cell-growth of WHCO1 oesophageal cancer cells. The *p*-methoxybenzyl analogue was threefold more active than ajoene and the most potent analogue of the set with an IC_{50} below 10 μM. The observed increase in the biological activity of this analogue relative to ajoene was attributed to increased lipophilic character. Inclusion into the cyclodextrin TRIMEB resulted in reduced biological activity probably as a result of diminished delivery.

Future studies will focus on further functional group changes in search of an advanced lead by retaining the pharmacophore and changing the end groups to other lipophilic moieties such as benzyl and substituted benzyl derivatives. Biological evaluation will be carried out on these derivatives.

The mode of action of ajoene is believed to involve suppression of the anti-apoptotic protein bcl-2 but mechanistic detail is lacking on this process. A future avenue of research will be to probe the mechanisms behind the biological activity by using fluorescently tagged ajoenes.

References

1. Agarwal, K. C. *Med. Res. Rev.* **1996**, *16*, 111.
2. Thomson, M.; Ali, M. *Current Cancer Drug Targets.* **2003**, *3*, 67.
3. Kamel, A.; Saleh, M. *Stud. Nat. Prod. Chem.* **2000**, *23*, 455.
4. Lawson, L. D. *ACS Symp. Ser.* **1998**, *691*, 176.
5. Block, E. *Sci. Am.* **1985**, *252*, 114.
6. Ankri, S.; Mirelman, D. *Microbes and Infection*, **1999**, *2*, 125.
7. Cutler, R. R.; Wilson, P. *Brit. J. Biomed. Sci.* **2004**, *61*, 71.
8. Rahman, K. *Ageing Research Reviews.* **2003**, *2,* 39.
9. Scharfenberg, K.; Wagner, R.; Wagner. K. G. *Cancer Lett.* **1990**, *53*, 103.
10. S. M.; Takaha, T. *Chem. Rev.* **1998**, *98,* 1787.
11. Qwebani, T.; Hunter, R.; Caira, M. R.; Stellenboom, N.; Bourne, S. A.; Cele, K.; le Roex, T.
    ARKIVOC **2007**, *ix*, 53.
12. Harris, J. C.; Cottrel, S. L.; Plummer, S.; Lloyd, D. *Appl. Microbiol. Biotechnol.* **2001**, *57*, 282.
13. Wertheim, T. *Justus Liebigs Ann. Chem.* **1844**, *51*, 289.
14. Semmler, F. W. *Arch. Pharm.* **1892**, *230*, 434.
15. Cavallito, C. J.; Bailey, J. H. *J. Am. Chem. Soc.* **1944**, *66*, 1950.
16. Cavallito, C. J.; Buck, J. S.; Suter, C. M. *J. Am. Chem. Soc.* **1944**, *66*, 1952.
17. Small, L. V. D.; Bailey, J.; Cavallito, C. J. *J. Am. Chem. Soc.* **1947**, *69,* 1710.
18. Stoll, A.; Seebeck, E. *Adv. Enzymol.*, **1951**, *11*, 377.
19. Ellmore, G. S.; Feldberg, R. S. *Am. J. Bot.* **1994**, *81*, 89.
20. Kroemer, G.; Reed, J. C. *Nat. med.* **2000**, *6,* 513.
21. Freeman, F.; Kodera, Y. *J. Agric. Food Chem.* **1995**, *43*, 2332.
22. Shen, C.; Xiao, H.; Parkin, K. L.; *J. Agric. Food Chem.* **2002**, *50*, 2644.
23. Block, E.; Naganathan, S.; Putman, D.; Zhao, S.H. *Pure Appl. Chem.* **1993**, *65*, 625.
24. Block, E. *Angew. Chem. Int. Ed. Engl.* **1992**, *31,* 1135
25. Lawson, L. D.; Hughes, B. G. *Planta Med.* **1992**, *58*, 345.
26. Block, E.; O'Connor, J. *J. Am. Chem. Soc.* **1974**, *96*, 3929.
27. Block, E.; Ahmad, S.; Catalfamo, J. L. *J. Am. Chem. Soc.* **1986**, *108*, 7045.
28. Block, E.; Ahmad, S.; Jain, M.K.; Crecely, R.W.; Apitz-Castro, R.; Cruz, M. R. *J. Am. Chem. Soc.* **1984**, *106*, 8295
29. Block, E.; Ahmad, S.; Jain, M. K.; Apitz-Castro, R. W. *J. Amer. Chem. Soc.* **1986**, *108*, 7045.
30. Hunter, R.; Caira, M. Stellenboom, N. *Ann. N.Y. Acad. Sci* .**2005**, *1056,* 234.

31. Ibert, B.; Winkler, G.; Knoblock, K. *Planta. Med.* **1990**, *56*, 202.
32. Yoshida, S.; Kasuga, S.; Hayashi, N.; Ushiroguchi, T.; Matsuura, H.; Nakagawa, S. *Appl. Environ. Microbiol.* **1987**, *53*, 615.
33. San-Blas, G.; San-Blas, F.; Gill, F.; Marino, L.; Apitz-Castro, R. *Antimicrob. Agents Chemother.* **1989**, *33*, 1642.
34. Urbina, J.; Marchan, E.; Lazardi, K.; Visbal, G.; Apitz-Castro, R.; Gil, F.Aguirre, T.; Piras, M. *Biochem. Pharmacol.* **1993**, *45*, 2381.
35. Scharfenberg, K.; Wagner, R.; Wagner. K. G. *Cancer Lett.* **1990**, *53*, 103.
36. Hassan, H. T. *Leukemia Res.* **2004**, *28*, 667.
37. Naganawa, R.; Iwata, N.; Ishikawa, K.; Fukuda, H.; Fujino, T.; Suzuki A. *Appl. Environ. Microbiol.* **1996**, *62*, 4238.
38. Yang, J. Y.; Della-Fera, M.; Nelson-Dooley, C.; Baile, C. A. *Obesity.* **2006**, *14*, 388.
39. Yang, J. Y.; Della-Fera, M.; Hausman, D. B.; Baile, C. A. *Apoptosis.* **2007**, *12*, 1117.
40. Srivastava, K. C.; Tyagi, O. C. *Prostaglandins, Leukot. Essent. Fatty Acids.***1993**, *49*, 587.
41. Villar, R.; Alvarino, M. T. *Biochim. Biophys. Acta,* **1997**, *1337*, 233.
42. Barone, E. F.; Tansey, M. R. *Mycologia.* **1997**, *69*, 793.
43. Rendu, F.; Daveloose, D.; Denouzy, J. C.; Bourdeau, N.; Bourdeau, N.; Levy-Toledano, S.; Jain, M. K.; Apitz-Castro, R. *Biochem. Pharmacol.* **1989**, *38*, 1321.
44. Apitz-Castro, R.; Badimon, J.; Badimon, L. *Thromb. Res.* **1994**, *75*, 243.
45. Mathew, B. C.; Daniel, R. S.; Augusti, K. T. *Indian J. Exp. Biol.* **1996**, *34*, 337.
46. Yang, J. Y.; Della-Fera, M. A.; Nelson-Dooley, C.; Baile, C. A. *Obesity.* **2006**,*14,* 388.
47. Perez, H.; De La Rosa, M.; Apitz, R. *Antimicrob. Agents Chemother* **1994,** *38*, 337.
48. Gargouri, Y.; Moreau, H.; Jain, M. K.; De Haas, G. H.; Verger, R. *Biochim. Biophys. Acta.* **1989**, *1006,* 137.
49. Ackerman, R.T.; Mulrow, C.D.; Ramirez, G *et al. Arch. Intern. Med.* **2001**, *161*, 813.
50. Wagner, H.; Wierer, M.; Fessler, B. *Planta medica* **1987,** *53*, 305.
51. Gebhardt, R.; Beck, H.; Wagner, K. G. *Biochimica et biophysica acta* **1994,** *1213*, 57.
52. Belman, S.; Solomon, J.; Segal, A.; Block, E.; Barany, G. *J. Biochem. Toxicol.* **1989**, *4,* 151.
53. Dirsch, V. M.; Vollmar, A. M. *Biochem. Pharmacol.* **2001,** *61*, 587.
54. Dirsch, V. M.; Gerbes, A. L.; Vollmar, A. M. *Mol. Pharmacol.* **1998**, *53*, 402
55. Gallwitz, H.; Bonse, S.; Martinez-Cruz, A.; Schlichting, I.; Schumacher, K.; Krauth-Siegel, R. *J. Med. Chem.* **1999,** *42*, 364.
56. Sjöström, J.; Mäkelä, T. *Encyclopedia of life sciences.* **2006**.
57. Reed, J.C. *Ame. J. Pathol.* **2000**, *157,* 1415.

58. Dirsch, V. M.; Antlsperger, D. S. M.; Hentze, H.; Vollmar, A.M. *Leukemia.* **2002**, *16*, 74.
59. Nishikawa, T.; Yamada, N.; Hattori, A.; Fukuda, H.; Fujino, T.; *Biosci. Biotechnol. Biochem.* **2002**, *66*, 2221.
60. Li, M.; Cui, J.R.; Ye, Y.; Min, J. M.; Zhang, L. H.; Wang, K et al. *Carcinogenesis.* **2002**, *23*, 573.
61. Johnson, M. G.; Vaughn, R. H. *Appl. Microbiol.* **1969**, *17*, 903-905
62. Davies, N.M.; Sharkey, K.A.; Asfaha, S.; Macnaughto, W.K.; Wallace, J.L *Aliment Pharmacol Ther.* **1997**, *9*, 934.
63. Taketo, M. M *J Nat. Cancer Inst.* **1998**, *90,* 1609.
64. Ibert, B.; Winkler, G.; Knobloch, K *HPLC. Planta Med.* **1990,** *56,* 202.
65. Sigounas, G.; Hooker, J. L.; Li, W.; Anagnostou, A.; Steiner, M *Nutr Cancer.* **1997**, *8,* 153.
66. Pai, E. F.; Schulz, G. E *J. Biol. Chem.* **1983**, *258,* 1752.
67. Gallwitz, H.; Bonse, S.; Martinez-Cruz, A.; Schlichting, I.; Schumacher, K.; Krauth-Siegel, R. *J. Med. Chem.* **1999,** *42*, 364.
68. Sugoh, K.; Kuniyasu, H.; Sugae, T.; Ohtaka, A.; Takai, Y.; Tanaka, A.; Machino, C.; Kambe, N.; Kurosawa, H. *J. Am. Chem. Soc.* **2001**, *123*, 5108.
69. Ogawa, A.; Ikeda, T.; Kimura, K.; Hirao, T. *J. Am. Chem. Soc.* **1999**, *121*, 5108.
70. Koelle, U.; Rietmann, C.; Tjoe, J.; Wagner, T.; Englert, U. *Organometallics.* **1995**, *14*, 703.
71. Backvall, J. E.; Ericsson, A. *J. Org. Chem.* **1994**, *59*, 5850.
72. Kuniyasu, H.; Ogawa, A.; Sato, K. I.; Ryu, I.; Kambe, N.; Sonoda, N. *J. Am. Chem. Soc.* **1992**, *114*, 5902.
73. Mcdonald, J. W.; Corbin, J. L.; Newton, W. E. *Inorg. Chem.* **1976**, *15*, 2056.
74. Hartwig, J. F. *Nature.* **2008**, *455*, 314.
75. Sader, H. S.; Johnson, D. M.; Jones, R. N. *Antimicrob. Agents Chemother.* **2004**, *48*, 53.
76. Johannesson, P.; Lindeberg, G.; Johanson, A.; Nikiforovich, G. V.; Gogoll, A.; Synnergren, B.; Le Greves, M.; Nyberg, F.; Karlen, A.; Hallberg, A. *J. Med. Chem.* **2002**, *45*, 1767.
77. Ceruti, M.; Balliano, G.; Rocco, F.; Milla, P.; Arpicco, S.; Cattel, L.; Viola, F. *Lipids* **2001**, *36*, 629.
78. Marcantoni, E.; Massaccesi, M.; Petrini, M.; Bartoli, G.; Bellucci, M. C.; Bosco, M.; Sambri, L. *J. Org. Chem.* **2000**, *65*, 4553.
79. Lam, H. W.; Cooke, P. A.; Pattenden, G.; Bandaranayake, W. M.; Wickramasinghe, W. A. *J. Chem. Soc.* **1999**, *1,* 847.

80. Morimoto, K.; Tsuji, K.; Iio, T.; Miyata, N.; Uchida, A.; Osawa, R.;Kitsutaka, H.; Takahashi, A. *Carcinogenesis* **1991**, *12*, 703.
81. Monte, A.; Kabir, Shahjahan, M.; Cook, J. M.; Rott, M.; Schwan, W. R.; Defoe, L. U.S. *Pat. Appl. Publ.* **2007**, *37*. 11.
82. (a) Kiener, C. A.; Shu, C.; Incarvito, C.; Hartwig, J. F. *J. Am. Chem. Soc.* **2003**, *125*, 14272.
    (b) Vorogushin, A. V.; Huang, X.; Buchwald, S. L. *J. Am. Chem. Soc.* **2005**, *127*, 8146.
83. Bates, C. G.; Saejueng, P.; Doherty, M. Q.; Venkataraman, D. *Org. Lett.* **2004**, *6*, 5005.
84. Behringer, H. *Ann.* **1949**, *564,* 219.
85. Kampmeier, J. A; Chen, G. *J. Amer. Chem. Soc.* **1965**, 2602.
86. Bader, H.; Cross, L. C.; Heilbron, I.; Jones, E. R. H. *J. Chem. Soc.* **1949,** 619.
87. (a) Hunter, R.; Kaschula, C. H..; Parker, I. M.; Caira, M. R.; Richards, P.; Travis, S.; Taute, F.; Qwebani, T. *Bioorg. Med. Chem. Lett.* **2008**, *18,* 5277. (b) Muzart, J.; Pale, P.; Pete, J. P.; Riahi, A. *Bull. Soc. chim Fr.* **1988**, *4*, 731.
88. (a) Kimicheskaya, S. *Bull. Acta. Sci.* **1978**, *11,* 2539. (b) Boldyrev, B. G.; Trofimova, T. A. *Zh. Ob. Khimii.* **1957**, *27*, 1006.
89. Szejtli, J. *Pure. Appl. Chem.* **2004**, *76,* 1825.
90. Frömming, K. H.; Szejtli, J. *Cyclodextrins in pharmacy.* **1996**, 25.
91. Mosinger, J.; Tománková, V.; Němcová, I.; Zyka, J. *Anal. Lett.* **2001**, *34,* 1979.
92. Villiers, A. *Compt. Rend.* **1891**, *112,* 536.
93. Szejtli, J. *Cyclodextrin Technology*, Kluwer, Dordrecht. **1988**.
94. Cramer, F.; Freudenberg, K.; Plieninger, H. *Ger. Patent.* **1953**, 895.
95. Szejtli, J. *Med. Res. Rev.* **1994**, *14, 353.*
96. Atwood, J. L.; Davies, J. E. D.; Osa, T.; Reidel, D. *Third Int. Symp. on cyclodextrins.* Kluwer. Dordrecht, **1985**.
97. Cramer, F.; Szejtli *J. Proceedings of the First International Symposium on Cyclodextrins*, D. Reidel, Dordrecht. **1982**, 3.
98. Huber, O.; Szejtli, J. *Fourth Int. Symp. Cyclodextrins*, Dordrecht. **1988**, 407.
99. Brewster, M.E. *New Trends in Cyclodextrins and Derivatives. Editions de Santé,* Paris **1991**, 313.
100. Hedges, A, R. *Sixth Int. Symp. Cyclodextrins. Editions de Santé.* **1992.**
101. Osa, T. *Publ. Office of Business Centre for Academic Societies of Japan.* **1994**.
102. French, A. D.; Murphy, V.G. *Carbohydr. Res.* **1973**, *27,* 391.
103. Reuscher, H. Hirsenkorn, R.; Szejtli, j.; Szente, L. *Eighth Int. Symp. Cyclodextrins.* Kluwer, Dordrecht. **1996**, 553

104. Sato, Y.; Suzuki, K.; Ito, K.; Shingawa, T.; Szejtli, J.; Osu, T. *US Patent 5156866.* **1992**.

105. Szejtli, J.; Osu, T. *Compre. Supramol. Chem.* **1996**.

106. Szejtli, J. *Academic. Press.* **1984, 3**.331

107. Denter, U.; Buschmann, H. J.; Knittel. D.; Schollmeyer, E. *Angew. Makromol. Chem.* **1997**, *165*, 248.

108. Hedges, A. *Chem Rev.* **1998**, *98,* 2035.

109. Konno, A.; Misaki, M.; Toda, J.; Wade, T.; Yasumatsu, K. *Agric Biol Chem.* **1986**, *46,* 2203.

110. Ducheˇne, D.; Ponchel, G.; Bochot, A. *Eur. J. Pharm. Sci.* **2005**, 25S1, S1–S2.

111. Connors, K. *Chem. Rev.* **1997**, *97,* 1325.

112. Szejtli, J. *Chem. Rev.* **1998**, *98,* 1743.

113. Hooft, R. *COLLECT*, Nonius B. V Delf. **1998**. The Netherlands

114. Ergert, E.; Shelrick, G. M. *Acta Crystallogr.* **1985**, *A41*, 262.

115. Sheldrick, G. M. *SHELXL-97. Program for Crystal Structure Refinement,* University of Go¨ttingen, Germany, **1997**.

116. Drioli, E.; Gordano, A.; Manferti, C.; Trotta, F. *Sep. Purif. Technol.* **2002**, *28,* 61.

117. Durst, D. H.; Gan, L. H.; Johnson, E.; Menger, F. M. *J. Am. Chem. Soc.* **1987**, *109,* 2800.

118. Ketula, R. A.; Soderstrom, F. M. *J. Anal. Chem.* **1994**, *350,* 126.

119. Caira, M. R.; Hunter, R.; Bourne, S, A.; Smith, V. J. *Supramol. Chem.* **2004**, *16,* 395.

120. Bender, M.; Komiyama, M. *Cyclodextrin Chemistry.* **1978**.

121. Otwinowski, Z.; Minor, W.; Carter, C. W.; Sweet, R. M. *Academic Press.***1997**, *207,* 307.

122. Dressnandt, G.; Rockinger, H.; Prigge, H.; Treiber, A. *Patent EP0721940.* **1996**.

123. Kálmán , A.; Párkányi, L. *Adv. Mol. Struct. Res..* **1997**, 189.

124. Caira, M. R.; Griffith, V. J.; Nassimbeni, L. R.; van Oudtshoorn, B. *J. Incl. Phenom.* **1995**, *20*, 277.

125. Slater, T. F.; Sawyer, B,; Strauli, U. *Biochim Biophys Acta*, **1963**, *77*, 383.

126. Veale, R. B *et al. South African Journal of Science.* **1989**, *85*, 375.